

Alma Mater Studiorum – Università di Bologna

DOTTORATO DI RICERCA IN
Biologia Cellulare e Molecolare

Ciclo XXXV

Settore Concorsuale: 5/E2 - BIOLOGIA MOLECOLARE

Settore Scientifico Disciplinare: BIO/11 - BIOLOGIA MOLECOLARE

TITOLO TESI

Exploring the potential of self-assembling nanoparticles in displaying structurally defined antigens
for vaccines development

Presentata da: Luigia Cappelli

Coordinatore Dottorato

Vincenzo Scarlato

Supervisore

Vincenzo Scarlato

Co-supervisore
Roberta Cozzi

Esame finale anno 2023

Index

Abstract

Introduction

1. Nanoparticle's introduction
2. Biological function and distribution of self-assembling protein nanoparticles
3. Self-assembling protein nanoparticles for vaccine development
4. Engineerization of protein nanoparticles external surface
 - 4.1. Chemical conjugation of protein and sugar antigens
 - 4.2. Protein ligation systems for protein antigen display
 - 4.3. Genetic fusion of protein antigens
5. Natural and synthetic nanoparticles used as platform for antigen display
 - 5.1. VLP-based platform
 - 5.1.1. Hepatitis B virus core antigen HBcAg
 - 5.1.2. Bacteriophage coat protein Q β
 - 5.1.3. AP205 bacteriophage coat protein CP3
 - 5.2. Non-viral based platform
 - 5.2.1. Ferritin
 - 5.2.2. Encapsulin
 - 5.3. Synthetic nanoparticles
 - 5.3.1. mI3
6. Protein and sugar antigens target of this study
 - 6.1. *Neisseria meningitidis* Factor-H binding protein
 - 6.2. *Streptococcus agalactiae*
 - 6.2.1. Pilin proteins
 - 6.2.2. Capsular Polysaccharide
 - 6.3. *Neisseria gonorrhoeae*
 - 6.3.1. Opacity-associated proteins
 - 6.3.2. Porin B

Aim of the study

Materials and Methods

7. Protein design and 3D structure prediction
 - 7.1. Structure-based design

- 7.2. Rosetta homology modelling
- 8. Production of recombinant protein
 - 8.1. Strains
 - 8.2. Expression vectors
 - 8.3. Genes
 - 8.4. Cloning
 - 8.4.1. Vector amplification
 - 8.4.1.1. DpnI digestion
 - 8.4.1.2. Agarose gel electrophoresis
 - 8.4.2. PIPE cloning
 - 8.5. Plasmid transformation
 - 8.6. Recombinant protein expression in *E. coli* BL21(DE3)
 - 8.6.1. Pre-culture and glycerol stock preservation
 - 8.6.2. Batch culture at 20 °C
 - 8.6.3. Batch culture at 37 °C
 - 8.6.4. Small scale analysis of protein expression and solubility
 - 8.6.5. SDS-PAGE
 - 8.6.6. Harvest and cell lysis
 - 8.7. Purification of recombinant proteins
 - 8.7.1. Immobilized metal affinity chromatography (IMAC)
 - 8.7.2. Size exclusion chromatography (SEC)
 - 8.8. Protein content evaluation
- 9. Polysaccharide chemical conjugation
- 10. Structural and functional characterization
 - 10.1. Transmission electron microscopy (TEM)
 - 10.2. Western and Dot Blot
 - 10.3. His-tag removal
 - 10.4. Differential scanning fluorimetry (DSF)
 - 10.5. Differential scanning calorimetry (DSC)
 - 10.6. Dynamic light scattering (DLS)
 - 10.7. SEC-Multi Angle Light Scattering (SEC-MALS)
 - 10.8. Surface Plasmon Resonance (SPR)
 - 10.9. Protein crystallization and structure determination
 - 10.10. *In Vivo* study

10.11. Luminex assay

Results and discussion

11. Self-assembling protein nanoparticles and virus like particles correctly display β -barrel from meningococcal factor H-binding protein through genetic fusion

11.1. Rosetta comparative modelling for the structural assessment of chimeric NPs

11.2. Correctly assembled NPs were detected for all tested molecules, except Q β

11.3. β barrel antigen is correctly displayed on NP surface

11.4. Discussion

12. Domain 3 of Group B Streptococcus pilus protein as scaffold for epitopes identification and display on NP surface

12.1. Structural analysis of GBS D3 allowed the identification of potential engineerable sites

12.2. Structural prediction and identification of extracellular loops of PorB.1b and OpaB

12.3. D3 site2 is the optimal site for the insertion of OpaB and PorB1b loops

12.4. D3 correctly displays gonococcal epitopes

12.5. Crystal structure resolution of D3porBloop5 confirmed the correct epitope display

12.6. D3 scaffold prevented epitope degradation when displayed on mI3 surface

12.7. Discussion

13. Production of a polyvalent nanoparticle displaying both protein and sugar antigens of Group B streptococcus (GBS)

13.1. Pilus fusion protein covers all protein variants of GBS pilus type 2

13.2. mI3 NP correctly displays chimeric pilus antigen

13.3. Chimeric mI3-pilus fusion protein successfully conjugated with GBS PSII

13.4. GBS PSII and pilus fusion protein are more immunogenic when displayed on mI3 surface

13.5. Discussion

Conclusions and future perspective

Transparency statement and sponsorship

Trademarks

References

Abstract

To meet the growing need for medical interventions against infectious diseases, several vaccines containing isolated and highly purified antigenic proteins have been developed. Compared to traditional vaccines, they are safer but show a lower capability to induce high level of protective immunity. To overcome the latter, the use of nanoparticles for the display of target antigens is a promising strategy [1]. Virus-like particles (VLPs) and protein nanoparticles (NPs), thanks to their repetitive and highly ordered structure, can present multiple copies of the target antigens. These supra-molecular assemblages can mimic the size and the shape of the natural host-pathogen surface interactions with potential to induce potent B- and T-cell response [2].

The present work is focused on (i) the identification of NPs prone to genetic fusion with a target protein antigen, (ii) the development of a new strategy for the epitope display and (iii) the design and development of a polyvalent NP. Different NPs and VLPs (e.g. I03, ferritin, encapsuline, Qbeta, CP3 and HBcAg) were genetically fused to a meningococcal antigen. The Domain 3 of Group B *Streptococcus pilus* protein has been successfully engineered with foreign epitopes allowing the display on a NP surface. Combining structural and computational biology each chimeric molecule has been designed and its 3D has been predicted. Computationally designed molecules were produced in *Escherichia coli* and biochemically and structurally characterized. Furthermore, by combining genetic fusion and chemical conjugation approaches, a polyvalent NP has been developed displaying simultaneously two different streptococcal antigens

Results obtained show that particles, can maintain their ability to self-assemble when genetically fused with a foreign protein. The antigen resulted correctly displayed on NPs surface and recognized by a functional human monoclonal antibody with increased avidity. The use of a foreign protein scaffold (D3) allowed the identification of most immunogenic epitopes from unsoluble membrane antigens as well as its display on mI3 surface. Moreover, the *in vivo* study conducted with the polyvalent NP revealed that the use of the NP as scaffold increased the immunogenicity of both streptococcal antigens.

In conclusion, this work represents a template strategy for the development of new effective NP-based vaccines against bacterial pathogens

Introduction

1. Nanoparticle's introduction

A nanoparticle (NP) can be defined as an ordered set of atoms or molecules with a diameter ranging from 1 to 100 nm [3]. During the last years, the use of NPs has evoked a global interest thanks to their novelty and applicability in different research fields [4, 5]. In fact, their small size and unique properties make them attractive for bio-catalysis [6], drug and gene delivery [7, 8], fluorescent biological labels [9, 10], cancer therapy [11] and vaccine development [12]. Their versatility is also due to the possibility to have NPs of different shapes made up of various materials such as: metallic [13], lipidic [14], polymeric [15] and protein [16] (Figure 1). Metal nanocluster based on silver are mainly used in electronics and nanoconductor while noble metal NPs, like gold NPs, find wide applications also in nanomedicine [17, 18]. They can be easily produced with both top-down and bottom-up approaches using for example condensation/evaporation, pyrolytic methods, atomic layer deposition techniques [19, 20]. Their major drawbacks are represented by the intrinsic toxicity and organ-level accumulation [21]. Lipid NPs are produced using phospholipids comprising both a hydrophilic and hydrophobic portion. Using an aqueous solvent, they assemble into micelles able to encapsulate in their core therapeutics finding wide application for drug delivery [22]. For the same purpose, they are used also cages based on polymers. They can be composed by natural sources like chitosan and sodium alginate [23] or can be chemically synthesized [24]. Among biopolymer-based NP, there are nanoparticles formed by proteins (pNPs) like albumin, gliadin and ferritin [16]. This class of cages present a lot of advantages: biodegradability, stability, possibility to modify their surface, biocompatibility, easy control of particle size and low toxicity and immunogenicity [25, 26]. Their non-antigenic property makes them useful not only for drug delivery, cancer/tumor therapy but also for vaccine production [27-29]. In addition, not toxic compounds or organic solvents are needed for their production. In fact, the assembly of pNPs can be achieved using several different approaches like: desolvation, coacervation, emulsification, nanoprecipitation and nano spray drying [30]. In some cases, a sub-class of pNPs, known as self-assembling protein nanoparticles, are composed by proteins that spontaneously assemble into nanoparticles.

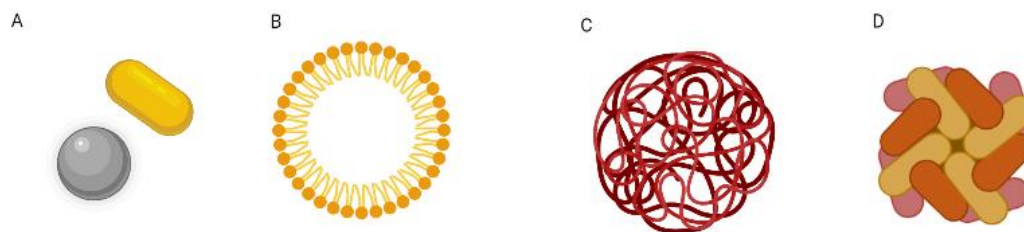


Figure 1: Representation of most common nanoparticles used in different research fields. (A) Gold nanorod (yellow) and silver spherical cage (grey), (B) lipidic micella, (C) polymeric nanoparticle, (D) protein-based nanoparticle (ferritin). Image created with BioRender.

2. Biological function and distribution of self-assembling protein nanoparticles

The term self-assembling protein nanoparticles is referred to molecules that have the intrinsic ability to spontaneously assemble into nanocages. Self-assembly can be directed dissolving in a solution an individual protein chain exceeded the critical micelles concentration (CMC) at the critical solution temperature (CMT) [30] or can occur naturally. The spontaneous assembly is a peculiarity of a class of proteins that in nature are organized in nanostructure to carry out their biological function. They are ubiquitously expressed both in bacterial, eukaryotic, archaeal, and viral organisms. First evidence of bacterial micro-compartment (BMC) came from 1973 when polyhedral organelles, named carboxisomes, were identified and visualized by electron microscopy in cyanobacteria and chemoautotrophs [31]. From then, seven functionally distinct organelles distributed among over at least 40 bacteria genera have been identified through genome analysis [32]. They resulted to be crucial in different metabolic pathways. In fact, their role is to segregate specific compounds like toxic or volatile intermediates allowing at the same time the permeation of enzyme substrates, products and cofactors [33]. Together with carboxisomes, the other major prokaryotic MC is represented by encapsulins. These proteins belong to the organelles involved in the protection of the bacterium from oxidative stress [34, 35]. Some nanocages identified in bacterial cells are shared also with eukaryotic organisms. This is the case of ferritins that are involved in the iron storage and regulation of iron availability and homeostasis [36]. First eukaryotic ferritin has been isolated from horse spleen and crystallized by Laufberger in 1937 [37] and currently they represent the most studied eukaryotic nanocages. Another class of eukaryotic compartments are the vaults. They are ribonucleoproteins with a barrel structure that self-assemble into cages (67 nm × 40 nm) with internal hole (3.87 × 10⁷ Å³) and they are involved in intracellular transport, multidrug resistance, and cell signalling [38, 39]. The use of protein nano-compartment widely spread also among not living organisms like viruses. In fact, they envelope their entire replicative machinery in a protein capsid composed by multiple copies

of a single or few proteins that self-assemble into nanocage. Nevertheless, the recombinant protein capsid is not infective and not replicative but it is still able to maintain its symmetric structure resembling the original virus; for these reasons they are known as virus-like particles (VLPs) [40]. One of the first evidence of their existence comes from 1950s. Rod-shaped particles were extracted from a tobacco mosaic virus (TMV) with a morphology resembling the original TMV devoid of genetic material [41]. Thanks to genetic engineering and biochemical manipulations, both VLPs eukaryotic and procaryotic nanocages have been explored for several biotechnological uses such as drug delivery, cancer therapy, biocatalysis and vaccine development (Table 1).

Table 1: Summary of different types of protein nano-compartment, their source, function, and applications

Protein nano-compartment	Organisms	Function	Main applications
Bacterial micro-compartment [42]	Prokaryotes	Metabolism	Catalysis
Encapsuline [34]	Bacteria and Archaea	Protection in oxidative stress	Drug delivery, vaccine development
Ferritin [43]	Animals, microbes, plants	Iron-storage	Drug delivery, vaccine development
Vault [44]	Eukaryotes	Immune response	Drug delivery, vaccine development
Virus-like particle [45]	Viruses	Protection	Vaccine development and catalysis

3. Self-assembling protein nanoparticles for vaccine development

Nowadays vaccines represent one of the most powerful weapons to defeat bacteria causing severe diseases. First vaccine was developed by Edward Jenner in the 1976. He sensed that, by immunizing James Phipps with derivative of cows pustules, it would have made him immune to smallpox [46]. Since then, several new vaccines have been developed and multiple diseases eradicated [47]. First vaccine preparations were made by live attenuated or killed pathogens [48]. They were highly immunogenic, but their major drawback is that they could revert into a pathogenic state under certain conditions [49]. To overcome this issue, new vaccine preparations have been formulated using highly purified antigenic proteins. However, despite their safety, vaccines based on recombinant proteins

are poorly immunogenic due to their small size [50, 51]. The protein antigen display on a larger scaffold represents an efficient strategy to improve vaccine immunogenicity. For this reason, protein-nanoparticle are actually widely explored as platform for antigen display [1]. In fact, when NPs are intravenously injected, they travel through circulatory and lymph vessels with rapid accumulation in the spleen and thyroid stimulation the humoral immunity [52]. Therefore, the use of the larger scaffold for antigen display improves the antigen presenting cells (APC) uptake and their retention into the follicles [2, 53]. Moreover, the multicopy display allow an efficient binding and activation of B-cell receptors (BCR) [1]. In this way, a potent T-and B-cells response is induced with the resulting production of antigen-specific antibodies by plasma cells [1]. NPs sizes, shape and surface charge can impact the immune response induced [54]. Several studies have shown that the optimal size range to obtain a significant drainage and retention into lymph node is 20-45 nm [54] and that spherical NPs are internalized faster than rod or cubic shaped once [55]. In addition, positively charged NPs are internalized more efficiently than neutral or negatively charged molecules [56]. During the years, self-assembling protein NPs have been widely used in the vaccinology also thanks to their versatility. They have been used as antigen themselves, as carrier for peptide, adjuvant or drugs and as platform for foreign antigen display. The first evidence of the possibility to use NPs as antigen comes from 1970 when the hepatitis B virus surface antigen (HBsAg) was purified from infected human sera resulting in a non-infective nanoparticle [57]. This discovery represented a milestone that changed for ever the vaccinology field allowing also, 10 years later, to licence Engerix-B, the first effective vaccine against HBV produced by Glaxo Smith Klein (GSK) [58, 59]. Following this direction several other analogue vaccines have been produced: Recombivax-HB (Merk), GenHevac B (Pasteur), Fendrix (GSK) and HBvaxPRO (Merck Sharp and Dohome Limited) [60-63]. On the other hand, Xiamen Innovax Biotech has produced Hecolin vaccine to fight hepatitis E virus (HEV) using a recombinant peptide of capsid protein able to self-assemble into a homodimer of 23nm [64, 65]. In the first years of the new century, another nanoparticle-based vaccine (Cervarix) has been licensed. In this case the pathogen targeted is the Human papilloma virus (HPV) that causes the most common sexually transmitted infection (STI) leading the development of genital warts and even cervix, throat, and anus cancers [66-68]. Cervarix main antigens are capsid proteins (L1) of HPV types 16 and 18 that, when recombinantly produced, self-assemble into virus-like particles (VLPs) [69, 70]. Against the same pathogen a nine-valent vaccine has been produce by Merck known as Gardasil 9 [66]. Moreover, thanks to their unique structure, self-assembling protein NPs can encapsulate and carry in their hollow core target molecules like antigenic peptides, proteins, dsRNA, ssRNA and adjuvants [71-74]. The internal space is not their only portion that can be exploited. In fact, even the external surface has been extensively investigated for the display of the target antigen. The most recent

research in this field has led to the Mosquirix vaccine license in October 2021 [75]. Mosquirix represent the first approved vaccine to fight malaria disease [76]. It takes advantage of HBV VLP for the ordered display of 240 copies of circumsporozoite protein central repeat region [77, 78]. In general, during the last decades nanoparticle technology has been widely exploited for the design of vaccines against various pathogens like norwalk, influenzae, rotavirus, HIV viruses, chlamydia [79-82]. NP technology has confirmed its potential also for the fight against Sars-Co2 virus. Since Spike protein identification, several chimeric nanoparticles displaying target antigen have been designed and tested resulting able to elicit robust protective immune response in mice and monkeys [83-85].

4. Engineerization of protein nanoparticles external surface

An effective vaccine should be able to induce a potent and long-lasting antibody response. The generation of this response assumes that both B- and T-cells have to be activated [86]. Therefore, the preservation of antigen native conformation and its correctly display are essential features for vaccine design [87]. This aspect must be considered to choose the best method for their display on nanoparticles surface. Currently, three different approaches can be used for antigen display: chemical conjugation, protein ligation system and genetic fusion (Figure 2).

4.1. Chemical conjugation of protein and polysaccharide antigens

Chemical conjugation is mainly based on the modification of specific chemical group on the NP surface like carboxylic, amino, hydroxyl or thiol groups [88]. In particular, the amine group, due to their positive charge at physical pH, tend to be exposed on the protein surface, making them available for conjugation [89]. One of the main modifications is the lysine reacting with N-hydroxy-succinimide esters (NHS esters) with the formation of amide bond [90]. Alternative amino group modifications are done by utilizing click chemistry and hydrazone chemistry [91, 92]. All these modifications could be easily obtained with commercial kit that allow the rapid modification of activation of free amino groups. However, the major drawback of amine group modification is the possible protein structure disruption and loss of their conformational properties [93]. For a more site-directed conjugation, thiols can be modified. They are naturally not exposed on the protein surface and they are generally involved in the formation of disulphide bond [94]. However, thiols group can be artificially created with thiolation reagent that insert new thiol group into the protein or disrupting disulphide bond through reducing agents [89, 95]. Furthermore, also the carboxylic groups located at C-term of each protein and in the side chains of aspartic and glutamic acids can me modified [96]. They can form amide bond reacting with an amine, but the reaction needs the addiction of activation reagents [97]. The main concern in this case is the possible cross-reaction between the same protein or different molecules. In some cases, NP surfaces are modified attaching chemical linker that expose

reactive chemical groups as azides and maleimides able to react with the antigen [98]. At the same time the antigen needs to be modified to bind the scaffold. In the case of protein antigen their activation is achieved with the almost the same modifications described for the scaffold in this paragraph. While, in the case of sugar antigens, they can be activated with non-selective activation based on random hydrolysis reaction with agents that generate cyanide groups able to react with amines. However, also a chemoselective reaction is possible by the activation of carboxyl groups of sialic acid [98]. These are few examples of the main groups that can be modified through a variety of chemical reactions. The choice of the best approach strictly depends on the nature of the NP scaffold and the antigen. During the years chemical conjugation has been widely explored for the display of both protein/peptides and sugar antigens on NPs surface. Chemically conjugated NPs have been applied for a variety of purposes from the design of vaccines against asthma, hypertension nicotine [99-101] to the development of immunotherapy for neurodegenerative diseases [102, 103].

4.2. Protein ligation systems for protein antigen display

Another approach for a modular NP decoration is based on the use of protein ligation systems. As for chemical conjugation approach, also in this case, the final NP-based vaccine candidate is obtained in more than one step. Antigen and NP scaffold are separately produced and then they are *in vitro* mixed to direct the attachment of the antigen to the scaffold. The bond can be non-covalent exploit His-tag/NiNTA and biotin-avidin affinities [104-106]. However, the weak nature of the bond can lead to loss of antigen during the production processes. To overcome this issue and to increase the overall stability, antigen and NP can be also covalently linked. Halo-tag, SNAP-tag, Sortase, Split-inteins and SpyTag-SpyCatcher are just few examples of techniques that can be used for the formation of covalent bond [107-111]. Despite the major complexity of production process, this strategy allows to choose the best conditions that give the optimal yield, post-translational modification and conformation for both antigen and NP [112]. Modular assembly also meets the urgent needs to produce personalized vaccines [113]. In fact, the pre-production of modular scaffolds, which need just to be mixed with the *ad hoc* antigen, could reduce significantly the time needed for vaccines preparation [114]. Modular assembly also gives the possibility to increase the number of different antigens displayed on the same nanoparticle [115, 116]. This could make a huge contribution for the development of multi-target vaccines. The major drawback remains the difficulty in analytics and incomplete-inefficient reaction. More in general modular decoration has different limitations connected with not yet explored industrial scale production and efficiency of coupling reactions [110, 117].

4.3. Genetic fusion of protein antigens

Genetic fusion is the simplest method used for chimeric NP production allowing the site-specific antigen display. In fact, assuming that both antigen and scaffold are successfully produced with the same expression system, it is possible to obtain the desired molecule in a single step process [112]. In fact, both antigen and scaffold are encoded by the same plasmid and produced directly as chimeric molecule. This aspect facilitates the entire production and characterization process. In fact, the number of displayed antigens on a single NP is constant for all the molecules of the same sample. Moreover, correctly assembled NP can be easily purified from all the other proteins thanks to their high molecular weight and size. The only concern is about the display of large or bulky antigens and the rational structure-based design needed to produce a properly folded chimeric NP [118]. The gene sequence encoding for target antigen can be fused both at the N- and at the C-terminus of protein nanoparticle scaffold [119]. The engineerization of loops internal to the scaffold in the primary structure but well exposed in the tertiary structure can be exploited for the display of short epitopes too [120]. The choice of best insertion position is determined by the identification of more flexible region that could potentially accept foreign antigen thus maintaining the entire structure. Moreover, in the case of multimeric antigens, it is important that the fusion site has the same symmetry of the antigen to prevent scaffold destabilization [112]. In all cases an aminoacidic linker is needed to correctly space the antigen avoiding clashes between multiple copies [121]. Usually glycine-serine linkers are the best solution to obtain good flexibility and structure stability in aqueous solvent [122].

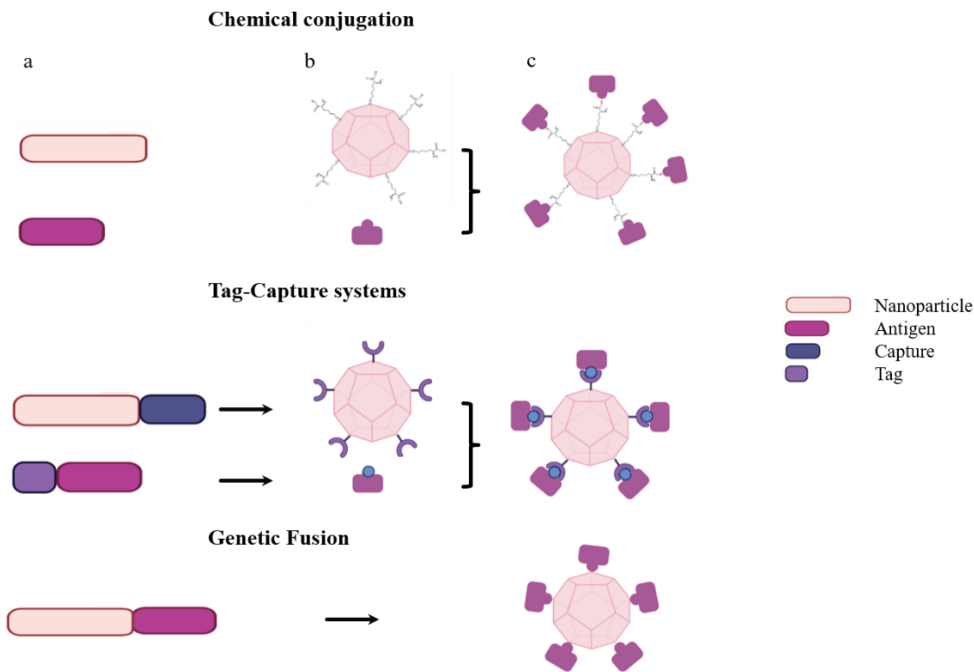


Figure 2: Schematic representation of the main approaches used for nanoparticle decoration. (a) First column reports genes coding for each component (b) in the second column intermediated products needed for *in vitro* assembly are indicated (c) third column reports final chimera.

5. Natural and synthetic nanoparticles used as platform for antigen display

Virus like particles (VLPs) have been the first self-assembling molecules exploited as platform for antigen display both in clinical trials and in licensed vaccines [123, 124]. Over time, other non-viral protein nanoparticles have been explored. Recently, the rapid progress in computational design enabled the development of synthetic self-assembling NPs. Starting from dimeric, trimeric, tetrameric and pentameric proteins is now possible, through both rational and computational approach, to predict mutations that allow them to self-assemble into nanoparticles [125]. Several different parameters must be considered for the *de novo* design of new scaffolds. The choice of building blocks determines the shape and the geometric symmetry of the final nanoparticle. Self-assembly must be guaranteed by engineerization of building block interfaces or fusing small domains able to promote spontaneous assembly. Finally, to be used as scaffold for antigen display through genetic fusion, it is needed that at least one terminus of the NP monomeric building block is exposed and accessible [126].

5.1.VLP-based platform

5.1.1. Hepatitis B virus core antigen HBcAg

The hepatitis B core antigen (HBcAg) represents the internal protein envelope of Hepatitis B virus, that encloses the viral DNA [127]. HBcAg is a single chain of 20kDa and, when recombinantly produced in *E. coli*, self-assembles into non-infectious VLP [128] (Table 2). The protein is largely

structured as α -helices and two monomers strongly interact to form compact dimers organized in four-helical bundle that protrudes from the surface of the cage. Dimers are the only intermediate needed for the VLP formation. The entire assembly process is guided by the interactions among proline-rich loops located into $\alpha 5$ of each dimer. The resulting VLP is a fenestrated icosahedral nanoparticle with two possible symmetries T=3 or T=4 corresponding to a different number of subunits: 180 and 240 subunits respectively [129]. The removal of C-terminal portion, needed for DNA binding, leads to the predominant formation of T=4 VLPs with an external diameter of 34nm [130, 131]. Over the years, HBcAg has been successfully used as platform for the display of both protein antigens and epitopes. Chimeric HBcAg can be easily obtained using both prokaryotic and eukaryotic expression systems and foreign antigens/epitopes can be successfully attached both at its N- and C-terminus [132]. In addition, also the immunodominant loop (loop1) can be engineered for the display of small epitopes with a resulting immune-response 10-fold stronger [133]. Both malaria and influenzae epitopes have been inserted into loop1 and tested in preclinical and clinical studies [134]. With this in mind, recently HBcAg loop1 has been also engineered with hepatitis E virus epitope obtaining multimeric VLPs that could represent a starting point for the production of a bivalent hepatitis vaccine [135]. However, since the loop engineerization does not allow the display of large or hydrophobic epitopes, “Split-core” technique has been developed [136]. Cutting HBcAg loop1, monomers can be divided in two different cores (CoreN and CoreC) able of reconstructing their monomeric structure and to self-assemble into VLPs. CoreN and CoreC can be expressed by two different plasmids or encoded by a single vector spacing the two sequences with a STOP codon and a new ribosome binding domain (RBD) [136]. In this way N- and C- term of each core can be engineered with both chemical/enzymatic modification and through genetic fusion of target antigen [137]. Several studies confirm that HBcAg is a promising carrier able to enhance antigen immunogenicity demonstrating its effectiveness in animal models and safety in different human clinical trials [138, 139].

5.1.2. Bacteriophage coat protein Q β

Q β VLPs are nanocages composed by 180 copies of a 14.4 KDa protein capsid able to form 3D structures that resemble the native single-stranded RNA (ssRNA) bacteriophage Q β . Each monomer has a β -strand organization at the N-term while C-term portion is structured as two contiguous α -helices. Monomers are linked into dimers by a shared hydrophobic core. Disulphide bonds, occurring between Cys74 and Cys80, connect five or six dimers, in a stoichiometric ratio of 12:20, at five-fold and three-fold axis respectively [140, 141]. Q β VLPs have size ranging from 25 to 30nm and an icosahedral symmetry (T=3) [142] with pores of around 14 Å and 7 Å in diameter [140] (Table 2).

Naturally Q β particles package ssRNA thanks to the interactions of RNA sugar-phosphate backbone with three residues (Asn58, Arg59, Lys63) located into EF loop and β strand F of the dimer [143]. This ability has been further exploited to *in vitro* and *in vivo* encapsulate siRNA or tRNA to develop new delivery tools for cancer therapy [144-147]. Its intrinsic structural stability makes Q β VLPs tolerant to a wide range of organic solvents, high temperatures and extreme pH conditions [148, 149]. Furthermore, Q β VLPs can be easily recombinantly produced using different expression systems like *E. coli*, yeast, and cell-free protein synthesis reactions [150-152]. For these reasons, Q β VLPs have been widely used as platform for the display of peptides and glycopeptides for vaccine development [153, 154]. They can be easily engineered using exposed residues like lysines, cysteines, and tyrosine or can be genetically fused with small peptides for up to 20 amino acids [155]. No data are reported about the Q β ability to display entire proteins or protein subdomains through genetic fusion. Indeed, different clinical studies have shown the Q β VLP efficiency to induce a potent immune response and their safety in human [156]. In fact, they have been successfully conjugated with antigens for allergen-specific immune therapy in human and with several epitopes/peptides to develop vaccine and drug to fight diseases like nicotine dependence, hypertension, cancer, and Alzheimer [100, 101, 103, 157, 158].

5.1.3. AP205 bacteriophage coat protein CP3

CP3 is an icosahedral VLP composed by 180 copies of *Acinetobacter* phage 205 (AP205) capsid protein [159] (Table 2). As the majority of *Leviviridae* proteins, the N-term of each CP3 monomer is structured as β -hairpin connected with the two C-term α -helices through a five-stranded β -sheet. Two monomers are taken together by hydrophobic and polar interactions and present an α/β double sandwich topology [160]. Accordingly, β -hairpin and α -helices compose the external surface of the capsid while 10-stranded β -sheets form the internal surface responsible also of the RNA-binding. Despite some structural similarities, CP3 has some feature that distinguish it from the others. With its 29 nm of diameter results to be the biggest *Leviviridae* capsid known. Furthermore, it presents a smooth and completely closed surface. Finally, also the encapsulated RNA seems to not strictly interact with the protein capsid [160]. In the 3D structure both N- and C-termini are located at threefold axis of the hexameric facets. In this way, both peptides and trimeric antigens fused at each vertex, can be thoroughly exposed on the surface without disrupting the VLP structure [161]. Taking advantage of this peculiarities, CP3 has been successfully decorated with peptides and small proteins (up to 55 amino acids) through genetic fusion at its C-term [162]. Unfortunately, CP3 does not always allow the gene fusion, in fact it can lose its solubility and ability to self-assemble when highly expressed in the *E. coli* cytoplasm [163]. To overcome this issue, SpyTag-SpyCapture system has

been successfully used for the correct display of spike protein from SARS-CoV-2 as well as *E. coli* toxins and trimeric proteins [164, 165]. No data are available about the CP3 engineerization through chemical conjugation. However, given its structure, intrinsic immunogenicity and manufacturability, CP3 is a promising platform for antigen display to develop new vaccines [166-168].

5.2. Non-viral based platform

5.2.1. Ferritin

Ferritins are protein microcompartments ubiquitously expressed responsible of iron oxidation into ferric oxide and iron storage [169]. Despite several different ferritins have been described in literature, the *Helicobacter pylori* ferritin is the most explored one for vaccine development due to its low sequence identity with human ferritin variant [2]. *Helicobacter pylori* Ferritin NP is a hollow globular molecule (474 KDa) composed by twenty-four copies of the same protein subunit [170]. The building block is organized as trimer in which each monomer has four- α -helix bundle organization [171]. Eight trimers further interact to form a 10-12nm NP with octahedral symmetry presenting both three- and four-fold axis [172] (Table 2). Ferritin NPs are stable at high temperature, up to 75°C for 10min, and stable in presence of denaturant agents [43]. NPs disassembly occurs at pH 2.5 but the entire structure is restored returning to pH 7.5 [173]. Moreover, recombinant ferritin can be produced both in mammalian cells and in *E. coli* expression systems [174, 175]. Its peculiar structure and physiochemical properties allow to use ferritin NPs for both drug delivery and antigen display [176]. The hollow inner part can be loaded with adjuvants, enzymes and metals [177]. On the other hand, the external surface can be exploited for the display of functional molecules through several different approaches. In particular, the N-terminus, located at the three-fold axis, represents an ideal attachment site for trimeric antigens, while the C-term is hidden and not available for the direct antigen fusion [178]. In fact, the ferritin N-terminus has been successfully engineered with hemagglutinin (HA) from *Haemophilus influenzae* obtaining a molecule able to lead an increase of the antibody protection against influenza greater than the protection given by commercial influenza vaccines [179]. In addition, for the display of small epitopes, also flexible regions of Hpf have been tested. Wang et al. report the successful engineerization of loop, connecting helices αA and αB , with *Neisseria gonorrhoeae* peptides without disrupting the NP structure [180]. Taken together all this data confirm that ferritin is a sturdy and well-established platform applicable for many purposes.

5.2.2. Encapsulin

Encapsulins were serendipitously discovered in 1994 by Valdes-Staube and Scherer as proteinaceous aggregates in the supernatant of *Brevibacterium linens* and at first they were identified as antimicrobial peptides [181]. Later, these compartments have been discovered also in *Mycobacterium*

tuberculosis and *Thermotoga maritima* and it has been discovered that their function is merely structural. In fact, encapsulins are involved in the segregation of enzymes and small molecules to protect bacteria during oxidative stress [35, 182]. First structural analysis conducted in the early 2000s, revealed that encapsulins may assemble into three different architectures: 60 subunits with 20–24 nm diameter, 180 subunits with 30–32 nm, and 240 subunits with 43 nm diameter [183, 184]. *T. maritima* encapsuline, used in this work, is composed by 60 copies of a single protomer that self-assembles into icosahedrally symmetrical shell (T=1) with a diameter of 24 nm and a thickness of 2–5 nm [35] (Table 2). Each monomer consists of a main body in α/β structures that contains the N-term and a hydrophobic core. This portion is connected by a loop to the C-term regions that consists of three helical segments and a five-stranded β -sheet [35]. C-terminal sequence is highly conserved among species, and it is used for peptides encapsulation for the packaging of cargo molecules. This portion has also been fused with heterologous proteins like luciferase and green fluorescent protein [185, 186]. In particular, thanks to its high stability in presence of high temperature or denaturing agents [187], *T. maritima* encapsuline, has been exploited as delivery system of both therapeutic drugs, IgG-Fc domain-binding peptide and fluorescent probes [188-190]. Moreover, in 2018 Lagoutte et al. validated the proof of concept of the use of *T. maritima* encapsuline for rational vaccine design. Matrix protein 2 ectodomain (M2e) of influenza A virus and Gp350 from Epstein–Barr virus were successfully displayed on the external surface through genetic fusion [191, 192].

5.3. Synthetic NPs



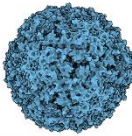
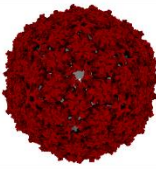
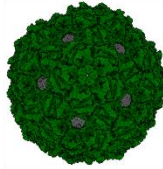
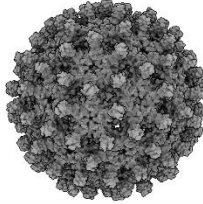
While many natural proteins have acquired self-assembling properties during evolution [13], the *de novo* design of new self-assembling nanoparticles remained challenging for several years. The idea of rational manipulation of substance at atomic and molecular level to generate new material was conceived for the first time in 1960 by Richard Feynman in 1960 [193]. Some years later the idea to use proteins as building blocks for the construction of self-assembling higher-ordered structures was proposed [194]. However, it is only with the development of computational tools that became possible the optimization and *de novo* design of new self-assembling molecules [195]. By choosing appropriate protein build blocks, nowadays is possible to design nanoparticles for *ad hoc* application with the most varied geometries. Trimeric proteins are the most common building blocks used. After the engineerization, the trimers can form nanostructures with tetrahedral, octahedral, and icosahedral symmetry. Tetrahedral nano-scaffolds are obtained introducing dimeric interfaces on each monomer of the trimer [126, 196]. The same strategy can be used also to direct the self-assembly of 8 trimers producing an octahedral NP [197]. While icosahedral NPs can be obtained by the self-assembly of either 20 trimers or 12 pentamers [198]. Using the first method Hsia et al., designed a hyper stable

dodecahedron known as I03-01 starting from *T. maritima* KDPG aldolase [199, 200]. They adopted a combined approach based on the alignment of trimeric structure on the three-fold axes of an icosahedron and the dimeric interface optimization with RosettaDesign [201, 202]. The result of this approach was the production of a new icosahedral scaffold with 25nm of diameter highly stable at 80°C as well as in 6.7 M Guanidinium Chloride (GuHCl). The only reversible dissociation has been observed in the presence of 2.25M Guanidinium thiocyanate (GITC). I03-01 maintains its stability even when C- or N-term are genetically fused with GFP [199]. Following this direction, Mercandalli et al, *de novo* designed the first two-component NP [203]. Through the interface engineering of 12 pentamers and 20 trimers they designed an icosahedral NP with 120 subunits and 44nm of diameter. The genetic fusion of respiratory syncytial virus glycoprotein at trimer subunits led the 10-fold increase in the neutralizing antibody production in mice and non-human primates [203].

5.3.1. mI3

The acronymous mI3 stands for “mutated I03” and it is referred to a new NP obtained from a next cycle of optimization performed on I03 scaffold described also in the previous paragraph. Compared to the original I03, mI3 has the Cys76 and Cys100 replaced with alanine avoiding the formation of undesired disulphide bond [168] (Table 2). Over the years, SpyTag-SpyCatcher technology has been widely used for the display of protein antigens on mI3 surface. It allowed the production of chimeric mI3 displaying spike receptor-binding domain (RBD) from SARS-CoV-2. In mice and pigs, RDB-mI3 was able to induce a stronger neutralizing antibody response than convalescent human sera [204, 205]. The *in vitro*, reaction needed for the antigen coupling on NP surface, allowed the production of a mosaic mI3 displaying from 4 to 8 different RDB variants. The heterotypic display resulted in the production of neutralizing antibodies with superior cross-reactive recognition of heterologous RDBs [206]. With the same strategy, multi-specific mI3 displaying hemagglutinin (HA) trimers from both group 1 and group 2 influenza A strains has been produced [207]. Moreover, chimeric mI3 can be easily obtained in *E. coli* and its intrinsic stability makes it stable at room temperature, resistant to freeze-thaw cycles and it can be also lyophilized without losing immunogenicity or activity [204]. All these features make mI3 attractive for vaccines production.

Table 2: General overview of the main features of six different self-assembling nanoparticles used in this work. In red are reported the names of non-viral NPs, in blue the name of computationally derived NP and in black the names of VLPs.

Name	Ferritin	mI3	Encapsulin	AP205 (CP3)	Q β	HBcAg
3D Structure						
Organism	<i>H. pylori</i>	*computationally designed	<i>T. maritima</i>	AP205 bacteriophage	Bacteriophage Q β	Human hepatitis B virus
MW (kDa)	15	25	32	15	16	16
PDB code	3BVE	5KP9	3DKT	5LQP	1QBE	1QGT
N° Subunit	24	60	60	180	180	240
MW NP (kDa)	360	1500	1920	2700	2880	3840
Diameter (nm)	10-12	25-30	24	30	30	34
Phase study	Preclinical	Preclinical	Preclinical	Preclinical	Clinical	Clinical

6. Protein and sugar antigens target of the study

Five different antigens (protein and sugars) have been investigated in the present work. They have been chosen from three human pathogens (*Neisseria meningitidis*, *Group B streptococcus* and *Neisseria gonorrhoeae*) which are main targets for vaccine development.

6.1. *Neisseria meningitidis* Factor-H binding protein

Neisseria meningitidis is responsible of meningitis and/or septicaemia in children and young adults worldwide [208]. Several virulence factors are involved in the pathogenicity like pili, lipopolysaccharide (LOS), and surface exposed membrane proteins [209]. Among them the lipoprotein Factor H binding protein (fHbp) play a crucial role in the survival of the bacterium in the human blood [210, 211]. Due to its widespread distribution in the most circulating meningococcal strains, it has become one of the protein targets for the vaccine development against *N. meningitidis* [212, 213]. In fact, the combination of factor H binding protein (fHbp), with other recombinant proteins and detoxified outer membrane vesicles (dOMV) led to the approval of Bexsero (GSK, 2015) and Trumenba (Pfizer, 2017) vaccines [214, 215]. FHbp is a 29 kDa protein structured in two β -barrel domains connected by a short loop [216] (Figure 3a). Starting from the N-term, six anti-parallel strands form the first β -sheet with a high intrinsic flexibility [217]. A five amino acid linker connects

the N-terminal domain with the C-terminal β -barrel composed by eight anti-parallel strands and filled by the hydrophobic side chains [218]. The dense network of hydrogen bonds contributes to β -barrel stabilization [219]. The different structural organization between the two domains is also reflected in two different unfolding profiles. The N-terminal domain melts in a range of 37 to 70°C along variants 2, 3 and 1. In contrast, in all variants the C-term β -barrel melts above 80°C [220]. Regarding their native orientation, it has been supposed that fHbp is completely exposed and it is anchored on the external membrane of the bacterium through the lipidated N-term cysteine [217]. Several epitope mapping studies allowed the identification of multiple bactericidal epitopes located along both the N- and the C-terminal domain [221].

6.2. *Streptococcus agalactiae*

Another pathogenic bacterium that creates concern and for which a vaccine is urgently needed is Group B streptococcus (GBS). The World Health Organization estimates that GBS is responsible of around 150.000 cases of neonatal death and foetal infections [222]. Naturally it is a member of intestinal and genitourinary flora of healthy women asymptotically [223]. However, it can cause severe diseases like meningitidis, sepsis and life-threatening pneumonia both in infant and adult patients [224]. Several different factors are involved in the pathogenicity of this bacterium. In particular, GBS colonization, persistence and invasion are mainly dependent on its ability to adhere to host cells and to evade the human immune system [225]. For these reasons the most studied antigens for vaccine development are capsular polysaccharide and surface exposed proteins.

6.2.1. Pilin proteins

Pili are filamentous protein structures that extend from the surface of the bacterium, and they are involved in the adhesion to the host cell [226]. Genome sequencing analysis of GBS isolates revealed the presence of three genomic islands which encode for three distinct pilus structures PI-1, PI-2a, and PI-2b [227]. Each pilus is composed by three major proteins: a backbone protein (BP) and two ancillary proteins AP1 and AP2. AP1 and BP have already been described as vaccine candidates able to induce protective antibodies in mice [228]. All three proteins are highly conserved in different GBS strains carrying the same genomic island. Only for BP-2a six immunologically distinct variants have been detected [228]. Further functional and structural studies on BP-2a led the identification of Domain 3 (D3) as the most immunogenic region [229]. D3 is one of the four domains that builds up the BP-2a and it is organized as β -sandwich composed by three- and four-stranded sheets connected with 6 loops (Figure 3b). As the other two domains (D2 and D4) it contains an internal isopeptide bond that stabilizes the entire structure [230]. Each domain folds independently giving the possibility to recombinantly produce each domain as a single recombinant protein in *E. coli*. Interestingly, the

overall organization is shared with the other five 2a variants and the most immunogenic epitopes seem to maintain the same localization [229]. Due to their surface exposure, abundance on bacterial surface and high immunogenicity, pilin proteins have been widely investigated as target antigen to develop an effective vaccine against GBS.

6.2.2. Capsular polysaccharides

The external surface of GBS is coated by a polysaccharide capsule (CPS) composed by multiple repeating units (RU) of four to seven monosaccharides forming one or two side chains [231]. The terminus of each chain is linked with sialic acid that mimic the surface of human cell glycocalyx [232]. CPS plays a crucial role in the pathogenesis at different levels. It interferes not only with complement-dependent cascade defence but also mediates biofilm formation in the presence of human plasma [233, 234]. So far, ten different CPS serotypes (Ia, Ib, and II–IX) have been identified from GBS isolates each one characterized by unique structural and antigenic features [235]. High variability has been also observed in terms of specific geographical distribution of different serotypes [223]. However, CPS has been the target of several studies for the development of CPS-based vaccine against GBS. First data about the capability of GBS CPS to induce the production of serotype-specific protective antibodies in mice comes from 1966 by Lancefield et al. [236]. In subsequent years, following the examples of meningococcal, pneumococcal and *H. influenzae* type b conjugate vaccines, several other preparations have been tested [237-239]. The most recent data are about the phase 1/2 clinical trials conducted on hexavalent CPS-based vaccine. It has been reported that, CPS variants Ia, Ib, II, III, IV, and V conjugated with CRM and formulated with aluminium phosphate were able to induce an immune response for at least 6 months [240]. However, one of the major drawbacks of CPS-based vaccine is the high capsular variability and the low of cross-protection induced by multivalent vaccines for which a deca-valent vaccine preparation should be the solution [241]. For the purpose of this study, polysaccharide type II (PSII) has been investigated (Figure 3c).

6.3. *Neisseria gonorrhoeae*

Neisseria gonorrhoeae is a Gram-negative bacterium that causes 87.7 million of cases of pelvic inflammatory diseases in women, blindness in new-borns and epididymitis in men worldwide [242-244]. This pathogen is also associated with human immunodeficiency virus (HIV) infections and other sexually transmitted infections (STIs) [245]. Due to the resistance to multiple antibiotics, vaccine remain the only efficacious solution to eradicate gonococcal diseases [246]. For this reason, a lot of efforts have been focused on the identification of potential vaccine target and optimization of delivery systems [247]. The most tested vaccine preparations are based on the use of a lipooligosaccharide epitope, formalin-inactivated whole-cell pathogen, outer-membrane vesicles, and

purified proteins [248-251]. For the development of protein-based vaccines a broad panel of antigens have been identified and characterized [252]. Most of them are proteins involved in colonization, nutrient acquisition, evasion of human immune systems and structural proteins [253, 254]. In this work two classes of membrane proteins involved in the colonization of host cells have been investigated.

6.3.1. Opacity-associated proteins

Colony opacity-associated proteins (Opa) are a family of integral outer membrane proteins. The genome of a single gonococcal strain encodes for about 8-10 antigenically distinct Opa variants [255]. Despite each gene is constitutively transcribed, the expression of each variant is phase-variable [256]. However, to date hundreds of Opa alleles have been annotated suggesting that intra-chromosomal and horizontal gene transfer continually occurs [255]. This phenomenon also suggests the pathogen needs to maintain Opa genes as they are involved in its pathogenicity. In fact, it has been shown that through the binding to the human carcinoembryonic antigen-related cellular adhesion molecule (CEACAM), Opa mediate the adhesion and invasion of host cells [257, 258]. Furthermore, it has been observed that the expression of Opa proteins leads to better resist to complement-mediated bacteriolysis [259]. Each protein has been predicted to be structured as a β -barrel composed by 8 highly conserved transmembrane sequences connected by four variable loops exposed in the extracellular environment (Figure 3d) [260]. A study conducted on Opa proteins expressed by *N. gonorrhoeae* FA1090 revealed that most immunogenic and functional epitopes are exactly located on the hypervariable (HV) and semi-variable (SV) loops [261]. The high variability that characterizes this class of proteins makes difficult to obtain a full knowledge of their mechanism of action. However, the identification of their functional epitopes could accelerate the development of an effective vaccine.

6.3.2. Porin B

The porin B (PorB), is the most abundant protein constitutively expressed on the outer membrane of *N. gonorrhoeae*. Naturally PorB is present as homotrimer in which each monomer has been predicted to be organized as β -barrel with 16 membrane-spanning sequences connected by 8 surface-exposed loops (Figure 3e) [262]. Although the β -sheets are conserved, the extracellular loops are highly variable among different strains generating different gonococcal serogroups and serovariant [263]. This aspect makes the production of PorB-based vaccine challenging. However, PorB remains a crucial protein for the pathogenicity of *N. gonorrhoeae*. In fact, it is involved in apoptosis, serum complement resistance and invasion of host cells [264-266]. In addition, trimeric PorB, could be able to inhibit dendritic cell stimulation of CD4⁺ T cell proliferation suppressing as result the adaptive

immune response [267]. Moreover, PorB has an intrinsic TLR2-dependent adjuvant effect that make it an attractive antigen for vaccine development [268].

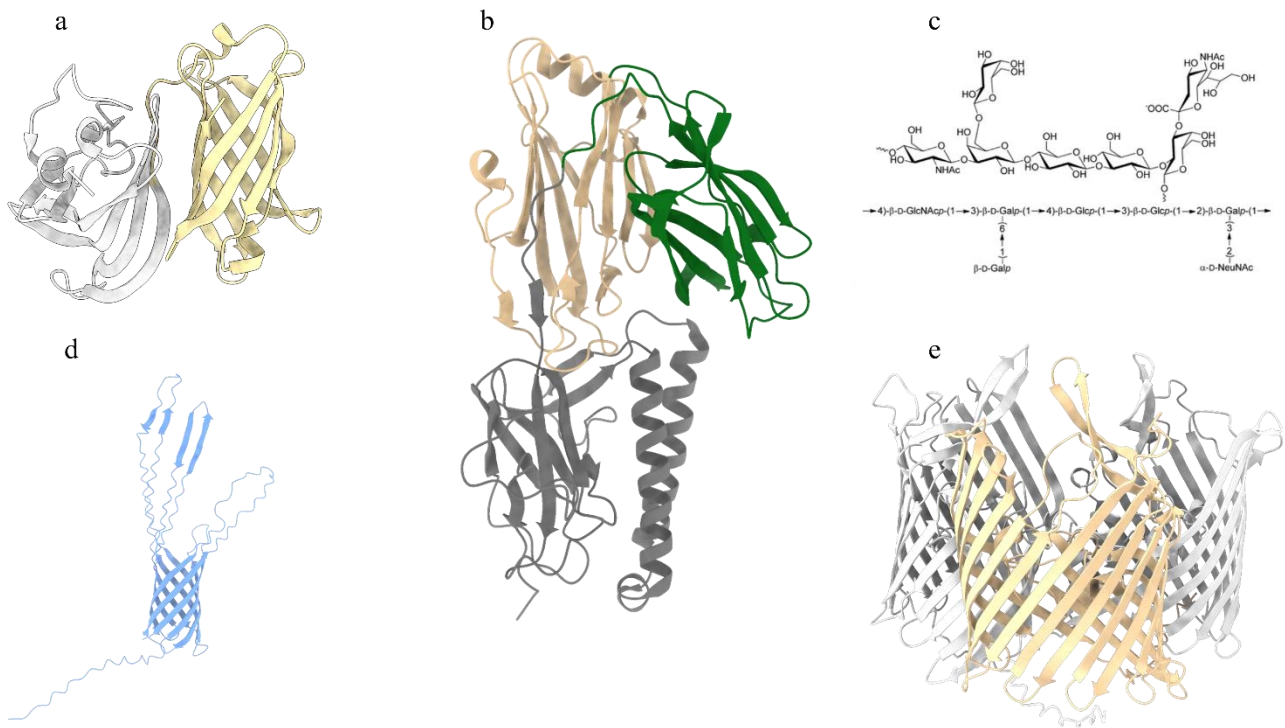


Figure 3: Cartoon representation of 3D structures of antigens tested in this work. (a) fHbp antigen (PDB code 3KVD), in yellow is shown the C-terminal β barrel domain while in grey the N-term domain. (b) GBS pilus protein type 2a (PDB code 2XTL). Domain 2 (D2) light brown, domain 3 (D3) green, domain 4 (D4) grey. (c) Repeating unit of GBS capsular polysaccharide type II. (d) predicted 3D model of OpaB protein. (e) predicted 3D model of PorB 1b protein.

Aim of the study

Self-assembling protein nanoparticles are a class of proteins able to spontaneously assemble into nanocages with precise shape and geometry. Since their discovery, they found widely application in drug delivery, bioimaging and vaccine production [269]. In particular, in vaccinology they can be used both as carrier of adjuvant and as platform for antigen display [72, 270]. In fact, the highly symmetric and ordered structure allows the multicopy display of target antigen enabling an efficient activation of both B- and T-cell immune response [1]. The nanoparticle surfaces can be decorated with either functional protein antigens/epitopes and with polysaccharide antigens. Different methods are now available for NP engineering like genetic fusion, chemical conjugation or protein ligation systems [2]. Currently, thanks to their unique properties, self-assembling protein NPs are a cutting-edge technology to produce effective vaccines. For this reason, the aim of the project was to explore the potentiality of self-assembling nanoparticle technology to display vaccine target. The purpose was to explore three main areas: (i) the identification of more suitable NP scaffolds for the display of protein antigen through genetic fusion; (ii) the setup of a new strategy for the identification of immunogenic epitopes from membrane antigens and their display on NP surface; (iii) the production of a polyvalent NP decorated simultaneously with protein and sugar antigens.

- I- By combining computational and structure-based approaches six self-assembling protein NPs and VLPs have been investigated for their ability to correctly display a protein antigen on their surface through genetic fusion. The antigen chosen for the study was the lipoprotein Factor H binding protein (fHbp) from serogroup B Meningococcus (MenB) [217]. As a highly protective antigen, fHbp is a key component of two different vaccines against MenB, namely MenB-fHbp (Trumenba) and 4C MenB (Bexero) [212, 213, 271]. fHbp is a 27 KDa protein structured in two β -barrels connected by a short linker [218]. Recently, a set of human monoclonal antibodies (mAbs) have been reported in literature to recognize fHbp [272, 273]. A crystal structure of fHbp complexed with the bactericidal human mAb 4B3 has been obtained revealing the presence of conformational and cross-protective epitopes [220]. Previous studies have shown that the most protective epitopes are harboured in the C-term β -barrel (e.g. targeted by the cross-protective humAb 4B3 [274] and the cross-reactive humAb 1A12 [275]). However, in the total set of human mAbs analysed, such cross-reactive mAbs were relatively rare (approximately only 10%). Therefore, to promote a beneficial immuno-focusing effect, only the C-terminal β -barrel domain of fHbp (residues 119-249 PDB code 3KVD), was selected to be tested in this study (Figure 5A).

II- The second goal of this project was to find a new strategy to investigate insoluble membrane antigens in order to find the most immunogenic/immunodominant portions. In fact, the main vaccine targets for the development of an effective protein-based vaccine are virulence factors involved in the bacterial adhesion, permeation, and evasion of immune system of host cells [276, 277]. These proteins are naturally exposed on the external membrane of the pathogen anchored into the lipidic bilayer through an extended hydrophobic portion while, the functional regions are exposed in the extracellular environment [278]. The presence of large hydrophobic domains makes membrane proteins insoluble and, when recombinantly produced in *E. coli* as whole antigens, they could form inclusion bodies complicating considerably the entire production process. Moreover, the hydrophobic regions, naturally not exposed to the immune system, result to be accessible deviating the immune response. For these reasons, the identification and production of functional epitopes could represent a valid alternative. Immunodominant epitopes in a protein antigen can be identified by (i) protein or peptide array, (ii) genetic manipulation and (iii) hydrogen deuterium exchange (HDX) experiments [221, 279, 280]. Alternatively, the protein antigen could be dissected producing sub-portions that can be produced and studied separately in a foreign protein scaffold. The dissection strategy has already been used for the study of antigenic loops extrapolated from meningococcal PorA, chlamydial MOMPA and gonococcal MtrE [180, 281, 282]. In the last case, the protein scaffold used is the ferritin nanoparticle. The peptide has been successfully fused at the N-term of the scaffold and also inserted into the primary sequence of ferritin, among two α -helices. However, the epitope displays on NP surface remain challenging. In fact, the engineerization of NP main structure inserting foreign and long peptides could disrupt the NP 3D structure. Furthermore, the peptides genetically fused at one end of the scaffold, could be exposed to exoproteases which could degrade them. To avoid all these troubles, this work has the aim to identify a new protein scaffold that can be engineered with foreign epitopes extrapolated from membrane antigens and that can be easily displayed on NP surface. For these reasons, the domain 3 (D3) of Group B Streptococcus (GBS) pilus 2a backbone protein (BP) has been chosen as scaffold. D3 is one of the four domains of the GBS pilus BP and the most immunogenic pilus domain able to induce functional antibodies [229] (Figure 12a). D3 is a small and highly stable protein (~15 KDa), thanks to the presence of an internal isopeptide bond, and can be easily produced as soluble His-tagged protein in *E. coli* (Figure 12c) [229, 283]. While as case-study antigens, Porin B.1b (porB1b) and opacity-associated protein B (OpaB) of *Neisseria gonorrhoeae* have been

investigated. They are two of the most highly abundant outer membrane proteins involved in the pathogenicity of *N. gonorrhoeae* and their 3D structure is not public available.

III- The last aim of this project was to produce a polyvalent NP decorated with two different types of antigens to produce multivalent vaccines. In fact, the combination of multiple components to produce an effective vaccine able to target simultaneously different variants of the same target or multiple pathogens is a well-established practice [284]. The first polyvalent vaccine produced was the vaccine against poliovirus [285]. After this, several other polyvalent vaccines like for example 4CMenB, Bexero, DPT have been licensed [214, 286, 287]. To produce a polyvalent vaccine each component must be produced separately and then combined in a single preparation during the manufacture or mixed before the administration. Furthermore, it is essential to ascertain that the combination of several different elements does not alter the physio-chemical properties of each individual antigen [287]. Therefore, the entire production process requires a lot of quality controls with the resulting increase of costs and time [288]. However, thanks to the rapid development of genetic engineer and recombinant DNA manipulation techniques, it is now possible to combine multiple protective antigens on a single molecule [289]. Actually, a promising strategy for the multicopy antigen display is based on the use of self-assembling NPs and different polyvalent NP based molecules have already been produced. In particular, they have been produced as single NP displaying different variants of the target protein antigen to achieve a broad protection against the same pathogen [75, 206]. Furthermore, despite several data about conjugated NPs, only the polyvalent display of protein antigen is reported in literature [207]. For these reasons, the aim of this project was to take a step forward by producing a chimeric NP decorated simultaneously with both protein and sugar antigens. In particular, the GBS pilus proteins and its capsular polysaccharide type II (PSII) have been taken in consideration as target antigens. In fact, they play a crucial role in the pathogenicity of the bacterium and several studies have been focused on their investigation as antigens for the development of an effective GBS vaccine [290].

Materials and Methods

7. Protein design and 3D structure prediction of target chimeras

7.1. Structure-based design

The design of target chimeras has been performed investigating the structure of both antigen and NP scaffold. Each structure has been analysed to identify structured regions and flexible portions of the protein. The investigation of NP structure was applied also to define residues involved in the interface interaction between each subunit needed for the NP assembly. The combination of these information was used to identify most suitable engineering sites. Particular attention was given to N-, C-terminus and exposed loops of both antigens and NPs.

The structures used for this analysis are deposited in the RCSB Protein Data Bank (PDB).

7.2. Rosetta homology modelling

The design and the 3D structure prediction of each chimeric NP displaying the target antigen were obtained with Rosetta comparative modelling tool [291]. Throughout this study, the high-resolution crystal structures available for both NPs scaffolds and antigens, were used. To obtain the 3D structure prediction of antigen-decorated NPs, a model composed of the nanoparticle monomer and the antigen was obtained in Chimera and aligned to the asymmetric unit of the self-assembling particle [292]. Then, a linker connecting the two portions was conformationally sampled using a fragment-based loop-modelling protocol, with refinement in Rosetta to minimize energetics and resolve clashes [293]. Finally, symmetric constraints were applied to generate the other subunits to obtain a 3D structure prediction of the entire nanoparticle. Pymol [294], Chimera and ChimeraX [295] software packages were used for structural investigation, molecules visualization and graphical representation.

8. Production of recombinant proteins

8.1. Strains

E. coli BL21(DE3) T1R (fhuA2 [lon] ompT gal (λ DE3) [dcm] Δ hsdS. λ DE3= λ sBamHIo Δ ecoRI-B int:(lacI::PlacUV5::T7 gene1) i21 λ nin5) cells provided by New England Biolabs (NEB) have been used for the expression of recombinant proteins.

E. coli Stellar (F-, endA1, supE44, thi-1, recA1, relA1, gyrA96, phoA, Φ 80d lacZ Δ M15, Δ (lacZYA-argF) U169, Δ (mrr-hsdRMS-mcrBC), Δ mcrA, λ -) strain provided by Takara has been used in the cloning procedure.

8.2. Expression vectors

Plasmids pET15TEV (derived from pET15b+ Merck) (Figure 4a), pET21b+ (Figure 4b) (Merck) and pET24b+ (Fig 4c) (Merck) were used to clone the genes coding for the recombinant proteins. All plasmids were previously modified internally to use them for Polymerase Incomplete Primer Extension (PIPE) cloning method [296]. According to this method, modified plasmids called pET15-TEV-ccdB, pET21-ccdB, and pET24-ccdB were PCR amplified and the gene coding for the protein of interest was cloned in the desired vector [274, 275]. All plasmids have IPTG-inducible T7 promoter and Ampicillin (pET15 and pET21) or kanamycin (pET24) resistance gene.

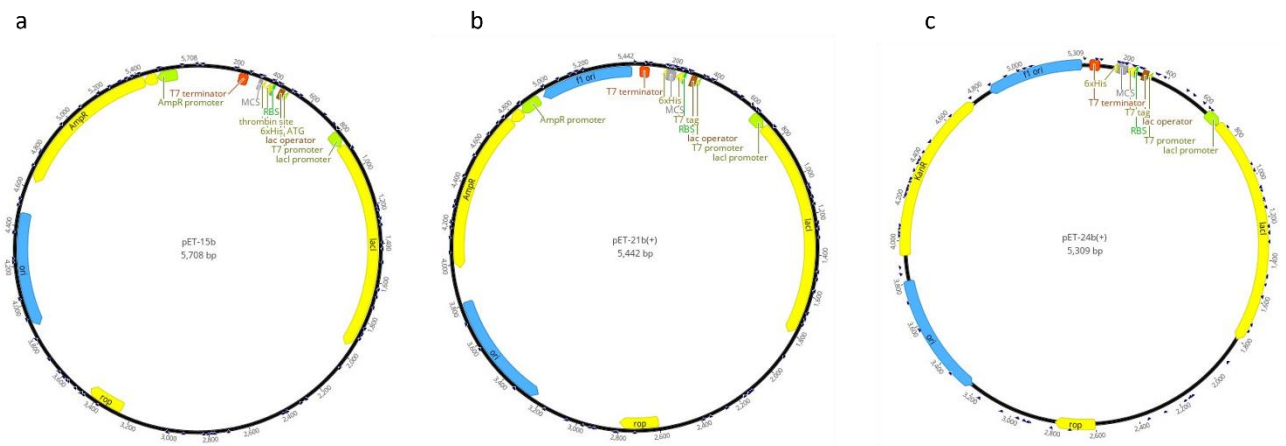


Figure 4: Plasmid map of commercially available vectors (a) pET15b+, (b) pET21b+ and (c) pET24b+. Map reconstruction performed with Geneious program.

8.3. Genes

Gene encoding for chimeric protein were provided by GeneArt (Thermo Fisher Scientific) as lyophilized synthetic DNA strings or by Twist (Twist Bioscience) as lyophilized recombinant plasmids. Synthetic strings were produced optimizing the codon usage for the expression in the *E. coli* host cells and by adding at the gene extremities the appropriate appendix (Table 3) for single step cloning into the expression vector. Both synthetic strings and recombinant plasmids, were resuspended in sterile DNase-free water with a final DNA concentration of 50ng/ μ L before their use.

Table 3: Flanking appendix of synthesized stings for the cloning in pET15-TEV-ccdb and pET21-ccdb vectors.

DNA appendix	Host plasmid	
	pET15-TEV-ccdB	pET21-ccdb
5'	CTGTACTTCCAGGGC	TAAGAAGGAGATATACATATG
3'	TAA CGCGACTTAATT	CATCACCATCACCATCACTGA

8.4. Cloning

9.4.1 Vector amplification

pET15TEV-ccdb and pET21-ccdb vectors were amplified with PCR (Table 4 and 5) and purified from agarose gel with Wizard® SV Gel and PCR Clean-Up System kit (Promega) following reported instructions.

Table 4: Nucleotide sequences of primer used for vector amplification of both pET15TEV-ccdb and pET21-ccdb

pET15-TEV-ccdB	<u>Forward</u>	5'TAACGCGACTTAATTCTAGCATAACCCCTTGG GGCCTCAAACGG 3'
	<u>Reverse</u>	5'GCCCTGGAAGTACAGGTTTTTCGTGATGATGAT GATGATGGCTGCTGCCCATGGTATATC 3'
pET21-ccdb	<u>Forward</u>	5'GTGGTGGTGGTGGTGCACCACCACCACC ACTGA 3'
	<u>Reverse</u>	5'GAAGGAGATATACATATGCATATGTATATCTC CTTCTTAAAGTTAAACAAAATTATTTCTAG 3'

Table 5: Vector amplification (a) mix prepared for each sample. Primer F (Forward) primer R (reverse) (b) running protocol. * Elongation time depends on the length of each vector.

a		b		
Component	Quantity [μ L]	Temperature [$^{\circ}$ C]	Time [s]	Cycles
Pfu Ultra II HotStart	12,5	95	120	
2X master mix		95	20	
Template [1ng/ μ L]	1	50-70	20	} 30
Primer F [10uM]	0,5	75	*	
Primer R [10uM]	0,5	72	180	
H ₂ O DNase free	10,5	10		
Total	25			

8.4.1.1. DpnI digestion

The hydrolysis reaction was set up to remove DNA template of pET15TEV-ccdb and pET21-ccdb vectors after PCR amplification. 1 μ L of DpnI (10 U/L) enzyme was added to PCR mix and incubated at 37 $^{\circ}$ C for 2h and 80 $^{\circ}$ C for 20 min.

8.4.1.2. Agarose gel electrophoresis

Agarose powder was dissolved in TAE 1X buffer (TRIS 242 g/L, acetic acid 51.7 mL/L, EDTA 18.6 g/L in 1L distilled water) at 1% final concentration. 1X SYBR safe DNA gel stain (Thermo Fisher Scientific) was added before solidification for DNA visualization. The mixture was allowed to solidify in the right apparatus with the comb. DNA samples and molecular weight marker were loaded on the gel. The run was performed in TAE 1X buffer with a constant voltage of 100V, 400mA for about 45min.

8.4.2. PIPE cloning

The cloning of target gene in the desired vector was performed with the Infusion cloning kit (Takara Bio) following manufacturer instructions. Recombinant plasmids were propagated in *E. coli* Stellar cells grown on selective Luria-Bertani (LB) agar plates (Tryptone 10g/L, yeast extract 5g/L, NaCl 10g/L 1.5% agar) containing ampicillin [100 μ g/mL] [297]. Grown colonies were screened through PCR (Table 6). The recombinant plasmid from positive colonies were extracted with E.Z.N.A Plasmid DNA Mini Kit (Omega Biotech) following manufacturer instructions and the correct sequence was further confirmed by next generation sequencing (NGS) analysis.

Table 6: Colony screening reaction mix (a) and protocol used (b). * The elongation time depends on the insert length. Primer F is the forward (5' TAATACGACTCACTATAGGGG 3') and primer R is the reverse (5' GATATCCGGATATAGTTCCTC 3').

a		b		
Component	Quantity [μL]	Temperature [°C]	Time [s]	Cycles
Go Taq Green	12,5	95	120	
Master mix 2X		95	30	
Template	Single colony	55	30	} 25
Primer F [10uM]	0,25	72	*	
Primer R [10uM]	0,25	72	300	
H ₂ O DNase free	12	4		
Total	25			

8.5. Plasmid transformation

Both recombinant pET29b+ provided by Twist and recombinant pET15TEV and pET21 plasmids cloned in house were transformed into *E. coli* BL21 (DE3) chemically competent cells following heat-shock procedure [298].

8.6. Recombinant protein expression in *E. coli* BL21 (DE3)

8.6.1. Pre-culture and glycerol stock preservation

The recombinant colonies grown on selective plates were picked and incubated with 5-10mL of LB (Tryptone 10g/L, yeast extract 5g/L, NaCl 10g/L) medium at 37 °C and 180 rpm overnight (about 16 h). Pre-culture was used to set up batch cultivation and 500 μL were mixed with 200 μL of 80% sterile glycerol and preserved in cryo vials at -80 °C.

8.6.2. Batch culture at 20 °C

The cultivation was set up in a 250 mL shaker flask with 75 mL of sterile HTMC medium (glycerol 15 g/L, yeast extract 30 g/L, MgSO₄ x7H₂O 0.5 g/L, KH₂PO₄ 5 g/L, K₂HPO₄ 20 g/L, KOH 1M at pH final 7.35±0.1), ampicillin [100 μg/mL] or kanamycin [50 μg/mL] and preculture diluted 1:100. The flask was incubated for 16h at 20 °C and 160 rpm. 500 μL of not-induced sample were collected in 1,5 mL eppendorf tube and stored at 4°C. The production of interest protein was induced with 1mM sterile IPTG and protein expression was followed for 24 h at 20 °C and 160 rpm. 500 μL of induced sample were collected in 1,5 mL eppendorf tube and stored at 4°C.

8.6.3. Batch culture at 37 °C

The culture was set up in 1 L shaker flask with 500 mL of sterile LB medium, ampicillin [100 µg/mL] or kanamycin [50 µg/mL] and preculture diluted 1:100. The flask was incubated at 37°C and 160 rpm until to reach OD_{600 nm} value of 0.8-1.2. 500 µL of not-induced sample were collected in 1,5 mL eppendorf tube and stored at 4°C. The production of interest protein was induced with 1mM sterile IPTG and the protein expression was followed for 3 h at 37 °C and 160 rpm. 500 µL of induced sample were collected in 1,5 mL eppendorf tube and stored at 4°C.

8.6.4. Small scale analysis of protein expression and solubility

500 µL of induced and not-induced samples collected from the growths were centrifuged at 14000 rpm for 10 min at 4°C. The medium was discarded, and pellets, after 1h at -20°C, were resuspended in 300 µL of CellLytic Express lysis buffer (Sigma-Aldrich) and incubated for 1h at room temperature (RT) under shaking conditions. Samples were diluted 1:2 with 1X Phosphate Buffered Saline (PBS) at pH 7.6 and 60 µL representing the total extract were collected in a new eppendorf tube. The remaining volumes were centrifuged at 14000 rpm for 10 min at 4 °C and 60 µL of the supernatant (soluble fraction) were collected in a separate eppendorf tube. Both total and soluble fractions were mixed with NuPAGE LDS Sample Buffer 4X (Thermo Fisher Scientific) and NuPAGE™ Sample Reducing Agent 10X. Samples were boiled at 98 °C for 10 min and analysed on SDS-PAGE.

8.6.5. SDS-PAGE

9µL of sample were mixed with 3µL of 4X reducing mix (LSD and DDT) and boiled at 98°C for 10 min. 12µL of samples and prestained protein molecular marker (Thermo Fisher Scientific) were loaded on precast polyacrylamide gels (Thermo Fisher Scientific). The run was performed in 1X 2-(N-morpholino) ethanesulfonic acid (MES), at 150 V 1000 mA and 180 W for 35min. Gels were stained with Coomassie ProBlue Safe stain (Giotto) for protein visualization and images were acquired with GelDoc (Bio-Rad).

8.6.6. Harvest and cell lysis

The whole cultivation was transferred in 50mL falcon and centrifuged for 8000 rpm at 4 °C for 10min. Medium was discarded and pellet, after 1h at -20°C, was lysed with CellLytic Express lysis buffer. Each g of pellet was resuspended with 10 mL of lysis buffer and incubated at RT for 1h under gently shaking. Alternatively soluble proteins are extracted from *E. coli* cytoplasm through mechanic lysis. Pellets were resuspended in lysis buffer (20 mM Tris, 150mM NaCl pH 8) and sonicated on ice with

40% amplitude 30s pulse and 30s stop for 10min. After lysis in both cases samples were diluted 1:2 with PBS or lysis buffer and centrifuged at 8000 rpm at 4°C for 10 min to collect soluble fraction.

8.7.Purification of recombinant proteins

8.7.1. Immobilized metal affinity chromatography (IMAC)

Empty PD10 column were prepared with the appropriate filter and filled with 2 mL of homogenous suspension of Ni-NTA Agarose resin (Thermo Fisher Scientific). When the matrix was settled, the resin was decanted and the leftover liquid was discarded, leaving 1 cm above the column head to prevent drying out. Alternatively, His-Trap fast flow crude (Cytiva) column was used connected to a peristaltic pump. The columns were washed with five column volumes (CV) of distilled water and then equilibrated with ten CV of equilibration buffer (PBS or 20 mM Tris, 150mM NaCl pH 8). Crude cell lysate was applied on the column, incubated for 10 min, and the flow through was collected. The column was washed with five CV of equilibration buffer supplied with 20 mM imidazole. Target protein was eluted with about 5-10 mL of elution buffer containing 350 mM imidazole. The column was washed with two CV of equilibration buffer, ten CV of distilled water and it was preserved in one CV of 20% ethanol. All fractions collected during IMAC purification were analysed with SDS-PAGE. The elution fractions containing interest proteins were transferred into ultrafiltration device (10-100-300 kDa) and centrifuged at 4500 rpm until to reach desired final volume.

8.7.2. Size exclusion chromatography (SEC)

Recombinant chimeric nanoparticles were purified with size exclusion chromatography in order to separate correctly assembled molecules from their monomers. 0.5, 1 or 5 mL of samples were loaded on preparative Superdex 200 10/300-26/600 or in Superose 6 columns equilibrated with 1X PBS. All the collected fractions were checked for the content of target protein by SDS-PAGE analysis. Fractions of interest were pooled, filtered at 22 µm, concentrated and stored at -20°C.

8.7.3. Size Exclusion-High Pressure Liquid Chromatography (SE-HPLC)

Oxidated PSII and chemically conjugated nanoparticles were purified with SE-HPLC. About 5 µg of each sample were loaded into SRT-C 2000 column using NaPi 100mM pH 7,2 + Na2SO4 100mM as running buffer. The absorbance at 214 nm, 280 nm e 254 nm was constantly measured. Elution fractions containing molecule of interest were collected, pooled, and stored at 4°C.

8.8. Protein content evaluation

Protein concentration was determined with Nanodrop measuring the absorbance at 280nm and normalizing with the calculated protein extinction coefficient. The first measurement was the blank

solution represented by the buffer alone. Then the concentration of each sample was measured, and the value obtained was expressed as mg/mL.

9. Polysaccharides chemical conjugation

Polysaccharide of GBS CPS serotype II (molecular weight ~100 kDa), internally purified, was oxidated using 5% of NaIO₄ and purified with a desalting column. Protein residues were activated with NaBH₃CN in NaPi buffer at pH 7.2 for 3 days at 37°C under circular rotation. PSII 20% oxidated in NaBH₄ 0,4M, NaPi 100mM pH 7,2 was added in different ratios (0.25:1, 0.5:1, 1:1, 2:2, 4:1). The conjugation reaction was incubated for 2h at room temperature. Conjugated proteins were then purified with Amicon 100kDa washing 30 times with PBS 1X, filtered in sterile conditions and protein concentration measured with BCA assay. Conjugates quality was finally assessed by SE-HPLC.

10. Structural and functional characterization

10.1. Transmission electron microscopy

The electron microscopy analysis was performed loading 5 µl of sample concentrated 20 ng/µL onto a glow discharged copper 300-square mesh grid for 30 s. Blotted the excess, the grid was negatively stained using NanoW for 30 seconds. The samples were analysed using a Tecnai G2 spirit and the images were acquired using a Tvips TemCam-F216 (EM-Menu software).

10.2. Western/Dot Blot

Purified recombinant proteins were directly spotted (Dot blot) or transferred to a nitrocellulose membrane after an SDS_PAGE run (western blot) using i-transfer and i-Blot Mini/regular kit (Thermo Fisher Scientific). The membrane was blocked with 3% milk in 1X PBS+ 0.1% TWEEN detergent for 1h at RT under gently agitation. Primary and secondary antibodies (Abs), diluted in 3% milk, were incubated with the membrane for at least 1h at RT. After the incubation with both antibodies, the membrane was washed three times with PBS+0.1% TWEEN for 5 min under shaking to remove unbound Ab. The chromogenic substrate 4-chloro-1-naphthol was added to acquire the signal using GelDoc XR+ imaging system.

10.3. His-tag removal

His-tag was removed through TEV digestion. Samples are mixed with TEV enzyme 1mg/ml diluted in a 1:50 ration, 1mM DTT and 0.5mM EDTA in 1mL of 2mM Tris-HCl at pH 8. The samples were incubated for about 48h at RT under shaking 200rpm. The enzyme removal and buffer exchange were performed by SEC.

10.4. Differential scanning fluorimetry (DSF)

A capillary filled with the sample was manually located in the apparatus of NanoDSF Tycho NT6 (Nanotemper). A linear temperature ramp from 35°C to 95°C with thermal ramp of 30 °C/min was applied to unfold proteins. During the scanning the increase of intrinsic tryptophan or tyrosine fluorescence was recorded and the melting temperature (T_m), corresponding to the midpoint of the transition from folded to unfolded, was evaluated. In particular, T_m is represented by the flex point of sigmoid curve obtained plotting fluorescence intensities in function of temperature. Data analysis and graphical manipulation were performed with GraphPad Prism.

10.5. Differential scanning calorimetry (DSC)

Using a MicroCal VP-Capillary DSC instrument (GE Healthcare), protein samples [10 μ M] were subjected to a temperature scan range from 10–110 °C with a rate of 180 °C/h, and a 4-s filter period. During the analysis the heat capacity of denaturation (C_p) was constantly measured as Kcal/mole/°C. The results, analysed with Origin 7 software, were reported as C_p in function of increasing temperature with a resulting Gaussian curve. The temperature corresponding to the maximum of the curve represents the T_m of the protein.

10.6. Dynamic light scattering (DLS)

The hydrodynamic diameter of NP in solution was measured with dynamic light scattering. The measurement was performed using Malvern Zetasizer Nano ZS equipped with a 633 nm He–Ne laser and using an angle of 173°. Scattering light detected was automatically adjusted by laser attenuation filters. For data analysis, the refractive index (RI) and viscosity of PBS were used at 25 °C. To analyse the data the Zetasizer software version 7.11 was used. Temperature was set at 25 °C. 80 μ L of the sample were transferred into a single-use polystyrene microcuvette (ZEN0040, Alfatest) with a path length of 10 mm. The hydrodynamic diameter of NPs was expressed by a Z-average providing also the polydisperse index.

10.7. SEC-Multi Angle Light Scattering (SEC-MALS)

The molecular weight of purified chimeric NPs was calculated with size exclusion chromatography Multi-Angle-Light-Scattering (SEC-MALS). HPLC-SEC with Tosoh TSK gel G6000PW (30 cm \times 7.5 mm) + G4000PW (30 cm \times 7.5 mm) columns was equilibrated in PBS and used in series with in-line UV, fluorescence emission, and MALS detectors. 100 μ l of the sample were injected and eluted with a flow rate of 0.5 mL/min for 40 min. ASTRA 6 software (Wyatt Technology) was used to

analysed collected data and the NPs size was measured as the number average geometric radius R_n , Z-average geometric radius R_z values and weight average geometric radius R_w .

10.8. Surface plasmon resonance (SPR)

The capability of human mAb 4B3 to recognize the fHbp1.1 β -barrel nanoparticles was assessed by SPR analysis using the Single Cycle Kinetics method. mAb was diluted to a concentration of 5 $\mu\text{g}/\text{mL}$ with running buffer HBS-EP+ (0.01 M HEPES, 0.15 M NaCl, 0.003 M EDTA and 0.05% v/v Surfactant P20) and captured on the surface of a CM5 sensor chip coated with a secondary anti-human IgG Fc. Increasing concentrations (1.25 nM, 2.5 nM, 5 nM, 10 nM, 20 nM) of each analyte were injected for 60 s on the surface of the sensor chip. After the last injection, dissociation of the protein was followed for 1500 s. After each cycle, the sensor chip was regenerated using 3 M MgCl_2 . The sensorgram, a plot of response (measured in Resonance Units [RU]) against time (measured in seconds [s]), was used to monitor the interaction. The response is directly proportional to the concentration of biomolecules on the surface. The sensorgrams resulted from the blank subtraction, based on the captured mAb but with injections of buffer instead of samples. Capture adjustment was applied to correct sample responses for variations in the levels of captured mAb between cycles by dividing the sample response with the response for captured ligand. Adjusted response levels were expressed as sample response divided by capture level.

10.9. Protein crystallization and structure determination

Purified recombinant protein D3porBLoop5 has been concentrated until to reach a concentration of 18mg/mL in 20mM Tris-HCl, 150mM NaCl at pH 8.0. Using a Crystal Gryphon robot (Art Robbins Instruments), 384 different crystallization conditions have been tested by using 200nl reservoir and 200nl protein sample. The best crystal was grown in buffer containing 0.1M HEPES with 20% w/v jeff ED-2001 as precipitant at pH 6.5. Crystals were soaked in the original mother liquor supplemented with 15% ethylene glycol prior to cryo-cooling in liquid nitrogen. Diffraction of the crystals was performed at beamline ID30A-1 of the European Synchrotron Radiation Facility (ESRF). 900 images were collected at 100K, at wavelength $\lambda = 0.96546 \text{ \AA}$. Data were processed using autoProc and they were reduced using Scala within the CCP4 program suite [299]. Crystals of the D3-Loop 5 chimera belong to space group F222, with the asymmetric unit containing two copies and a solvent content of 56.8 % (Matthew coefficient of 2.85 $\text{\AA}^3/\text{Da}$). The structure of the D3porBLoop5 was determined at 2.6 \AA resolution by molecular replacement with Phaser [300] using two separate search models obtained from homology modelling simulation and from 2XTL data collected in PDB database. Rigid body and restrained refinement were carried out with Refmac5 (from CCP4i suite). Structure quality was assessed using Molprobit, while protein-protein interface areas were analysed

and calculated using the Protein Interfaces, Surfaces and Assemblies service (PISA) [301] by PDBePISA. Figures were generated using PyMOL.

10.10. *In vivo* studies

Animal treatments were performed in compliance with the Italian laws and approved by the institutional review board (Animal Ethical Committee) of GSK Vaccines Siena, Italy.

Different amount (0.5 µg, 0.8 µg, 2 µg, 3.2 µg) of each purified protein, with low endotoxin level, mixed with Alum adjuvant has been used to immunize intramuscularly 10 mice CD1 Female 7 weeks old. Three different immunizations were performed at days 0, 21 and 37 or 42 collecting sera sample at each point.

10.11. Luminex assay

Luminex Magplex beads were equilibrated at RT. 100µL (1.25×10^6) of resuspended beads were transferred to a LoBind Eppendorf tube and placed into a magnetic separator for 2 min. The supernatant was removed, and the beads were washed with water and activated for 20 min with NHS and EDC (10 µL of each 50 mg/mL solution diluted in dH₂O) in 100 mM EDC in 100 mM of Monobasic sodium phosphate pH6.2 buffer and washed twice with 50mM MES. The activated beads were incubated 2 h with 20 µg/mL of molecule of interest. Coupled beads were finally washed twice with 1X PBS + 0.05 % Tween and stored in 500µL of assay buffer (1X PBS, 0.5 % TWEEN and 0.05% BSA) at 4°. After each step described above, beads were re-suspended by vortex for approximately 20 seconds and placed into a magnetic separator for 2 minutes.

Standard sera and sera from mice immunized with Outer membrane Vesicle (OMV) or recombinant proteins were pre-diluted in assay buffer 3-fold dilution were performed in 50 µL final volume for each well of Grainer microtiter plate. 50 µL of coupled beads were added to sera and the plate was incubated for 1h at RT in the dark on a plate shaker at 700 rpm. Unbound Ab were removed by washing plates three times with 200 µL of PBS using an automatic plate washer with magnetic plate holder. Each well was then loaded with 50 µL of secondary antibody conjugated with R-phycoerythrin-AffiniPure and incubated for 1 h at RT in the dark on a plate shaker at 700 rpm. After washing, beads were suspended in 100 µL of PBs and analysed with Bioplex 200. Data were acquired in real time by Bioplex Manager Software 6.1 (BioRad) and analysed and graphically represented with GraphPad.

Results

11. Self-assembling protein nanoparticles and virus like particles correctly display β -barrel from meningococcal factor H-binding protein through genetic fusion

11.1. Rosetta comparative modelling for the structural assessment of chimeric NPs

An *in-silico* analysis of the structures and the symmetry of each NP was performed to correctly design NP-antigen chimeras. Structural analysis of the selected NPs (Table 2) allowed the identification of potentially engineerable sites. In particular, it has been observed that the C-terminal portion of each NP was directed inside the scaffold or involved in the interface interactions needed for the particle assembly. In contrast, the N-terminal portion resulted to be exposed to the outside of the NP and it was therefore considered more suitable for antigen display, potentially achievable by genetic engineering (Figure 5B). In the case of HBcAg and encapsulin, a relatively long surface-exposed loop was also identified and selected to be tested as an additional antigen insertion site (Figure 5B) [136]. For HBcAg the connecting loop of $\alpha 3$ and $\alpha 4$ helices of each monomer, protruding from the surface of VLP in the 3D structure, has been identified as possible suitable site. This loop is also part of an immunodominant B-cell epitope already engineered in previously reported works [136, 302]. While the crystal structure analysis of naked encapsulin [35] revealed that the loop from residues 58-64 is flexible and is well exposed on NP surface. Based on the results of the structural analyses, the gene encoding for the antigen fragment was fused at the N terminus of each NP gene, spaced by a glycine-serine linker [121, 303] and in the gene sequence of exposed loop of HBcAg [136] and encapsulin. For each chimera a 6-His tag was inserted at the N-term of the antigen to allow protein purification and antigen detection. The only exception was the chimera based on mI3, in which the 6-His tag was placed at the C terminus of the scaffold spaced by a glycine-serine linker. In order to analyse the spatial disposition of the antigen on the NP surface, a structural prediction of the symmetric assembly was performed with Rosetta comparative modelling [304]. The chimeric sequences were threaded onto template structures consisting of both antigen and NPs, and an energetic analysis of these models was performed to ensure the absence of steric clashes, while assessing the conformational feasibility of repetitively displaying the fHbp β barrel on the NP surface in a symmetric manner (Figure 5C-D).

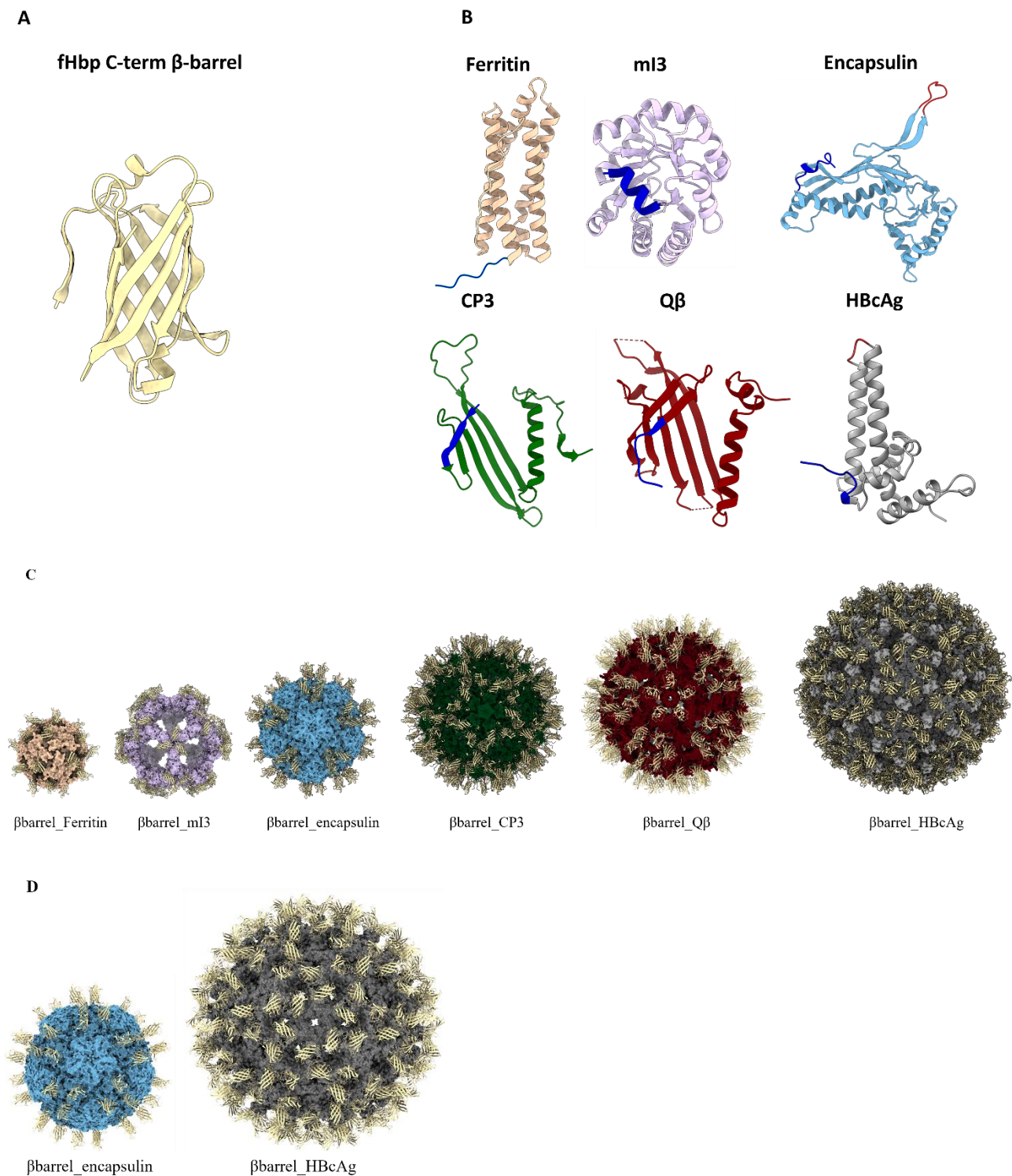


Figure 5: Design of chimeric NPs. (A) Cartoon representation of 3D structure of C-term β barrel from fHbp antigen. (B) Cartoon representation of 3D structure of monomers from each tested NP. In dark blue is highlighted the N terminus and in red the loops exploited for the genetic fusion of the antigen. (C) Cartoon representation of predicted 3D structure obtained with Rosetta homology modelling of each chimera displaying β barrel genetically fused at each N-term. (D) Cartoon representation of predicted 3D structure obtained with Rosetta homology modelling of encapsulin and HBcAg NPs displaying β barrel inserted into a surface exposed loop. The β barrel exposed is represented in yellow. Images obtained with ChimeraX (panel A, C, D) and Pymol (panel B).

11.2. Correctly assembled NPs were detected for all tested molecules, except Q β

All designed chimeras resulted to be well expressed and soluble only when recombinantly produced in *E. coli* BL21(DE3) in batch culture at 37°C (see section 9.6.3) and extracted with sonication. In fact, a first attempt to express chimeric NPs displaying β barrel fused at the N-term was made in batch culture at 20°C (see section 9.6.2) and recombinant proteins were extracted by using Cell-lytic detergent. In this case all chimeras were expressed in soluble form except β barrel-encapsulin which was not expressed. However, transmission electron microscopy conducted in negative staining revealed that only β barrel-mI3 and β barrel-HBcAg were properly assembled with a diameter respectively of 30 and 35nm. For β barrel-ferritin, β barrel-CP3, β barrel-Q β , only aggregates and protein fragments were detected (Figure 6).

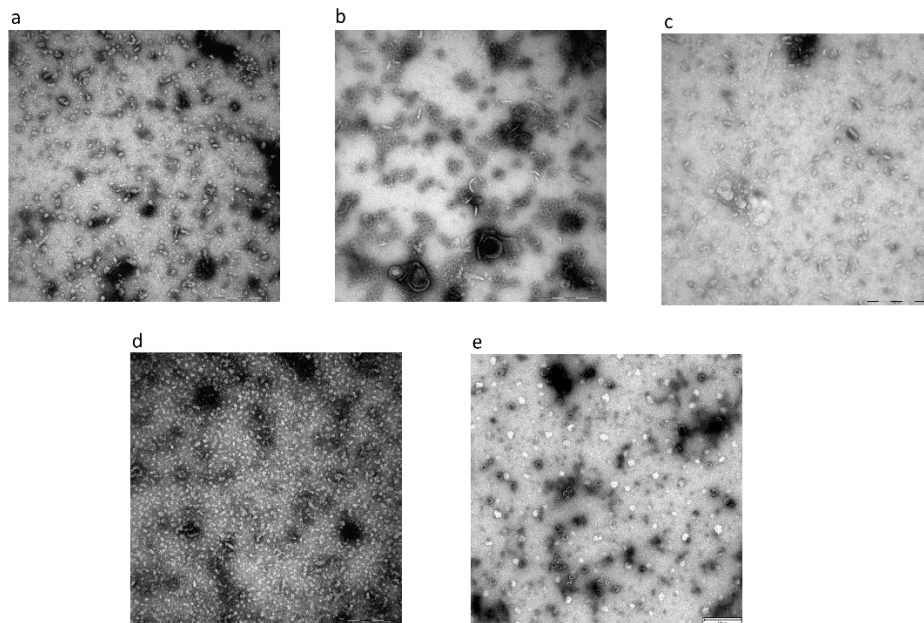


Figure 6: Negative staining transmission electron microscopy (NSTEM) of chimeric NPs displaying β barrel antigen after SEC purification. (a) β barrel-Ferritin (b) β barrel-mI3 presents a diameter of 30nm (c) β barrel-CP3 (d) β barrel-Q β (e) β barrel-HBcAg presents a diameter of 35nm. Scale bar inserted in the pictures and corresponding to 200nm

The optimization of both expression conditions and lysis method allowed the production of properly assembled chimeras. In fact, recombinant chimeric NPs were isolated from the soluble fraction after two steps of purification, affinity, and size exclusion chromatography (SEC) (Figure 7a). The integrity and purity of each sample was assessed with SDS-PAGE analysis in denaturing conditions (Figure 7b). Each monomer migrated at the expected molecular weight (MW). Furthermore, the shift in MW, by comparing chimeric constructs with naked NPs, confirmed that the polypeptide of the expected length was produced and that the chimeras were not susceptible to protease digestion. The

structure of the protein purified by SEC was analysed by negative staining with transmission electron microscopy (TEM). The genetic fusion of the antigen at the N-term of each NP was successful. In fact, all protein-based chimeric NPs resulted in a homogeneous population of correctly assembled NPs with a diameter ranging from 25 nm (β barrel-ferritin) to 30nm (β barrel-mI3 and β barrel-encapsulin) (Fig 8 a-c). For this last construct, we also observed a tendency of NPs to adhere to each other; in fact, NPs completely separated from the others were rare. On the other hand, not all chimeras based on VLPs were correctly structured. In fact, only for β barrel-CP3 and β barrel-HBcAg, properly structured NPs were detected, with a diameter of 30 and 35nm respectively. Despite several attempts, β barrel-Q β VLPs were not obtained as ordered structures, but only aggregated and precipitated proteins were detected in TEM analysis (Figure 8 d-f).

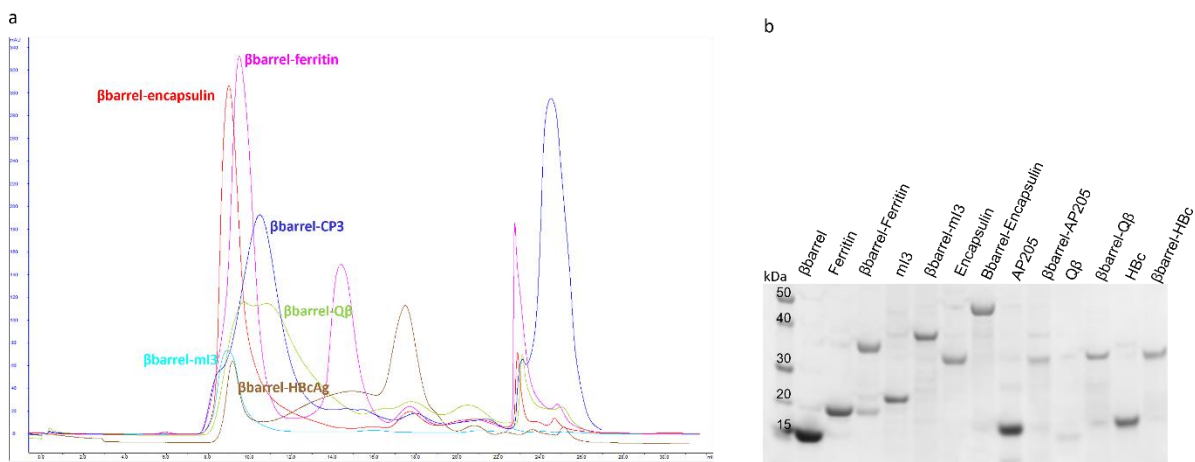


Figure 7: (a) Chromatograms of size exclusion purification of NPs displaying β barrel. X-axis mL of elution, Y-axis mAU of UV intensity detected at 280nm (b) SDS-PAGE analysis of purified monomeric antigen, naked and chimeric NPs after SEC purification, performed under denaturing conditions and stained with Coomassie Blue. First lane reports the molecular weight marker expressed in KDa. Theoretical molecular weights of each sample: β barrel 14KDa, Ferritin 21KDa, β barrel-Ferritin 34,8KDa, mI3 23,6 KDa, β barrel-mI3 37,3KDa, encapsulin 32,1 KDa, β barrel-encapsulin 45,9KDa, AP205 15,2 KDa, β barrel-CP3 29,5KDa, Q β 16,1 KDa, β barrel-Q β 29,7KDa, HBcAg 19KDa, β barrel-HBcAg 32,3 KDa

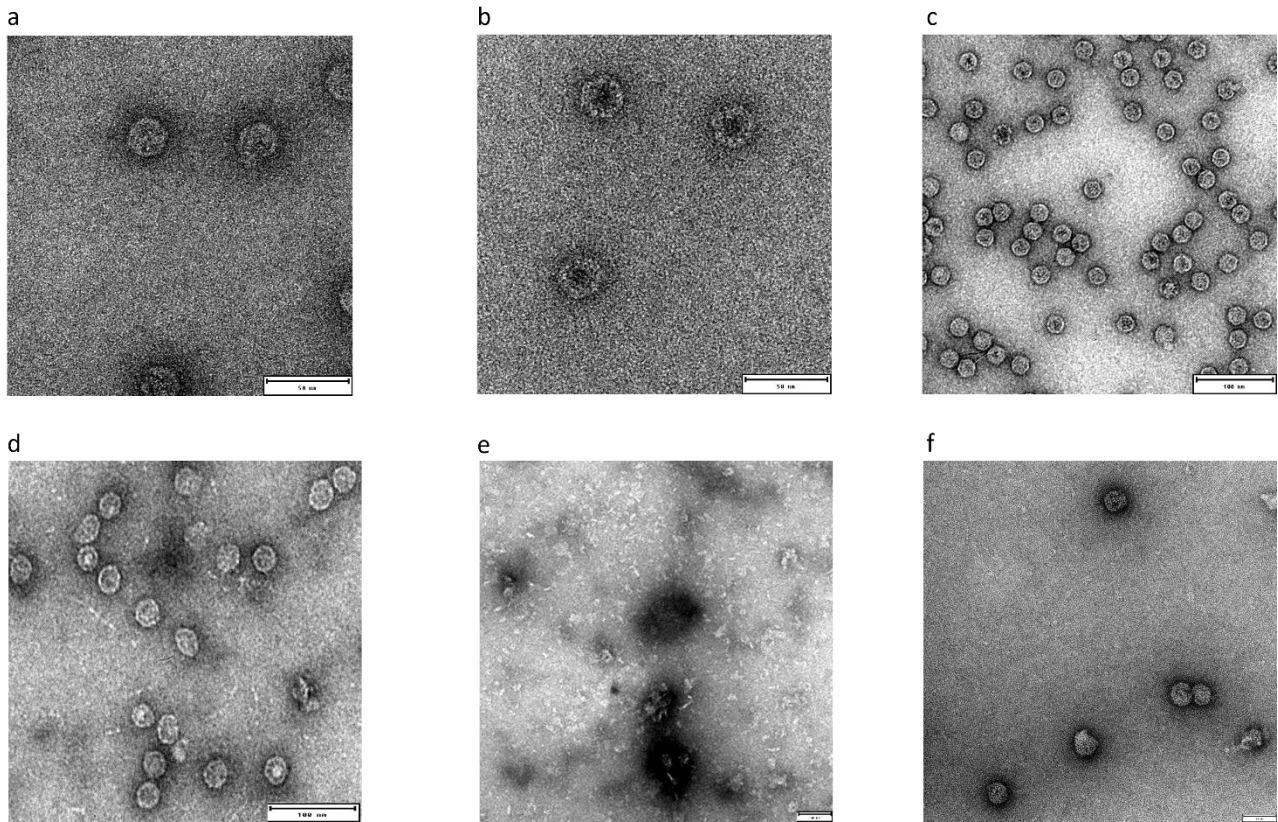


Figure 8: Negative staining transmission electron microscopy (NSTEM) of chimeric NPs displaying β barrel antigen after SEC purification. (a) β barrel-Ferritin presents a diameter of 25nm (b) β barrel-m13 presents a diameter of 30nm (c) β barrel-Encapsulin presents a diameter of 30nm (d) β barrel-CP3 presents a diameter of 30nm (e) β barrel-Q8 for which aggregates, or monomers were detected (f) β barrel-HBcAg presents a diameter of 35nm. Scale bar inserted in the pictures and corresponding to 50nm (a-b-e-f) and 100nm (c-d).

As regarding the engineerization of exposed loops of HBcAg and encapsulin with β barrel, it resulted to be not a successful strategy. In fact, the manipulation of HBcAg loop led the production of highly soluble protein in *E. coli* but only a minimal portion of proteins were correctly assembled. In fact, TEM analysis revealed that the majority of proteins were aggregated or only partially structured (Figure 9a). An analogous result was obtained by engineering the selected loop of encapsulin. The recombinant particles produced were heterogeneous differing by size and shape (Figure 9b). Moreover, further production attempts failed, and the chimeric protein was detected only as a monomer.

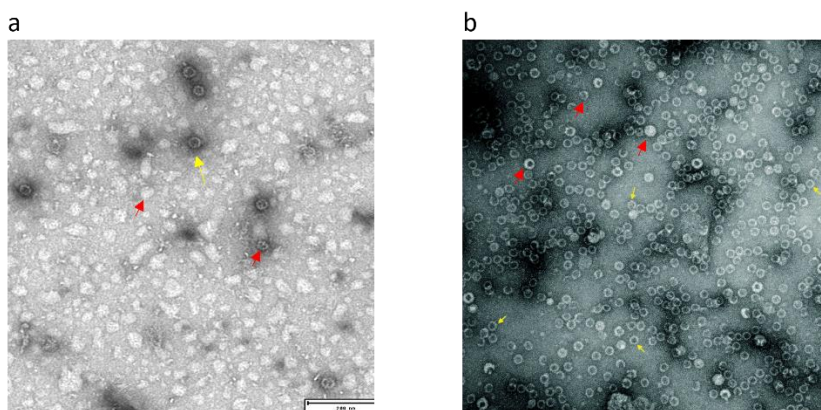


Figure 9: TEM analysis of HBcAg (a) and encapsulin (b) exposing β Barrel in the loop. Yellow arrows indicate correctly assembled NPs. Red arrows indicate incorrectly structured NPs like aggregates, NPs partially structured or NPs with unexpected size or geometry. Scale bar inserted in the pictures and corresponding to 200nm (a-b).

11.3. β barrel antigen is correctly displayed on NP surface

To further investigate the antigen structure and conformation on the NPs surface of properly assembled samples, a dot blot assay was performed using the human monoclonal antibody (hmAb) 4B3 able to bind a β barrel conformational epitope (Figure 10) [274]. An interaction between 4B3 and the antigen was observed by for monomeric β barrel used as positive control and for all NPs tested. These data confirm that not only the antigen is present, but it is also correctly structured and appropriately displayed to be accessible for antibody recognition. In accordance with this, no binding was detected between 4B3, and naked ferritin used as negative control.

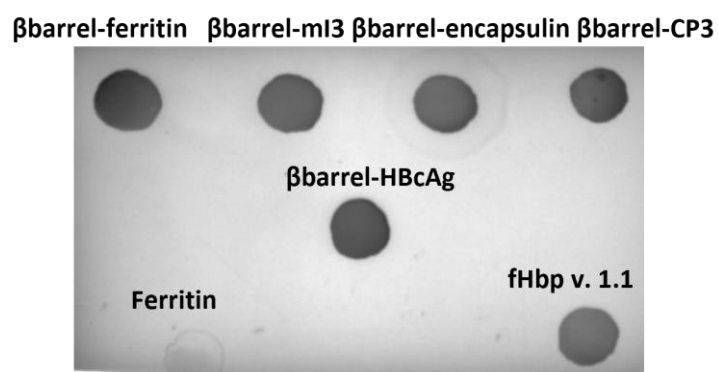


Figure 10: Dot Blot of properly assembled NPs displaying β barrel with human 4B3 antibody.

Moreover, one of the advantages to use NPs as a scaffold is the possibility to display multiple copies of a target antigen. This results in the improvement of the avidity that is crucial for the induction of potent and long-lasting immune responses [1, 2, 305]. For this reason, the avidity of the binding between β barrel and 4B3 has been evaluated with a surface plasmon resonance (SPR) assay (Figure 11). The hmAb was captured on the surface of a sensor chip and increasing concentrations of the

analytes (β barrel alone and chimeric β barrel-NPs) were applied (see Materials and Methods). The kinetic parameters of the interaction between monomeric β barrel and 4B3 were evaluated using the Langmuir 1:1 binding model; both association (k_{on}) and dissociation (k_{off}) constants were measured with a resulting KD of $1,114E-9 M \pm 0.219$ (Figure 10 red line). While, regarding the β barrel-NPs, the kinetic parameters evaluation was not applicable to all the samples because of the avidity effect. Indeed, during the dissociation phase, the complex formed between mAb, and some β barrel-NPs did not dissociate over time but remained stable. Notably, although the samples were normalized for protein content, the highest binding level was displayed by monomeric β barrel. Moreover, we observed an inversely proportional tendency between molecular weight (MW) and RU reached by the molecules. This could be explained by the fact that during the analyte injection, applying a constant flow rate, a higher number of binding events occur with molecules with lower MW because the higher MW molecules move slower over the sensor chip surface. This tendency was common to all chimeras except β barrel-Encapsulin for which it was impossible to evaluate the binding profile. Its tendency to adhere, highlighted also with TEM, likely masks some epitopes making them unavailable for the binding with the hmAb.

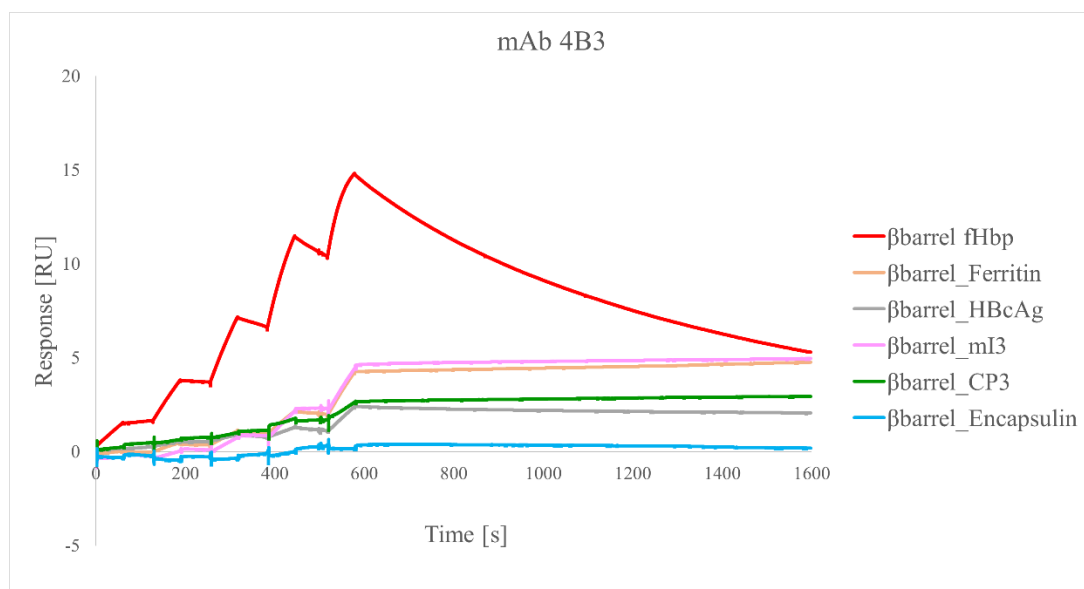


Figure 11: Biacore SPR analysis of monomeric β barrel and β barrel-NPs for evaluation of binding avidity with cross-bactericidal 4B3 hmAb. The interaction between the sample and the antibody has been observed during a time frame of 1500s

11.4. Discussions

This work represents one of the few pieces of evidence of the possibility to display bacterial protein antigens on NPs surface through genetic fusion. In fact, genetic fusion approach has been widely explored for the display on NP surface of viral antigens or short bacterial peptides [121, 163, 164, 204, 207, 306]. While only few examples of bacterial antigens displayed on NPs have been reported

so far [165, 307-309]. Compared to other systems, the genetic fusion approach has the enormous advantage to allow the generation of the final nanoparticle by producing a single recombinant protein. However, it is essential that both scaffold and antigen preserve their correct structure after the fusion [54, 74]. This could be particularly challenging in the case of large and bulky antigens as well as multimeric proteins [1]. However, genetic fusion remains the more straightforward approach to produce chimeric NP displaying the protein antigen of interest. In the present work the feasibility to use genetic fusion for the display of a structured protein antigen on the surface of six different NPs has been investigated. Immuno-focusing by displaying multiple copies of a key epitope on a nanoparticle was previously demonstrated [310]. The β barrel of fHbp v. 1.1, containing most of the cross-reactive epitopes, has been fused to ferritin, mI3, encapsulin, CP3, Q β and HBcAg NPs. Through a structural analysis the N-terminus of each molecule resulted to be suitable for foreign protein insertion and in the case of encapsulin and HBcAg an exposed loop was also identified as potential insertion site. However, the loop design led the production of inhomogeneous samples containing aggregates and partially formed assemblies. Conceivably, the design at the level of amino acid sequence of the scaffold interfered with the correct assembly of the NP. This result is in accordance with the recently published work of Aston-Deaville et al., which reports the potential disruption of HBcAg 3D structure following the loop engineering with β barrel antigen [307]. However, in addition to their data, here reported the possibility to successfully engineer also the HBcAg N-term with β barrel. In fact, the genetic fusion of the antigen at the N-term of each scaffold allowed the production of homogeneous and well-structured molecules with the only exception of Q β VLP. Despite several attempts, Q β VLPs displaying fHbp β barrel were not obtained, indicating that the genetic fusion of a protein antigen to the N-terminus of Q β VLP interfered with the assembly. In accordance, the approach reported in literature for the decoration of Q β VLP is the chemical conjugation of small protein peptides. On the other hand, all the remaining scaffolds were able to correctly display the β barrel obtaining NPs with a diameter ranging from 25 to 35 nm. SDS-PAGE analysis confirmed the presence of the antigen in each chimera and dot blot as well as SPR analysis, using functional 4B3 mAb, suggested that the displayed β barrel was properly folded. However, the SPR analysis revealed that the multicopy display of β barrel increased the binding avidity and it was impossible to determine the kinetic parameters of the binding. In fact, using self-assembling NPs as scaffold, from 24 (ferritin) to 240 (HBcAg) copies of target antigen were displayed simultaneously on the same molecule.

In conclusion, these data showed that ferritin, mI3, encapsulin, CP3 and HBcAg can be engineered through genetic fusion for the display of fHbp β barrel, a well-folded protein domain of approximately 15kDa. Chimeric NPs can be easily produced using a standard bacterial expression system and

purified as His-tagged proteins. Our data indicate that the design of an internal exposed loop of the NP scaffold is more challenging. In the two cases tested herein, it led to the disruption of the NP structure and the formation of heterogeneous samples. In contrast, the exploitation of flexible and exposed N-terminal regions preserved NP structure and correctly exposed the antigen. Although the choice of the best scaffold may be dependent on the antigen displayed, the identification of five different NPs that can potentially accept genetic fusion at the N-terminus represents a template approach to design and produce new chimeric molecules for both vaccine and drug development. However, an *in vivo* study of all these molecules is needed to better elucidate the contribution of antigen copy number, size, shape, and geometry in enhancing the immune response and to further investigate NPs mode of action.

12. Domain 3 of Group B Streptococcus pilus protein as scaffold for epitopes identification and display on NP surface

12.1. Structural analysis of GBS D3 allowed the identification of potential engineerable sites

By using a structure-based design approach six different D3 sites corresponding to its loops have been identified to be potentially engineerable. In fact, D3 folds into a β -barrel structure independently protruding from backbone protein BP. The β -barrel is composed by 6 spanning segments connected by 6 flexible loops (Figure 12b).

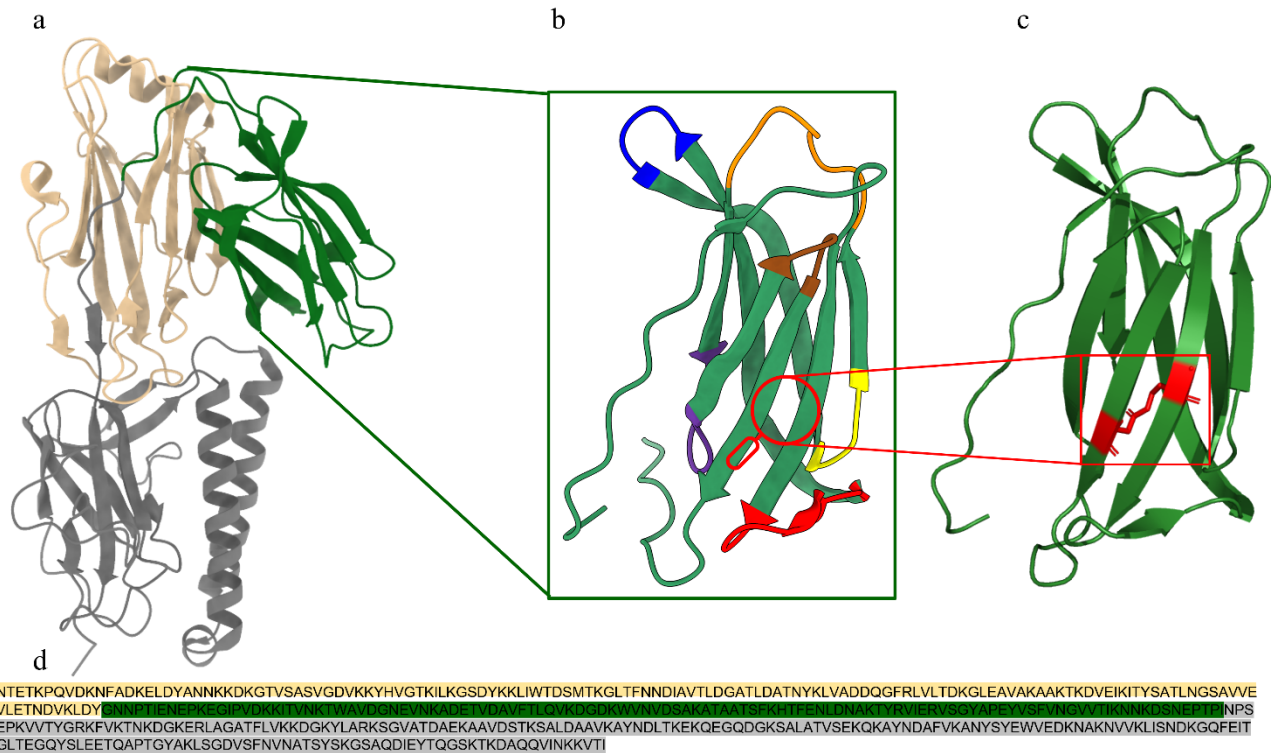


Figure 12: (A, D) Cartoon representation of 3D structure and aminoacidic sequence of GBS pilus protein type 2a (PDB code 2XTL). Domain 2 (D2) light brown, domain 3 (D3) green, domain 4 (D4) grey. (B) D3 magnification with residues 360-372 loop1 red, 380-384 loop2 blue, 393-399 loop3 yellow, 404-411 loop4 orange, 418-422 loop5 purple and 429-432 loop6 brown. (C) Magnification of isopeptide bond occurring between Lys355 and Asn437. Images obtained with ChimeraX.

12.2. Structural prediction and identification of extracellular loops of PorB.1b and OpaB

As reported in the introduction part, PorB.1b and OpaB are integral membrane proteins naturally exposed on the external surface of *N. gonorrhoeae* FA1090 [27]. They are anchored within the membrane through an extended and conserved hydrophobic core and they expose in the extracellular environment only few variable and flexible loops. Due to their hydrophobic nature their recombinant production is challenging. To study the immunodominant epitopes of these antigens, a structural analysis has been performed for the identification of extracellular porB.1b and OpaB loops. In particular, artificial intelligence (AI) approach named AlphaFold2 [311] has been applied to predict with high accuracy PorB.1b and OpaB 3D structure.

The analysis performed revealed the canonical 3-fold PorB symmetry with 16-stranded β -barrel, short turns connecting the strands on the periplasm and long inter-strands loops on the extracellular part of the pore for each of the monomer (Figure 13A). Interestingly, it has been observed that two of the eight loops present a secondary structure. Loop5 (L5) is structured as a β -hairpin which is solvent exposed and oriented towards the central channel pore of the monomer. While Loop3 present two

short-helical turns and it is predicted to be directed inside the pore (Figure 13B). The per-residue measurement of model local confidence (pLDDT) revealed high confidence for the transmembrane β -barrel predicted region ($pLDDT \geq 50$) but low confidence ($pLDDT \leq 30$) in the region of loops. This is probably due to the intrinsic flexibility of this region.

Alphafold prediction of OpaB model shows a structure made of 8 antiparallel β -strands, forming a barrel structure in the bacterial outer membrane, linked by 4 extracellular loops [257] (Fig 13C). Two out of four loops, namely Loop2 and Loop3, showed the same beta-hairpin structure previously observed in PorB.1b/L5 (Figure 13D). The pLDDT score revealed high confidence for the β -strands region ($pLDDT \geq 50$) but low confident in the OpaB/L2-L3 region ($pLDDT \leq 30$).

Finally, the 3D structure prediction of both porB.1b and OpaB antigens allowed the identification of 8 (porB.1b) and 4 (OpaB) extracellular loops (Figure 13B-D). In order to identify most immunogenic/immunodominant epitopes, they have been extrapolated and inserted into the previously described protein scaffold D3.

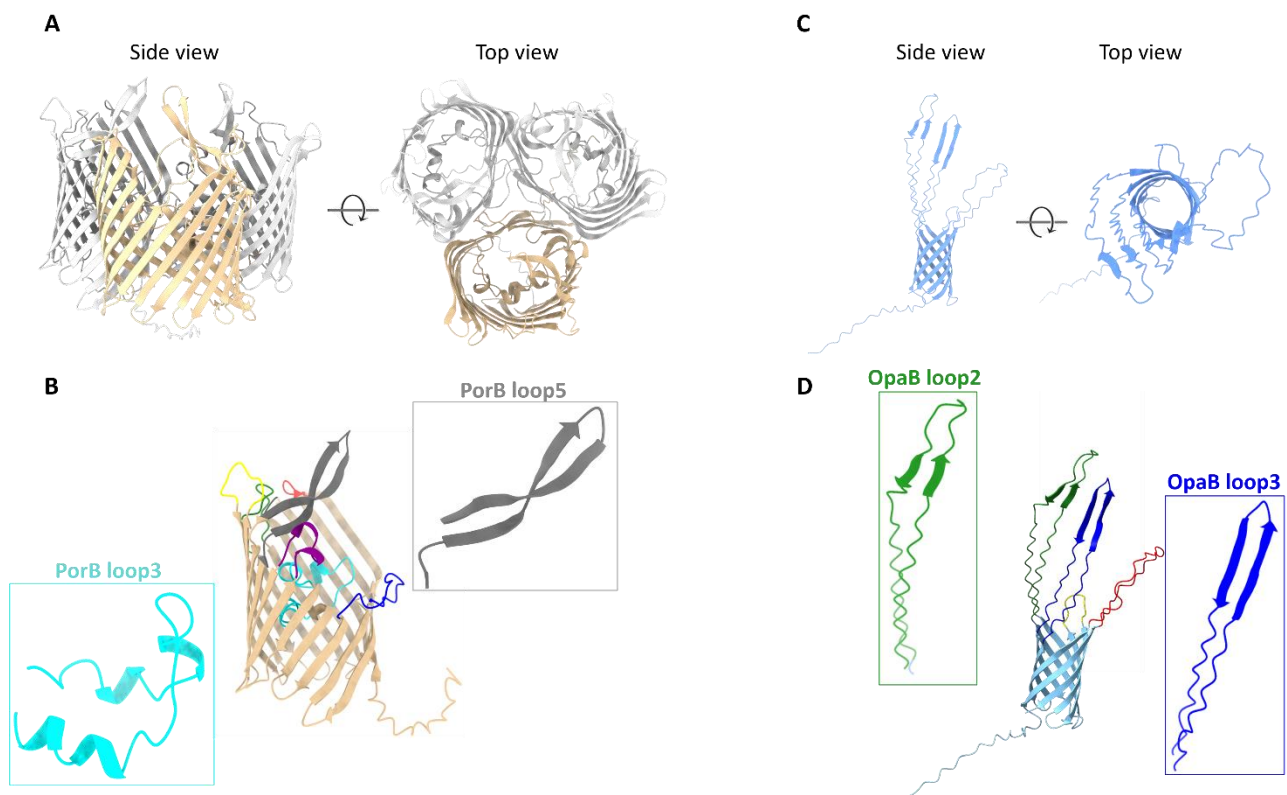


Figure 13: Cartoon representation of predicted 3D structures of rPorB.1b and rOpaB proteins. (A)porB.1b is predicted to form an homotrimer into the external membrane. (B) Identification of 8 extracellular loops: Loop1 red, Loop2 blue, loop3 cyan, loop4 purple, loop5 grey, loop6 yellow, loop7 green, loop8 black. Magnification of Loop3 and Loop5 that present a secondary structure (C) Side and top view of predicted model of OpaB (D) Identification of 4 extracellular loops: Loop1 red, Loop2 blue, Loop3 green, Loop4 yellow. Magnification of Loop2 and Loop3 presenting a secondary structure. Images obtained with ChimeraX.

12.3. D3 site2 is the optimal site for the insertion of OpaB and porB1b loops

The best engineerable D3 site has been selected considering the expression level (Figure 14A), the thermal stability (Figure 14B) and the ability to preserve the epitope conformation [278] of the 6 different chimeras. The analysis has been performed inserting the longest epitope identified in the model antigens (PorB.1b loop3) into each of the six D3 sites. All chimeras have been expressed in soluble form in *E. coli* at levels comparable to the empty D3, only the engineerization of D3 site4 seems to generate a less soluble chimera not correctly folded. In fact, from Nano DSF analysis it was not possible to appreciate for this chimera a transition between the folded and unfolded states suggesting that the protein is not properly structured (Figure 14B). Whereas the engineerization of all the other D3 sites has generated chimeras presenting a shift in the measured fluorescence at temperatures in the range of 45-76 °C (Figure 14C) suggesting that they are folded. Each chimera presents a T_m lower than the T_m detected for the empty scaffold (88 °C), but this is reasonably due to the insertion of a long and flexible foreign portion. Among all tested positions, the engineerization of site1 and site2 led the formation of most stable chimeras. The only note is that the higher initial ratio 350/330nm detected for site1 chimera suggests the presence of partially unfolded regions [312]. While the D3-Site2 shows a profile comparable to the empty D3 scaffold with the lowest initial 350/330 nm ratio. Another key factor for the choice of best insertion position is the ability to preserve the native epitope conformation. For this reason, the 3D structure of each chimeric D3 displaying PorB.1b loop3 has been computationally predicted with Alphafold (Figure 14D) and the epitope conformation has been compared with the one predicted in the native protein (Figure 14D). From this analysis, loop3 porB.1b resulted to maintain its α -helices conformation when inserted into D3 site2 and site6. In all the other sites the epitope is partially restructured respect to its predicted native conformation in the whole protein. Combining all these data, the engineerization of D3 site2 resulted to be the most promising strategy to produce soluble and stable chimeras able to correctly display the epitope of interest.

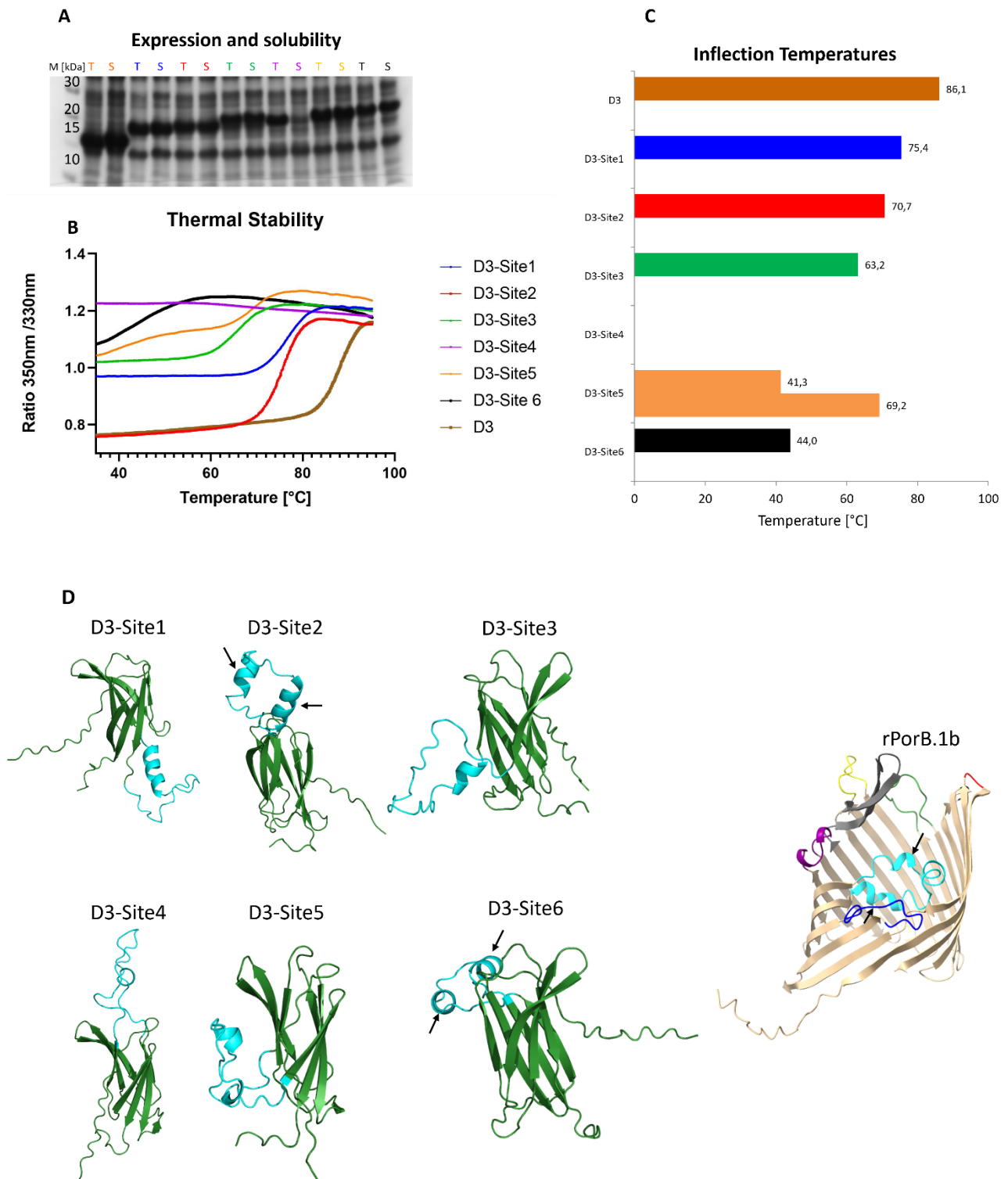


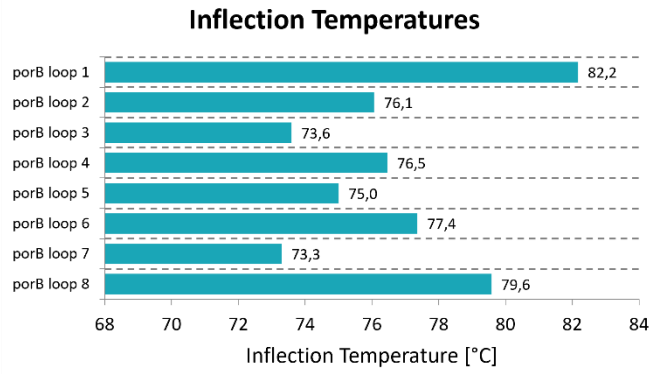
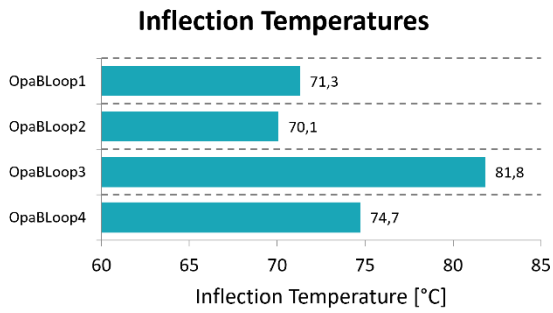
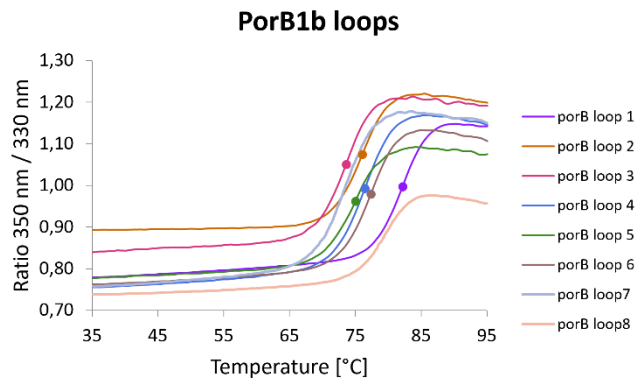
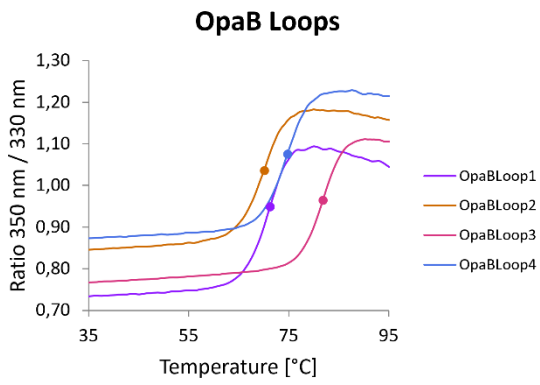
Figure 14: (A) SDS_PAGE analysis of expression and solubility of chimeric D3 displaying loop3 inserted into 6 different sites. M: Novex sharp protein marker (Invitrogen LC5800); T total fractions, S soluble fractions of *E. coli* extract. (B) Unfolding profiles of each chimeric D3 evaluated with NanoDSF. (C) Inflection temperatures corresponding to the medium melting temperature of each molecule calculated as inflection point of the curve. (D) Predicted 3D structure of D3 displaying porB.1b loop3 into each D3 site and rPorB.1b. Black arrows indicate the two α -helices structures of loop3 porB.1b detected in the native protein and maintained after the insertion into D3 site 2 and 6. Images generated with Pymol.

12.4. D3 correctly displays gonococcal epitopes

Once the best D3 site has been identified, all the PorB.1b and OpaB loops have been extrapolated and inserted into D3 site2. All chimeras have been obtained as His-tagged soluble proteins in the cytoplasm of *E. coli*. Thermo stability analysis revealed that each molecule is properly folded with a T_m ranging from 70 to 82 °C (Figure 15A). Furthermore, to identify the immunodominant loops in PorB.1b, a western blot with two different sera was performed. This analysis revealed that only porB.1b loops 1-3-5 and 6 were recognized by antisera raised with the recombinant purified PorB.1b (α -rPorB 1b serum) (Figure 15B-i). When the same experiment was conducted with sera raised by gonococcal outer membrane vesicles (α -OMV-FA1090 serum) (containing 70% of PorB as main protein), only the loop5 was recognized (Figure 15B-ii). This result has been also confirmed by Luminex assay (Figure 15C-i).

A similar experiment was conducted with the 4 loops of OpaB protein displayed on the D3 scaffold revealing that α -OMV-FA1090 serum is able to recognize only OpaB loop2 and loop3 (Figure 15B-iii). In fact, despite OpaB loop1 is poorly recognized in western blot by α -OMV-FA1090, it is not detected by the same serum in Luminex assay (Figure 15C-ii) as well as OpaB loop4. This is in accordance with the information reported by Cole at al., which defined Loop2 and Loop3 as the hypervariable loops of Opa proteins containing also the most immunogenic and functional epitope. While loop1 and loop4, although they were highly conserved among strains and variants, they are not able to induce the production of specific antibodies [261]. Moreover, the *in vivo* study conducted in mice revealed that designed chimeras are able to elicit immune response against the target epitopes. In this sense, sera α -D3PorBLoop5 and α -D3OpaBLoop2 are able to recognize in western blot native proteins present in the total cell-extracts and in the OMV of *N. gonorrhoeae* FA1090 (Figure 15B-iv-v). In accordance, due to the high sequence diversity of porB.1b Loop5 and OpaB loop2 between strains FA1090 and F62, both tested sera do not recognize the total extract of F62 strain (Figure 15D).

A



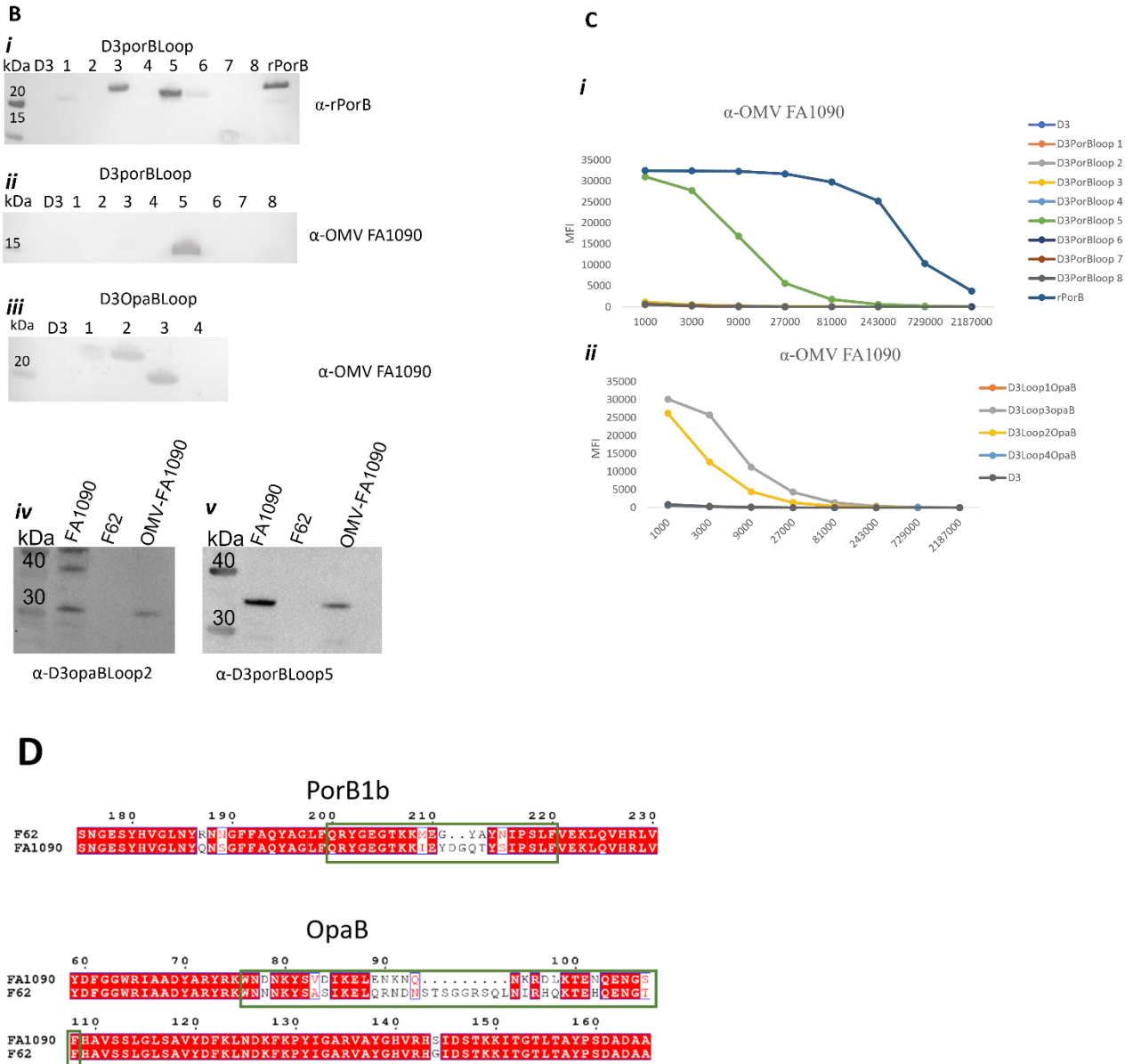


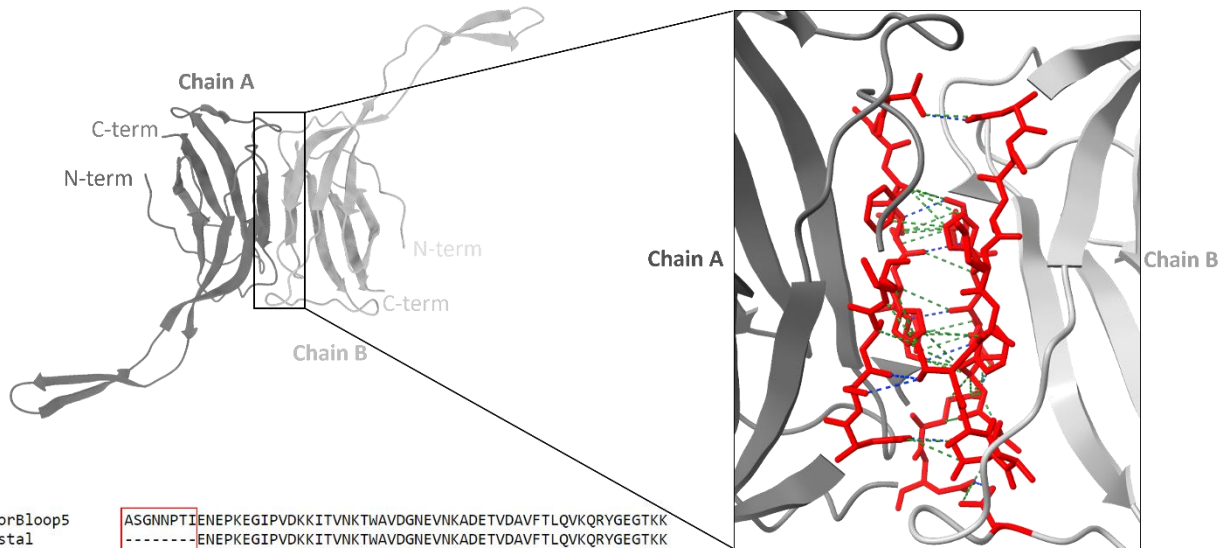
Figure 15: Thermal stability analysis of chimeric D3 displaying both *porB.1b* and *OpaB* loops with the respective inflection temperatures. (B) Western Blot analysis of chimeric D3 displaying *porB.1b* or *OpaB* loops. (B-i-ii) D3 *porB.1b* loops tested with α -*rporB 1b* and α -OMV-FA1090 sera, (B-iii) D3 *OpaB* loops tested with α -OMV-FA1090 sera. (B-iv-v) total cell extracts and purified OMV-FA1090 tested with α -*porB* loop5 and α -*OpaB* loop2 sera. (C) Luminex assay on D3 displaying *porB.1b* or *OpaB* loops testing α -OMV-FA1090 serum. X axis reports serum dilutions. (D) aminoacidic sequence alignment obtained with *clustalW* between *PorB 1b* and *OpaB* proteins produced by the strains F62 and FA1090. Green rectangles highlight loop5 *porB.1b* and Loop2 *opaB*.

12.5. Crystal structure resolution of D3porBloop5 confirmed the correct epitope display

The computational structural prediction of *porB.1b* has shown that loop5 adopts a β -hairpin structure in the native protein and the same structure is also predicted in the chimeric D3-loop5. In order to confirm the results of the *in-silico* analysis, recombinant pure D3-loop5 has been used to conduct a crystallization trial. Diffracting crystals were obtained and the 3D structure of D3-loop5 has been

solved by X-ray crystallography. Crystals were obtained after 6 days in buffer containing 0.1M HEPES with 20% w/v jeff ED-2001 precipitant at pH 6.5. The x-ray diffraction data were processed and the crystal structure of D3-loop5 was determined using the molecular replacement method by using Phaser (Suite Phenix). Electron density maps were of high quality and allowed the model building and structure refinement to a final resolution of 2.6 Å. Although crystallization was carried out using entire D3-loop5 chimera (139 a.a.), 8 N-terminal and 7 C-terminal residues were absent in the density map (Figure 16A). Based on the computational prediction, this is reasonably due to the high flexibility of these regions. The crystal asymmetric unit contains a dimer of two independent chains arranged in a mirror image. The second chain is rotated of 180° along y axes compared to the first chain (Figure 16A). The interface analysis performed with PISA revealed that the interface area represents about the 9% of the entire surface and the two monomers are taken together by multiple hydrogen bonds occurring between residues located in a β-strand (from residue 98 to 114) (Figure 16A). In addition, for each chain the presence of the internal isopeptide bond between residues K43 and N146 has been detected (Figure 16B). This result, in accordance with the data published by Nuccitelli et al. [229], suggests that the D3 engineerization with a foreign epitope did not alter its structure. Moreover, the foreign epitope displayed has maintained its native conformation. Density map of porB.1b loop5 region, confirms the β-hairpin organization of this epitope (Figure 16D). This result validates the computational structural prediction reported above of porB.1b. In addition, the model of chimeric D3-loop5 has been computationally predicted and compared with the crystal structure obtained (Figure 16C). The structures are aligned with an overall calculated root mean square deviation (RMSD) of 2.31 Å. In particular, the structure alignment presents the highest similarity between the structures of the scaffold with an RMSD of 1.12. While the structure of porBloop5 between crystallographic and predicted model presents a higher structural diversity with an RMSD of 2.53 (Figure 16C). Reasonably, the structural diversity detected is due to the flexibility of this region, anyhow its secondary structure as is β-hairpin maintained. These results suggest that the engineerization of D3 site 2 allow the preservation of epitope native conformation without destroying the scaffold structure. Atomic coordinates of D3porBloop5 have been deposited in the Protein Data Bank under accession PDB code 8C27.

A



D3porBloop5 crystal	ASGNNPTIENEPKEGIPVDKKITVNKTWAVDGNVKNKADETVDAVFTLQVKQRYGEGTKK -----ENEPKEGIPVDKKITVNKTWAVDGNVKNKADETVDAVFTLQVKQRYGEGTKK *****
D3porBloop5 crystal	IEYDGGQTYISPSLFVKWVNVDSAKATAATSFKHTFENLDNAKYRVIERSVGYAPEYVSF IEYDGGQTYISPSLFVKWVNVDSAKATAATSFKHTFENLDNAKYRVIERSVGYAPEYVSF *****
D3porBloop5 crystal	VNGVVTIKNNK[SNEPTPI VNGVVTIKNNK----- *****

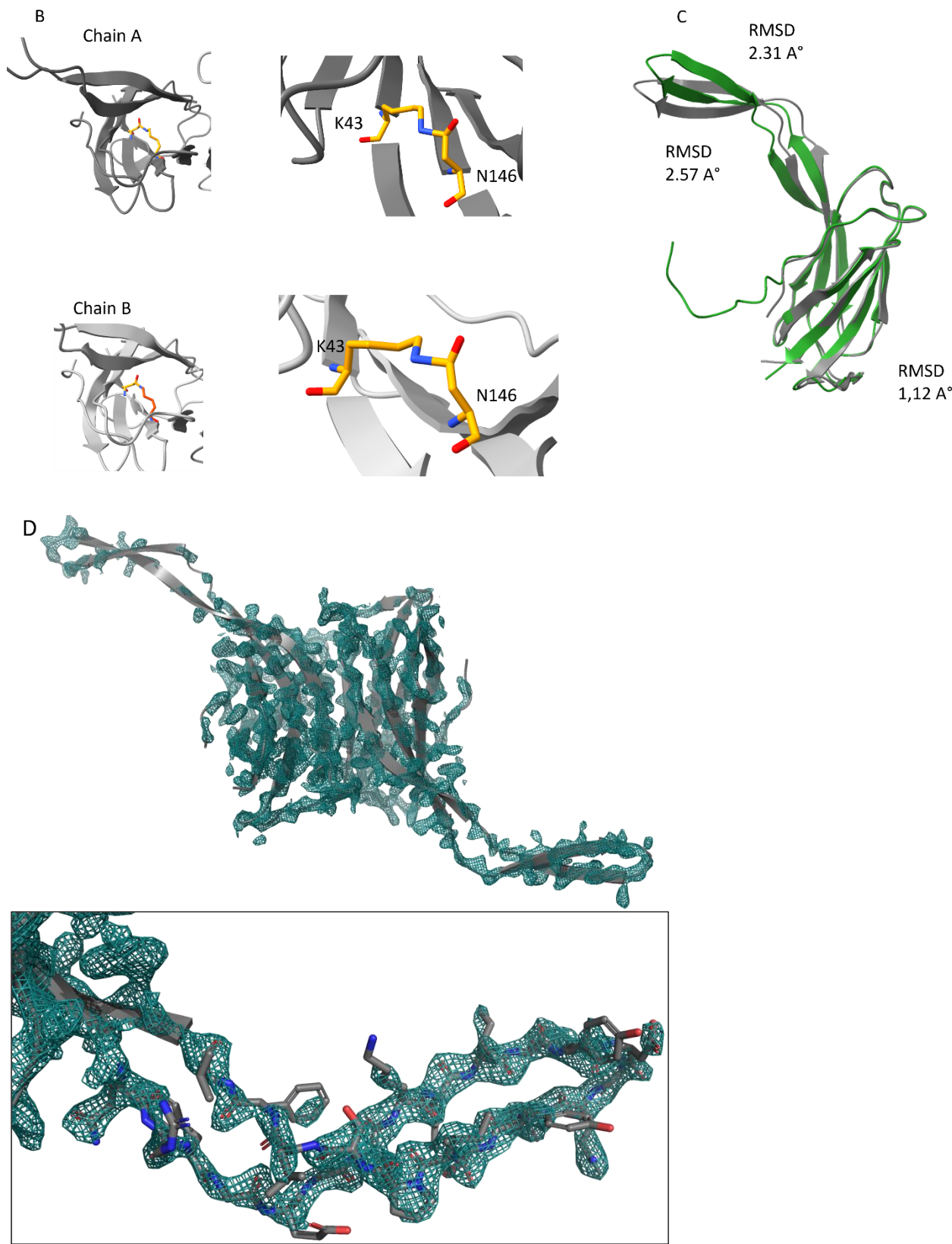


Figure 16: Crystal structure resolution of D3porBloop5. (A) Two chains (A dark grey and B light grey) have been detected in the crystal structure. Compared with the sequence of recombinant protein, in the crystal some residues at N- and c-terminus are absent (red rectangles). The connection between one chain and another are highlighted in the magnification reported in the left part of the section. Residues involved in the inter-chain bonds are reported as red sticks. Hydrogen bonds are highlighted in blue while all the other types of interactions are highlighted in green. (B) Identification of an internal isopeptide bond occurring within residues K43 and N146 of each chain. (C) Structural comparison of computationally predicted D3-loop5 models and resolved crystal structure and

evaluation of Root Mean Square Deviations (RMSD). (D) Density map shown for the entire crystal (up) and a magnification of density map around the loop5. Graphical representation and structural analysis performed with Pymol.

12.6. D3 scaffold prevented epitope degradation when displayed on mI3 surface

After the identification of most immunodominant epitopes, and the confirmation that the native structure of the epitope is maintained when inserted into D3 scaffold, PorB.1b loop5 has been displayed on mI3 surface. The nanoparticle has been decorated with both linear peptide (mI3-porBloop5) and with chimeric D3 displaying porB.1b loop5 (mI3-D3porBloop5). In both cases the antigens have been genetically fused to the N-term of mI3 NP. The molecules have been produced in *E. coli* and purified from the soluble fraction with affinity chromatography exploiting the 6x-his tag fused at the C-term of the scaffold (Figure 17A). Then assembled particles were separate from monomers with SEC. Expression analysis as well as SDS_PAGE analysis of purified protein of mI3-porBloop5 revealed the presence of a double bands at the expected molecular weight (Figure 17 B-C). This could be due to a mixed population of intact mI3-porBloop5 and partially degraded molecules. In order to understand which region, the N- or the C-terminus, of the chimera was degraded a western blot was performed using α -His antibody (Figure 17D). In this analysis both bands were detected indicating that the shift in the molecular weight was due to a degradation of the N-terminus corresponding to the linear peptide of porB.1b loop5. On the other hand, mI3-D3porBloop5 has been produced as soluble chimera with the expected molecular weight and no degradation has been observed in production and purification step. In fact, also microscopy analysis conducted in negative staining confirmed the formation of properly assembled mI3-D3porBloop5 NPs (Figure 17E) and as regarding mI3-porBloop5 a mixed population of nanoparticles was observed (Figure 17F). Properly folded molecules were detected among partially structured particles as well as aggregated proteins. All these data shown the importance to use a protein scaffold for the display of epitopes on NP surface. In fact, this strategy allows to prevent possible epitope degradation as well as to maintain native epitope conformation.

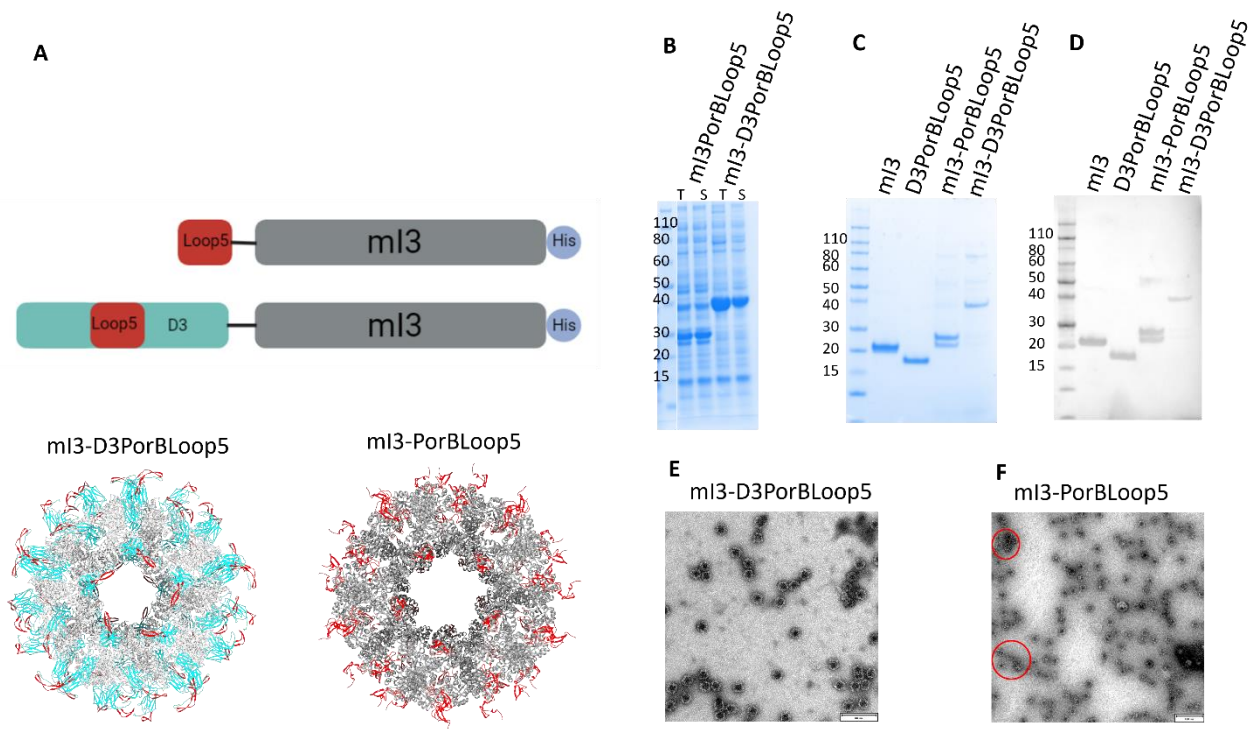


Figure 17: (A) Design (up) and Rosetta homology modelling derived 3D structure prediction of chimeric m13 displaying *porB* 1b loop5 and D3porB 1b loop5 (down). Images obtained with Chimera (B) SDS_PAGE analysis of expression and solubility of each chimera extracted with cell-lytic lysis buffer, T total fraction, S soluble fraction. (C) SDS_PAGE analysis of purified proteins after SEC inserting as control the naked m13 scaffold and monomer of D3 *porB*.1b loop5. (D) western blot with α -his antibody of purified protein. (E) electron microscopy in negative staining of m13-D3PorBloop5 (F) Electron microscopy in negative staining of m13-PorBloop5.

12.7. Discussion

The investigation of membrane protein as recombinant vaccine antigens is still challenging. In fact, the presence of large hydrophobic domains needed for the membrane anchoring makes them insoluble and usually they are produced in *E. coli* as inclusion bodies. The protein extraction and subsequent protein refolding requires the use of denaturing agents as well as detergents. In addition, of the whole antigen, only few epitopes are naturally exposed to the immune system when the protein is in the outer membrane. For these reasons, the identification and production of functional epitopes could represent a valid strategy to produce effective protein-based vaccines. Among the different techniques used for the epitope identification, a promising strategy is based on the dissection in sub-domains/fragments of target antigen and their production in a foreign scaffold. Different examples have already been reported in literature showing the possibility to extrapolate extracellular loops from membrane proteins and to display them both on a single protein and on NPs [179, 297, 298]. The use of NPs scaffold for epitope display is a well-established practice and it could be achieved by (i) engineering the primary NP sequence or (ii) by fusing at gene level the epitope with the protein

scaffold. As also shown by the results reported in the previous section of this work (section 12) the engineerization of aminoacidic sequence of the scaffold could led the disruption of the 3D structure. While, in the second case, the epitope could be degraded or even lost during the production process. For this reason, in this work the D3 of GBS has been investigated as protein scaffold for both the investigation of most immunogenic extracellular PorB.1b and OpaB loops and their display on mI3 surface. The analysis of reported D3 crystal structure allowed the identification of 6 potentially engineerable sites corresponding to its six loops. On the other hand, the structure of both PorB.1b and OpaB has not been reported yet. Only computational predictions are reported based on the sequence homology with structurally known proteins. From the reported data, PorB.1b should forms an homotrimer in which each monomer should be formed by 16 transmembrane-spanning segments and 8 highly flexible extracellular loops [313, 314]. While OpaB, has been predicted to be structured as eight spanning stranded forming a β -barrel, connected by four extracellular loops [315]. However, the low sequence identity within the loop regions, makes the predictions based on the homology modelling not entirely accurate. Instead, thanks to the advances in the structural prediction field is now possible to obtain models with a level of accuracy comparable to the experimental structures exploiting deep learning techniques. For this reason, AlphaFold2, a cutting-edge deep learning algorithm that outperforms in the latest protein folding competition CASP1 [316] has been used to computationally predict the 3D structure of both antigens. The analysis revealed that both proteins are organized as β -barrel with 8 (porB.1b) and 4 (OpaB) extracellular loops. This result is in accordance with other reported predictions based on the sequence homology [260, 262]. However, given the high sequence variability of loops among protein variants, the major structural diversity is detected for the loop conformation. Interestingly, a secondary structure has been predicted by AlphaFold for some of them. PorB.1b loop5 and OpaB loop2 and 3 are present as β -hairpin and porB.1b loop3 presents a double short helices conformation. Among them porB.1b loop3, the longest one, was used to perform a scanning engineerization of each D3 site. The production and characterization in terms of stability, solubility, and ability to preserve the epitope conformation of each chimera, led the identification of D3 site 2 as the best insertion point. Basing on that, all the other PorB.1b and OpaB loops have been extrapolated and inserted into the site 2. By combining western blot and Luminex analysis PorB.1b loop5 and OpaB loop2 and loop3 have been identified as the most immunogenic loops. However, it is not excluded the that all the other loops could be recognized when combined with other loops/epitopes supposing in this way the presence of conformational epitopes involving more than one single loop. Moreover, the crystal structure resolution of chimeric D3 displaying PorB-loop5 has experimentally confirmed the preservation of epitope conformation upon engineerization validating the computational structural prediction of

PorB.1b. Finally, the use of D3 scaffold resulted to be crucial also for the display of porB-loop5 epitope on mI3 NP surface. In fact, the presence of D3 scaffold prevented the epitope degradation during the recombinant expression and properly folded NPs correctly displaying the epitopes have been successfully produced.

All these data shown that D3 is an ideal protein scaffold easily engineerable. It can correctly display target epitope thus maintaining its physio-chemical properties. In fact, it has been successfully used to dissect two membrane protein antigens (porB.1b and OpaB) allowing the identification of 3 more immunogenic epitopes (PorB.1b-loop5, OpaB loop2 and Loop3). Moreover, it can be also used as scaffold for the display of epitopes on NP surface protecting the target antigen from degradation. However, the strategy adopted for the study requires an extensive structural investigation of both protein scaffold and antigens. The computational structure prediction was crucial for the identification of PorB.1b and OpaB extracellular loops and for the evaluation of best D3 engineerable site. In fact, further engineerization of D3 scaffold with longer epitope will probably require the *de novo* identification of the optimal engineerable site. At the same time, also the simultaneous display of two different epitopes in multiple D3 sites as well as the insertion of entire antigens should be investigated. In conclusion, the approach adopted in this work opens the door to a new way to study membrane and insoluble antigen as vaccine candidates. Lastly, it also represents a step forward in the development of new approaches for epitope display on protein NPs surface.

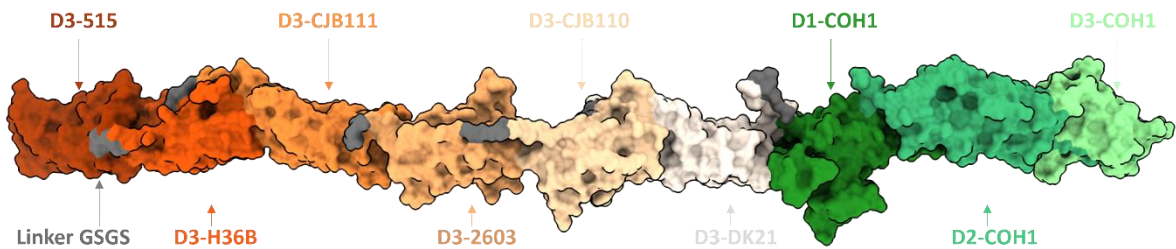
13. Production of a polyvalent nanoparticle displaying both protein and sugar antigens of Group B Streptococcus (GBS)

13.1. Pilus fusion protein covers all protein variants of GBS pilus type 2

Genomic analysis of GBS isolates revealed the presence of three distinct pilus islands: PI-1, PI-2a, and PI-2b each encoding for three different pilus types [229]. A single pilus is composed by a backbone protein (BP) and two anchor proteins (AP1 and AP2) highly conserved among GBS strains. The only exception is the BP from PI-2a for which six immunologically different variants have been discovered [228]. The overall BP structure solved for the variant 2a revealed an organization in 4 independent domains (D1-D2-D3-D4) differing from the BP types 1 and 2b that present three domains (D1-D2-D3) [317]. The variability of 2a BP is due to a sequence diversity located in the D3 which contains also the most immunogenic epitopes. Therefore, with the idea to cover all the circulating BP-2a variants Nuccitelli et al. have successfully produced a functional chimera collecting the D3 from each variant (6xD3) [229]. Taking a further step in this direction, here a new chimera

has been designed. The domain full length BP of type 2b GBS pilus has been genetically fused, spaced by a serine glycine linker, to the C-term of 6xD3 chimera covering in this way all possible variants of pilus type 2 (Figure 18A). The molecule has been successfully produced in *E. coli* and purified from the soluble fraction. The interest protein has been purified by SEC eluting at a volume compatible with the correct molecular weight (Figure 18C). SDS-PAGE analysis of purified protein showed a single band at the expected molecular weight confirming the production of a single polypeptide without signs of degradation (Figure 18B). Moreover, from nanoDSF analysis, two Tms have been detected revealing the presence of two regions with a different stability (Figure 18D). Reasonably, the less stable portion is represented by the full-length BP type 2b with a Tm of about 62°C. In fact, by comparing this result with the previously reported data, it should have a Tm of about 67°C [283]. While the 6 domains fused in the chimera 6xD3 are highly stable and they show a similar trend of stability with a Tm of about 80°C (Figure 18D).

A



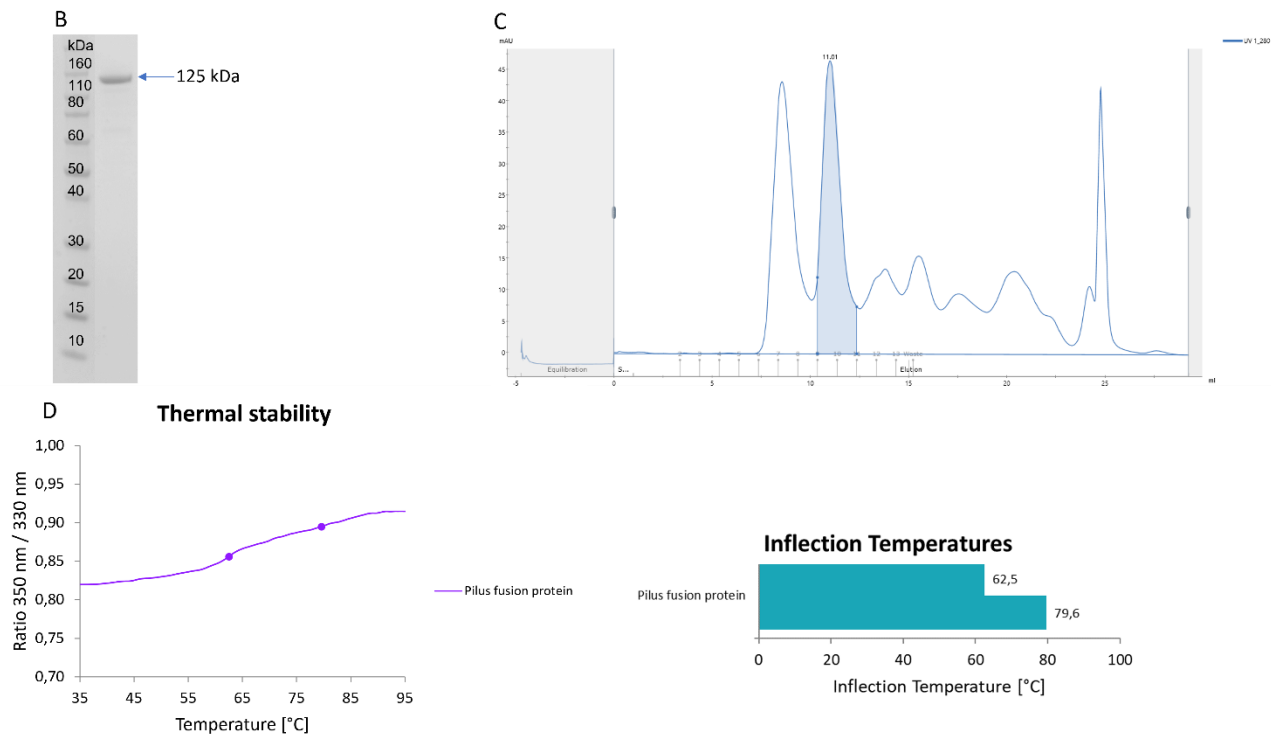
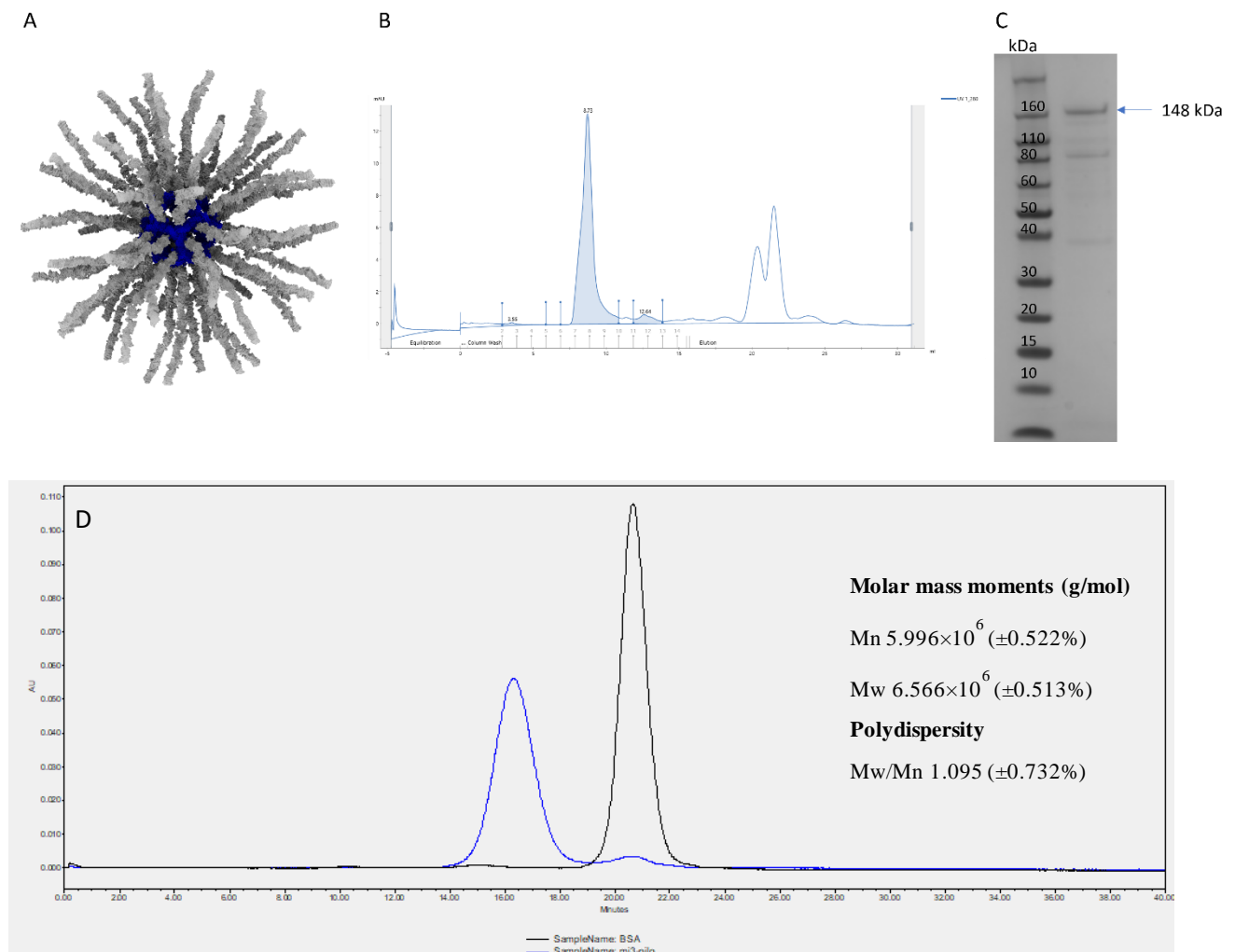


Figure 18: Design and production of chimeric pilus fusion protein. (A) Cartoon of designed chimeric pilus fusion protein reporting in the red scale the 6 D3 variants of GBS pilus type 2a from six different GBS strains (515, H36B, CJB111, 2603, CJB110, DK21) and in the green scale the domain 1, 2 and 3 of the GBS BP type 2b from the strain COH1. The glycine serine linker is reported in grey. Molecule representation has been performed with ChimeraX (B) SDS-PAGE analysis of purified protein. (C) Chromatogram of SEC purification reporting the UV absorbance at 280nm. Pilus fusion protein has been eluted in the peak highlighted in blue (D) NanoDSF analysis for thermal stability evaluation with the respective T_m detected for the chimeric pilus protein.

13.2. mI3 NP correctly displays chimeric pilus antigen

To improve protein antigen immunogenicity pilus fusion protein could be displayed on a NP surface. However, the high molecular weight and the long-extended structure of the fusion protein required a highly stable scaffold. For these reasons mI3 was selected as the most suitable NP for the display of the pilus fusion. As shown in the previous chapters of this work (section 11), the mI3 intrinsic structural stability, resistance at different physicochemical conditions, as well as its ability to correctly display a protein antigen through genetic fusion makes it ideal for the purpose of this study. Therefore, pilus fusion protein has been genetically fused at the N-terminus of mI3 adding a 6xhis-tag at the C-terminus of the scaffold. Rosetta comparative modelling has been used to *in silico* predict the 3D structure of designed chimera and to ensure the absence of steric clashes, while assessing the conformational feasibility of repetitively displaying the GBS pilus fusion protein on the mI3 surface in a symmetric manner (Figure 19A). The chimeric gene has been cloned into pET24b+ vector and the protein has been produced in soluble form in *E. coli*. The chimera has been purified from soluble

fraction and correctly assembled particles were separated from monomers by SEC collecting assembled particles in the dead volume of Superose 6 column (Figure 19B). SDS-PAGE analysis of elution fraction showed a band at the expected molecular weight and a slight lower band suggesting the presence of a degraded portion (Figure 19C). However, SEC-MALS analysis detected a monodisperse population of particles with molecular weight of 6500KDa compatible with correctly assembled chimeric mI3-pilus protein NPs (Figure 19D). The presence of few contaminants has been observed also with this case. In fact, after 21 min from the beginning of the run some other proteins have been eluted from mI3-pilus sample suggesting the presence of a small amount of degraded portion. Moreover, further structural characterization of this protein based on DLS and transmission electron microscopy analysis, confirmed that the NPs are correctly structured with a diameter of 35-40nm (Figure 19 E-F). Resulting chimeric NPs were also particularly stable with a T_m detected in DSC of about 120°C (Figure 19G).



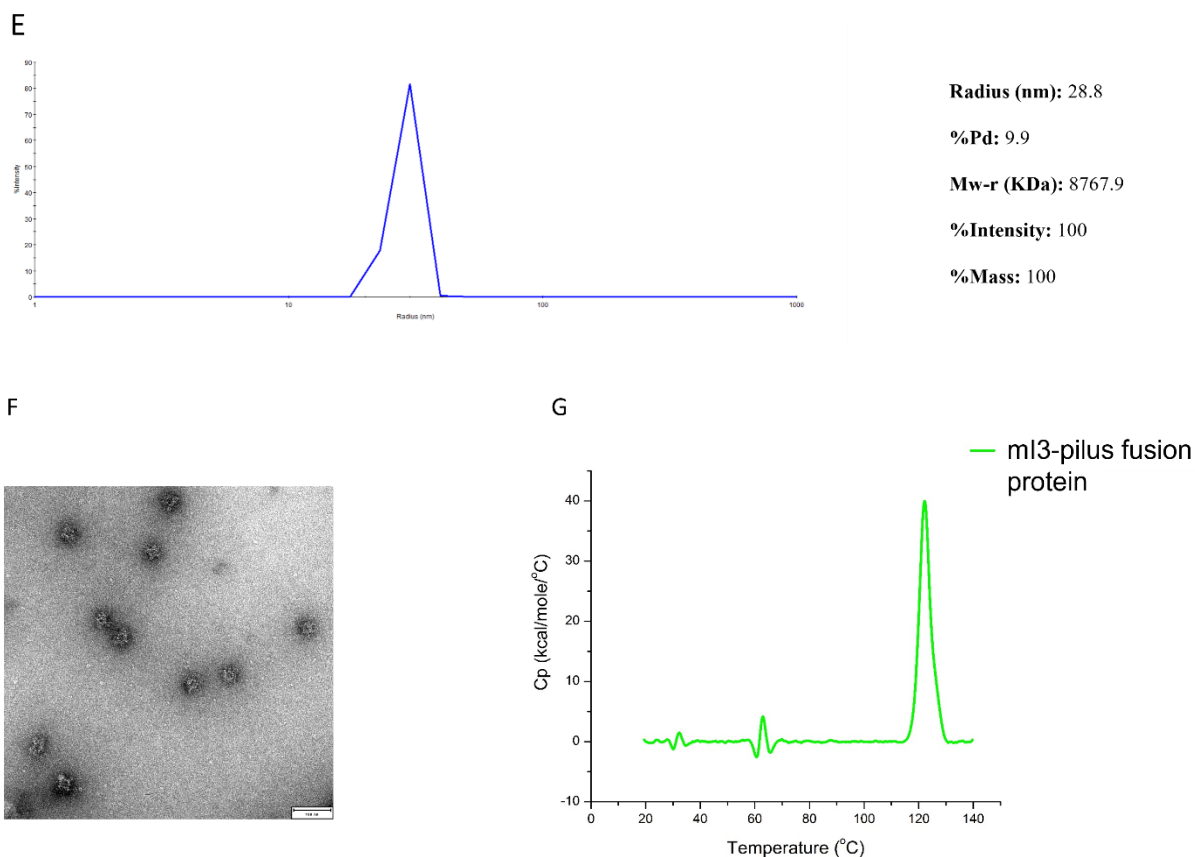


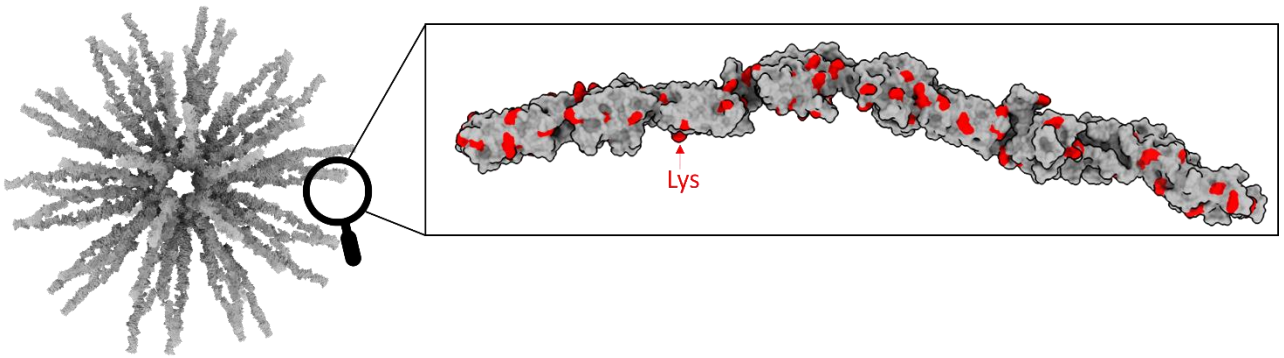
Figure 19: Production and characterization of mI3 pilus fusion protein. (A) Cartoon representation of predicted 3D structure of mI3-pilus fusion protein. In blue it is reported the mI3 scaffold while in grey the antigen (pilus fusion protein) exposed on the surface. Molecule representation and visualization has been performed with ChimeraX. (B) Chromatogram of SEC purification. Interest protein has been detected in the first peak highlighted in blue. (C) SDS-PAGE analysis of purified protein after SEC. The band indicated by the blue arrow correspond to mI3 pilus fusion protein with an estimated molecular weight of 148 kDa. Faint lower bands detected correspond to a degraded portion. (D) Chromatogram of SEC-MALS analysis of mI3 pilus fusion protein in blue and BSA used as standard in black. (E) DLS investigation of mI3 pilus fusion protein reporting the radius detected in function of signal intensity. (F) Transmission electron microscopy performed in negative staining confirms the presence of correctly assembled NPs. The scale bar reported is 100 nm. (G) Thermal stability evaluation with DSC revealed a T_m of about 120°C for mI3 pilus fusion protein.

13.3. Chimeric mI3-pilus fusion protein successfully conjugated with GBS PSII

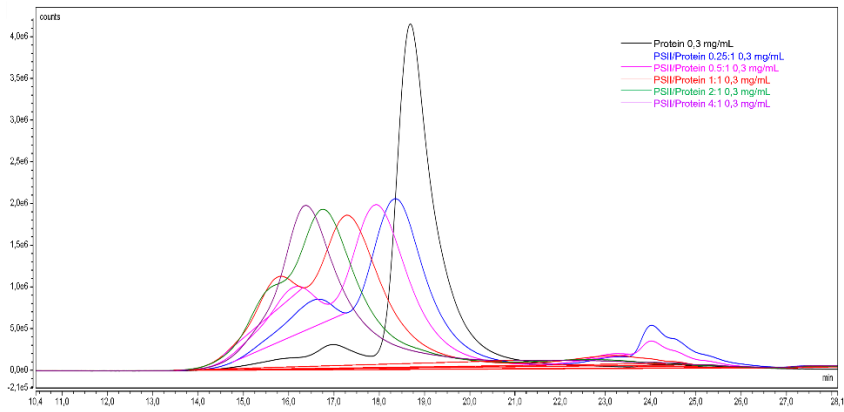
The high thermal stability of both pilus fusion protein and the chimeric mI3 produced, despite the presence of some degradation products, encouraged their further engineering. By combining structural and biochemical analysis almost 100 lysines have been identified to be well exposed on the surface of pilus fusion protein (Figure 20A). This result supported the possibility to firmly attach, at the exposed residues, a GBS sugar antigen. Basing on different CPS composition, ten distinct GBS serotypes have been identified [223]. Although serotype prevalence can change over time and geography, four main variants (Ia, II, III and V) have been detected in a large portion of invasive

isolates [318]. However, compared with the other CP types, the structure of CP type II is relatively simple making easier an *in vitro* chemical synthesis of this sugar. In this way no pathogenic bacteria must be manipulated and sugar with different lengths could be synthesized and tested. For these reasons PSII has been chosen to be chemically conjugated to mI3 pilus fusion protein obtaining a polyvalent molecule. The feasibility of this approach has been firstly assessed by an *in-silico* prediction with Rosetta software. As regarding the mI3-pilus fusion protein, the 3D rearrangement of the sugar on the chimera has been evaluated confirming the absence of clashes or steric hindrance. (Figure 20D). Both chimeric nanoparticle (mI3-pilus fusion protein) and the monomeric antigen (pilus fusion protein) have been activated and *in vitro* incubated with oxidated GBS PSII testing different ratios of protein/PSII. From the SE-HPLC analysis of the conjugation products, the ratios 4:1 and 2:1 resulted to be the best conditions to conjugate respectively mI3-pilus fusion protein and the monomeric protein antigen (Figure 20B-C) with the final ratio of saccharide/protein amount (μg) of 0.61 and 2,68 respectively. Desired conjugated proteins have been purified from the unconjugated protein as well as the exceeded sugar by centrifugation using a cut-off filter. Moreover, the electron microscopy analysis performed on mI3-pilus fusion protein, confirmed that the chimera has maintained its 3D structure and symmetric assembly even after the conjugation (Figure 20E). However, the presence of the sugar on the surface causes an increase of the adherence between the NPs (Figure 20E).

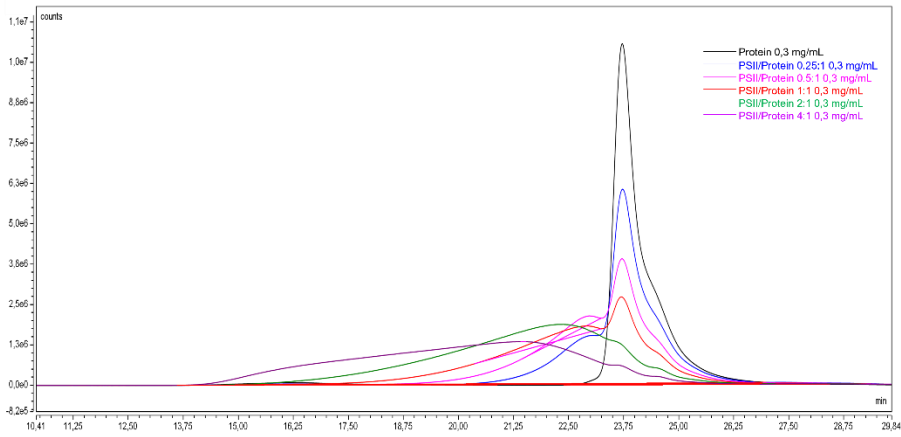
A



B



C



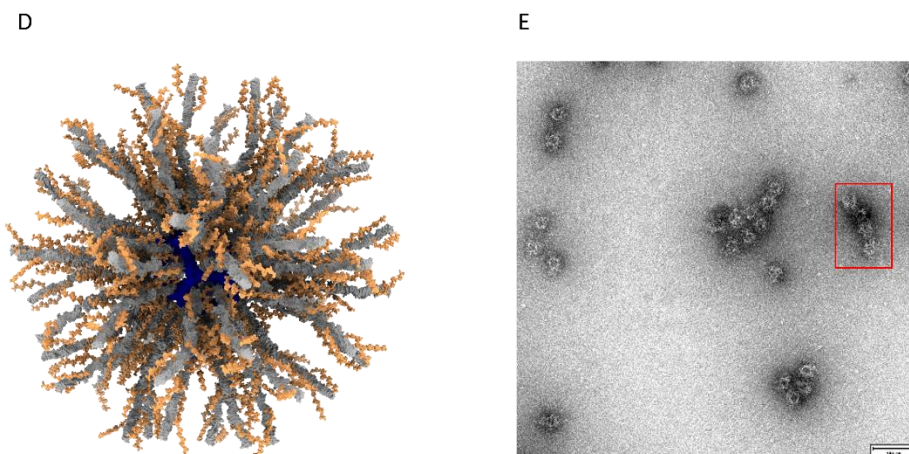


Figure 20: Chemical conjugation of GBS pilus fusion protein as monomeric antigen and displayed on mI3 surface. (A) Biochemical investigation of aminoacidic composition of pilus fusion protein reporting in red the identified exposed lysines (B-C) SE-HPLC chromatograms of conjugation products of mI3 pilus fusion protein (B) and monomeric antigen (C) obtained testing different ratios of protein/sugar (D) In silico prediction of 3D rearrangement of PSII on the surface of mI3-pilus fusion protein after chemical conjugation (E) TEM analysis of conjugated mI3-pilus fusion protein confirmed the presence of correctly assembled particles. Red section highlights NPs with tendency to adhere to each other. Images obtained with ChimeraX.

13.4. GBS PSII and pilus fusion protein are more immunogenic when displayed on mI3 surface

In order to evaluate the impact of the use of NP as scaffold on the immunogenicity elicited by both PSII and pilus fusion protein a preliminary *in vivo* study has been conducted in mice. Both antigens have been tested in different groups listed in the table 7. In particular, pilus fusion protein has been tested naked or conjugated with PSII and as monomeric antigen or displayed on mI3 surface. In addition, PSII conjugated with cross-reacting material 197 (CRM) [319] has been used as benchmark for the evaluation of PSII immunogenicity. Different antigen doses in formulation with Alum adjuvant [320] have been used to immunize 10 mice at day 1 and 22. Mice sera collected at day 0, 21 and 43 have been analysed with Luminex assay in order to evaluate the IgG titers raised against each antigen.

Table 7: Immunization scheme of the *in vivo* study reporting the antigens, the adjuvant and the doses used for the immunizations.

Group	Antigen-immunization 1	Antigen-Immunization 2	Adjuvant	Dose
1	PSII-CRM	PSII-CRM	Alum	0.5 ug
2	Pilus fusion protein	Pilus fusion protein	Alum	0,8 ug
3	Pilus fusion protein	Pilus fusion protein	Alum	3,2 ug
4	PSII-pilus fusion protein	PSII-pilus fusion protein	Alum	0.5 ug
5	PSII-Pilus fusion protein	PSII-Pilus fusion protein	Alum	2 ug
6	Pilus fusion protein-mI3	Pilus fusion protein-mI3	Alum	0,8 ug
7	Pilus fusion protein-mI3	Pilus fusion protein-mI3	Alum	3,2 ug
8	PSII Pilus fusion protein-mI3	PSII Pilus fusion protein-mI3	Alum	0.5 ug
9	PSII Pilus fusion protein-mI3	PSII Pilus fusion protein-mI3	Alum	2 ug

Results obtained showed that PSII is able to elicit the highest immune response when conjugated to a chimeric NP scaffold (Figure 21). In fact, 0.5 μ g of PSII conjugated with mI3-pilus fusion protein elicited an immune response 10 folds higher than its monomeric form (PSII-pilus fusion protein) and three times higher than the reference PSII-CRM. Accordingly, the IgG titers against PSII lower than the LLOQ (lower limit of quantification of 20.4 RLU/mL) have been detected in the negative controls represented by monomeric pilus fusion protein and chimeric mI3 displaying only the protein antigen.

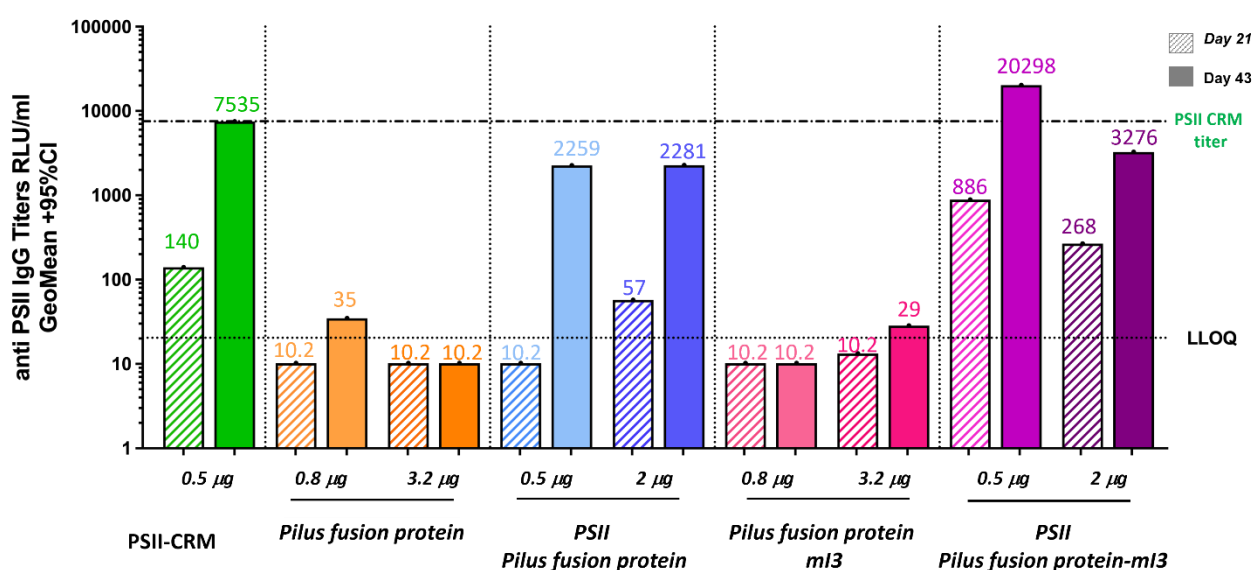


Figure 21: anti-PSII IgG titers evaluation by Luminex assay on pooled sera collected post 1 and post 2 doses. Graphical representation performed with GraphPad Prism.

As regarding the immunogenicity of pilus fusion protein, the naked antigen, at both concentrations tested, after 2 doses induced a higher IgG production compared to the conjugated form and to its multicopy display on mI3 (Figure 22). However, when the protein antigen is simultaneously conjugated with PSII and displayed on the NP surface, just 0.5 μ g of antigens are able to induce an immune response after one dose from 5 to 15 folds higher than the other doses and antigen tested. By increasing the dose up to 2 μ g, the same chimera induces the highest immune response both after first and second dose. In accordance, the number of antibodies specific for pilus fusion protein detected in the serum derived from CRM-PSII immunization is lower than limit of blank (LOB 0.3 RLU/mL). The result obtained highlights the advantages to multicopy display the target antigen on NP surface. In fact, by using NP scaffolds it is possible to use a lower antigen dose and potentially to also reduce the immunization numbers.

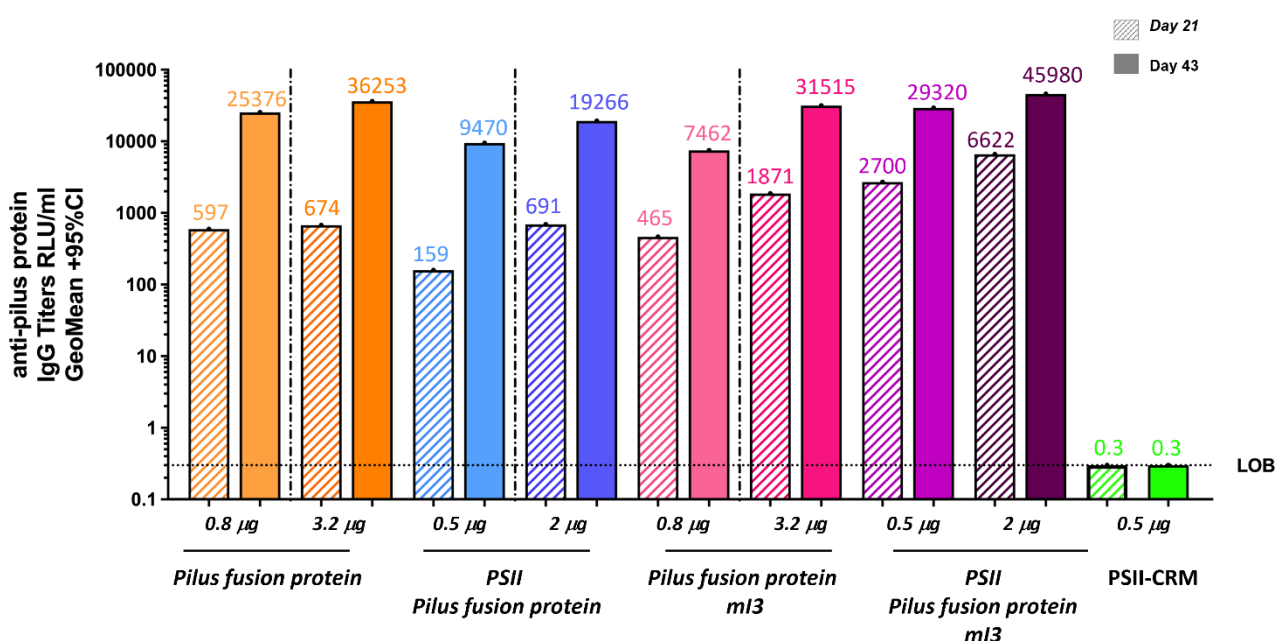


Figure 22: anti-pilus fusion protein IgG titers evaluation by Luminex assay on pooled sera collected post 1 and post 2 doses. Graphical representation performed with GraphPad Prism.

13.5. Discussion

Actually, polyvalent vaccines are one of the most powerful tools to protect from the infections of multiple pathogens [287]. Traditional polyvalent protein-based vaccines are composed by multiple recombinant antigens formulated in a single preparation. Therefore, their development is more challenging than the production of a mono-component vaccine. However, during the last years new approaches have been developed exploring the possibility to produce a single molecule comprising multiple antigens/epitopes. In this sense the use of self-assembling nanoparticles resulted to be crucial. In fact, their repetitive organization of subunits allows the multiple antigen display on a single

molecule. Although, the display of multiple protein antigens on a single NP has already been reported in literature, the NP decoration with different sugar antigens has not yet been explored [76, 206, 207]. By date, no published data are available about the NP decoration with simultaneously sugar and protein antigens. For these reasons, the work reported here has been conceived to fill this gap. Therefore, a polyvalent protein antigen has been developed starting from the GBS pilus proteins. Six different pilus domains and the entire BP 2b pilus protein have been successfully genetically fused in a single chimeric protein covering all BP variants of pilus type 2. The designed antigen has been then displayed in multiple copies through genetic fusion on mI3 surface. The intrinsic high stability of the chosen scaffold allowed the production of a properly folded chimera with an estimated diameter of 35-40nm. Some degradation occurred during the production process, but the expression condition and purification step can be improved to limit this process and to improve the quality of the final product. The chimera was able to maintain its structure even after the chemical conjugation with GBS PSII. Therefore, the combination of two different approaches (genetic fusions and chemical conjugation) allowed the production of the first polyvalent NP displaying both a protein and a sugar antigen. In addition, preliminary *in vivo* study conducted in mice revealed an increased immunogenicity of both antigens (pilus fusion protein and PSII) when simultaneously displayed on mI3 NP compared to all the other molecules tested. In particular, the anti-PSII-IgG titers induced by the polyvalent NP were higher even than IgG induced by the benchmark CRM-PSII. While as regarding the immunogenicity of the protein antigen an increased immunogenicity has been observed only in the case of the polyvalent NP. In fact, when the protein antigen is displayed on mI3 surface without the PSII its immunogenicity is comparable with the monomeric antigen. This is probably due to the partial degradation observed for this construct, which was removed when the chemical conjugation to the PSII occurred. For these reasons, further studies are needed to prevent antigen degradation and to better elucidate the NP contribution in the immunogenicity of pilus protein. *In vitro* assays are also needed to investigate the functionality of the elicited antibodies to neutralize GBS pathogenicity. However, all the results reported show the concrete possibility to combine multiple approaches to produce polyvalent molecules in few steps. In particular, mI3 NPs resulted to be a promising scaffold for the display of a protein antigen, even long fusion proteins, through genetic fusion as well as sugar antigens. In conclusions, the entire strategy adopted here could be further exploited to produce effective NP-based vaccines able to target multiple pathogens with a single preparation.

Conclusion and future perspective

Protein-based vaccines are safer than traditional vaccine preparations based on live-attenuated or killed pathogens [321]. However, the major drawback is the lower immune response induced by single purified proteins or oligo/polysaccharide components, and consequently fusion proteins with increased size, multiple doses and adjuvants are often required to achieve sufficient immunogenicity [12, 49, 322]. Moreover, the low efficiency of vaccine antigens could be due to immunologically subdominant but protective epitopes [323]. To overcome these issues, self-assembling protein NPs are now widely explored in vaccinology as scaffolds for antigen display [1]. In fact, the use of a larger scaffold combined with the multicopy display of target antigen allows an efficient activation of B-cell receptors and longer retention in lymphoid follicles [2]. The result is the potential induction of a potent B- and T-cell response. Currently, numerous chimeric NPs are under investigation in preclinical and clinical research world-wide [100, 205, 324]. In these studies, several different self-assembling protein NPs and VLPs have been decorated with protein antigens of interest through genetic fusion, protein ligation or chemical conjugation [112, 325, 326]. In literature are present several examples of viral antigens or small bacterial epitopes displayed on the surface of NP scaffold through genetic fusion [163, 164, 204, 306]. Only few examples of bacterial antigens displayed on NPs have been reported so far [165, 307]. Compared to other systems, the genetic fusion approach has the enormous advantage to allow the generation of the final nanoparticle by producing a single recombinant protein. However, it is essential that both scaffold and antigen preserve their correct structure after the fusion [54, 74]. This could be particularly challenging in the case of large and bulky antigens as well as multimeric proteins [1]. However, genetic fusion remains the more straightforward approach to produce chimeric NP displaying the protein antigen of interest. While for the display of sugar antigens on NP surface the chemical conjugation result to be the most suitable approach. During the years different chemical manipulations have been developed to firmly attach target saccharides on protein scaffolds for vaccine development [89, 118, 153].

In this context the present work had the aim to explore the use of self-assembling protein nanoparticles as platform for the display of protein/epitope and sugar antigens to develop new vaccine against bacterial pathogens. In order to achieve this goal, a preliminary study has been conducted to evaluate the feasibility to use genetic fusion for the display of a structured protein antigen (β barrel of fHbp v. 1.1) on the surface of six different NPs. From this study ferritin, mI3, encapsulin, CP3 and HBcAg have been identified as suitable scaffolds. It also emerged that the engineerization of NP exposed loops is more challenging than the modifications at the N-term. This result supported the setup of an innovative system for the epitope display. In fact, epitopes are usually inserted into the primary

sequence of the NP or attached on the surface by chemical conjugation or protein ligation systems in multi-step process. While the innovative strategy developed in this work is based on the use of a foreign protein scaffold (D3) engineered with the epitope of interest and then displayed on NP surface through genetic fusion. In this way the epitope is reasonably displayed with its native conformation, the possible epitope degradation is avoided, and the symmetric structure of the NP scaffold is maintained. Finally, nanoparticle platform has been exploited for the simultaneous display of two different types of antigens. In fact, taking advantage of the high intrinsic stability of protein NPs it has been possible to decorate it with both an extended protein and sugar antigens without destroy the scaffold structure.

In conclusion all the results achieved contribute to highlight the potentialities of nanoparticle technology and its impact in the development of new effective vaccines. In addition, this study lays the foundation for subsequent investigations. In particular, it would be interesting to better understand the impact of NP size, shape, geometry, and antigen density on the surface in the elicitation of a potent immune response *in vivo*. Moreover, the system developed for the decoration of NPs with epitopes could be further implemented by engineering two or more D3 sites with different epitopes at the same time. This could represent an additional approach applicable for polyvalent NPs production. These are just few examples of possible NP technology applications. Although not all potential NP engineerization have been tested, their further implementations could have a huge impact on vaccinology field.

Transparency statement and sponsorship

Luigia Cappelli is PhD students at University of Bologna and participate in a post graduate studentship program at GSK. This work was sponsored by GlaxoSmithKline Biologicals SA which was involved in all stages of the study conduct and analysis

Trademarks

Bexsero, Fendrix, Engerix-B, Cervarix, are trademarks owned by or licensed to the GSK group of companies. Trumenba is a registered trademark of Wyeth LLC, Pfizer Canada ULC, Licensee. Recombivax-HB, Gardasil 9 and HBvaxPRO are registered trademarks of Merck Sharp & Dohme LLC. GenHevac B is a trademark and brand of INSTITUT PASTEUR. Hecolin E is a trademark owned by XIAMEN INNOVAX BIOTECH CO., LTD.

References:

1. Lopez-Sagaseta, J., et al., *Self-assembling protein nanoparticles in the design of vaccines*. Comput Struct Biotechnol J, 2016. **14**: p. 58-68.
2. Nguyen, B. and N.H. Tolia, *Protein-based antigen presentation platforms for nanoparticle vaccines*. NPJ Vaccines, 2021. **6**(1): p. 70.
3. Khan, I., K. Saeed, and I. Khan, *Nanoparticles: Properties, applications and toxicities*. Arabian Journal of Chemistry, 2019. **12**(7): p. 908-931.
4. *Nano Tools Pave the Way to New Solutions in Infectious Disease*. ACS Infectious Diseases, 2017. **3**(8): p. 554-558.
5. Salata, O.V., *Applications of nanoparticles in biology and medicine*. Journal of nanobiotechnology, 2004. **2**(1): p. 3-3.
6. Astruc, D., *Introduction: Nanoparticles in Catalysis*. Chemical Reviews, 2020. **120**(2): p. 461-463.
7. Pantarotto, D., et al., *Immunization with peptide-functionalized carbon nanotubes enhances virus-specific neutralizing antibody responses*. 2003. **10**(10): p. 961-966.
8. Mah, C., et al., *Microsphere-mediated delivery of recombinant AAV vectors in vitro and in vivo*. 2000. **1**(5): p. S239-S242.
9. Bruchez, M., et al., *Semiconductor nanocrystals as fluorescent biological labels*. 1998. **281**(5385): p. 2013-2016.
10. Wang, S., et al., *Antigen/antibody immunocomplex from CdTe nanoparticle bioconjugates*. 2002. **2**(8): p. 817-822.
11. Mu, Q. and B. Yan, *Editorial: Nanoparticles in Cancer Therapy-Novel Concepts, Mechanisms, and Applications*. Front Pharmacol, 2018. **9**: p. 1552.
12. Kheirollahpour, M., et al., *Nanoparticles and Vaccine Development*. Pharm Nanotechnol, 2020. **8**(1): p. 6-21.
13. Mody, V.V., et al., *Introduction to metallic nanoparticles*. Journal of pharmacy & bioallied sciences, 2010. **2**(4): p. 282-289.
14. *Let's talk about lipid nanoparticles*. Nature Reviews Materials, 2021. **6**(2): p. 99-99.
15. Zielińska, A., et al., *Polymeric Nanoparticles: Production, Characterization, Toxicology and Ecotoxicology*. Molecules (Basel, Switzerland), 2020. **25**(16): p. 3731.
16. Hong, S., et al., *Protein-Based Nanoparticles as Drug Delivery Systems*. Pharmaceutics, 2020. **12**(7): p. 604.
17. Gautam, A., et al., *Recent Trends in Noble Metal Nanoparticles for Colorimetric Chemical Sensing and Micro-Electronic Packaging Applications*. Metals, 2021. **11**(2).
18. Carabineiro, S.A.C., *Applications of Gold Nanoparticles in Nanomedicine: Recent Advances in Vaccines*. Molecules (Basel, Switzerland), 2017. **22**(5): p. 857.
19. Jamkhande, P.G., et al., *Metal nanoparticles synthesis: An overview on methods of preparation, advantages and disadvantages, and applications*. Journal of Drug Delivery Science and Technology, 2019. **53**: p. 101174.
20. Marinescu, L., et al., *Optimized Synthesis Approaches of Metal Nanoparticles with Antimicrobial Applications*. Journal of Nanomaterials, 2020. **2020**: p. 1-14.
21. Ajdary, M., et al., *Health Concerns of Various Nanoparticles: A Review of Their in Vitro and in Vivo Toxicity*. Nanomaterials (Basel, Switzerland), 2018. **8**(9): p. 634.
22. Ganesan, P. and D. Narayanasamy, *Lipid nanoparticles: Different preparation techniques, characterization, hurdles, and strategies for the production of solid lipid nanoparticles and nanostructured lipid carriers for oral drug delivery*. Sustainable Chemistry and Pharmacy, 2017. **6**: p. 37-56.
23. Langer, R., *Biomaterials in Drug Delivery and Tissue Engineering: One Laboratory's Experience*. Accounts of Chemical Research, 2000. **33**(2): p. 94-101.

24. Kumari, R.M., et al., *Chapter 11 - Synthesis and evolution of polymeric nanoparticles: Development of an improved gene delivery system*, in *Design and Development of New Nanocarriers*, A.M. Grumezescu, Editor. 2018, William Andrew Publishing. p. 401-438.
25. Jacob, J., et al., *Biopolymer based nanomaterials in drug delivery systems: A review*. 2018. **9**: p. 43-55.
26. Langer, K., et al., *Optimization of the preparation process for human serum albumin (HSA) nanoparticles*. *International Journal of Pharmaceutics*, 2003. **257**(1): p. 169-180.
27. Saleh, T., T. Soudi, and S.A. Shojaosadati, *Aptamer functionalized curcumin-loaded human serum albumin (HSA) nanoparticles for targeted delivery to HER-2 positive breast cancer cells*. *International Journal of Biological Macromolecules*, 2019. **130**: p. 109-116.
28. Sahoo, N., et al., *Recent advancement of gelatin nanoparticles in drug and vaccine delivery*. *International Journal of Biological Macromolecules*, 2015. **81**: p. 317-331.
29. Sabra, S.A., et al., *Self-assembled amphiphilic zein-lactoferrin micelles for tumor targeted co-delivery of rapamycin and wogonin to breast cancer*. *European Journal of Pharmaceutics and Biopharmaceutics*, 2018. **128**: p. 156-169.
30. Tarhini, M., H. Greige-Gerges, and A. Elaissari, *Protein-based nanoparticles: From preparation to encapsulation of active molecules*. *International Journal of Pharmaceutics*, 2017. **522**(1): p. 172-197.
31. Shively Jm Fau - Ball, F., et al., *Functional organelles in prokaryotes: polyhedral inclusions (carboxysomes) of Thiobacillus neapolitanus*. (0036-8075 (Print)).
32. Corchero, J.L. and J. Cedano, *Self-assembling, protein-based intracellular bacterial organelles: emerging vehicles for encapsulating, targeting and delivering therapeutical cargoes*. *Microbial Cell Factories*, 2011. **10**(1): p. 92.
33. Cheng, S., et al., *Bacterial microcompartments: their properties and paradoxes*. (1521-1878 (Electronic)).
34. Gabashvili, A.N., et al., *Encapsulins-Bacterial Protein Nanocompartments: Structure, Properties, and Application*. *Biomolecules*, 2020. **10**(6).
35. Sutter, M., et al., *Structural basis of enzyme encapsulation into a bacterial nanocompartment*. *Nat Struct Mol Biol*, 2008. **15**(9): p. 939-47.
36. Goel, D. and S. Sinha, *Naturally occurring protein nano compartments: basic structure, function, and genetic engineering*. *Nano Express*, 2021. **2**(4).
37. Wang, W., et al., *Serum ferritin: Past, present and future*. *Biochimica et Biophysica Acta (BBA) - General Subjects*, 2010. **1800**(8): p. 760-769.
38. Benner, N.L., et al., *Vault Nanoparticles: Chemical Modifications for Imaging and Enhanced Delivery*. *ACS Nano*, 2017. **11**(1): p. 872-881.
39. Kickhoefer, V.A., et al., *Vaults are up-regulated in multidrug-resistant cancer cell lines*. (0021-9258 (Print)).
40. Nooraie, S., et al., *Virus-like particles: preparation, immunogenicity and their roles as nanovaccines and drug nanocarriers*. *Journal of Nanobiotechnology*, 2021. **19**(1): p. 59.
41. Takahashi, W.N. and M. Ishii, *An Abnormal Protein Associated with Tobacco Mosaic Virus Infection*. *Nature*, 1952. **169**(4297): p. 419-420.
42. Bari, N.K., et al., *Nanoparticle Fabrication on Bacterial Microcompartment Surface for the Development of Hybrid Enzyme-Inorganic Catalyst*. *ACS Catalysis*, 2018. **8**(9): p. 7742-7748.
43. Wang, Z., et al., *Functional ferritin nanoparticles for biomedical applications*. *Frontiers of chemical science and engineering*, 2017. **11**(4): p. 633-646.
44. Rome, L.H. and V.A. Kickhoefer, *Development of the Vault Particle as a Platform Technology*. *ACS Nano*, 2013. **7**(2): p. 889-902.
45. Ding, X., et al., *Virus-Like Particle Engineering: From Rational Design to Versatile Applications*. (1860-7314 (Electronic)).
46. Riedel, S., *Edward Jenner and the history of smallpox and vaccination*. *Proceedings (Baylor University Medical Center)*, 2005. **18**(1): p. 21-25.
47. Hinman, A., *Eradication of vaccine-preventable diseases*. (0163-7525 (Print)).
48. Plotkin, S., *History of vaccination*. 2014. **111**(34): p. 12283-12287.

49. Pati, R., M. Shevtsov, and A. Sonawane, *Nanoparticle Vaccines Against Infectious Diseases*. Frontiers in Immunology, 2018. **9**.
50. Nascimento, I.P. and L.C.C. Leite, *Recombinant vaccines and the development of new vaccine strategies*. Brazilian journal of medical and biological research = Revista brasileira de pesquisas medicas e biologicas, 2012. **45**(12): p. 1102-1111.
51. Ahire, E.D. and S.J. Kshirsagar, *Immune responses induced by different vaccine platforms against coronavirus disease-19*. 2021: p. 243-257.
52. Kaiser, C.R., et al., *Biodistribution studies of protein cage nanoparticles demonstrate broad tissue distribution and rapid clearance in vivo*. (1176-9114 (Print)).
53. Leeds, I.L. and S.H. Fang, *Anal cancer and intraepithelial neoplasia screening: A review*. (1948-9366 (Print)).
54. Bachmann, M.F. and G.T. Jennings, *Vaccine delivery: a matter of size, geometry, kinetics and molecular patterns*. Nature Reviews Immunology, 2010. **10**(11): p. 787-796.
55. Li, Y., M. Kröger, and W.K.J.N. Liu, *Shape effect in cellular uptake of PEGylated nanoparticles: comparison between sphere, rod, cube and disk*. 2015. **7**(40): p. 16631-16646.
56. Verma, A. and F.J.s. Stellacci, *Effect of surface properties on nanoparticle–cell interactions*. 2010. **6**(1): p. 12-21.
57. Gerin, J.L., P.V. Holland, and R.H. Purcell, *Australia Antigen: Large-Scale Purification from Human Serum and Biochemical Studies of Its Proteins*. Journal of Virology, 1971. **7**(5): p. 569-576.
58. Hilleman, M.R.J.V., *Vaccines in historic evolution and perspective: a narrative of vaccine discoveries*. 2000. **18**(15): p. 1436-1447.
59. Keating, G.M. and S. Noble, *Recombinant hepatitis B vaccine (Engerix-B): a review of its immunogenicity and protective efficacy against hepatitis B*. (0012-6667 (Print)).
60. Van Damme, P., et al., *Safety, tolerability and immunogenicity of a recombinant hepatitis B vaccine manufactured by a modified process in healthy young adults*. Human Vaccines, 2009. **5**(2): p. 92-97.
61. Soulie, J., et al., *Immunogenicity and safety in newborns of a new recombinant hepatitis B vaccine containing the S and pre-S2 antigens*. 1991. **9**(8): p. 545-548.
62. Beran, J.J.E.o.o.b.t., *Safety and immunogenicity of a new hepatitis B vaccine for the protection of patients with renal insufficiency including pre-haemodialysis and haemodialysis patients*. 2008. **8**(2): p. 235-247.
63. Cimica, V. and J.M. Galarza, *Adjuvant formulations for virus-like particle (VLP) based vaccines*. Clinical Immunology, 2017. **183**: p. 99-108.
64. Zhang, X., et al., *Robust manufacturing and comprehensive characterization of recombinant hepatitis E virus-like particles in Hecolin®*. (1873-2518 (Electronic)).
65. Wu, X., et al., *Hepatitis E virus: Current epidemiology and vaccine*. Human vaccines & immunotherapeutics, 2016. **12**(10): p. 2603-2610.
66. Cheng, L., Y. Wang, and J. Du, *Human Papillomavirus Vaccines: An Updated Review*. Vaccines, 2020. **8**(3): p. 391.
67. Brianti, P., E. De Flammineis, and S.R. Mercuri, *Review of HPV-related diseases and cancers*. (1121-7138 (Print)).
68. O'Rourke, J.P., D.S. Peabody, and B. Chackerian, *Affinity selection of epitope-based vaccines using a bacteriophage virus-like particle platform*. Curr Opin Virol, 2015. **11**: p. 76-82.
69. Wang, J.W. and R.B.S. Roden, *Virus-like particles for the prevention of human papillomavirus-associated malignancies*. Expert review of vaccines, 2013. **12**(2): p. 129-141.
70. Ljubojević, S., *The human papillomavirus vaccines*. (1330-027X (Print)).
71. Han, J.A., et al., *Ferritin protein cage nanoparticles as versatile antigen delivery nanoplatforms for dendritic cell (DC)-based vaccine development*. (1549-9642 (Electronic)).
72. Neek, M., et al., *Co-delivery of human cancer-testis antigens with adjuvant in protein nanoparticles induces higher cell-mediated immune responses*. Biomaterials, 2018. **156**: p. 194-203.
73. Molino, N.M., et al., *Biomimetic protein nanoparticles facilitate enhanced dendritic cell activation and cross-presentation*. 2013. **7**(11): p. 9743-9752.

74. Mohsen, M.O., et al., *Major findings and recent advances in virus-like particle (VLP)-based vaccines*. *Seminars in Immunology*, 2017. **34**: p. 123-132.
75. Laurens, M.B., *RTS,S/AS01 vaccine (Mosquirix™): an overview*. *Human vaccines & immunotherapeutics*, 2020. **16**(3): p. 480-489.
76. Wilby, K.J., et al., *Mosquirix (RTS,S): A Novel Vaccine for the Prevention of Plasmodium falciparum Malaria*. *Annals of Pharmacotherapy*, 2012. **46**(3): p. 384-393.
77. Dame John, B., et al., *Structure of the Gene Encoding the Immunodominant Surface Antigen on the Sporozoite of the Human Malaria Parasite Plasmodium falciparum*. *Science*, 1984. **225**(4662): p. 593-599.
78. Oyarzún, P. and B. Kobe, *Recombinant and epitope-based vaccines on the road to the market and implications for vaccine design and production*. *Human Vaccines & Immunotherapeutics*, 2015. **12**(3): p. 763-767.
79. Tan, M. and X. Jiang, *Norovirus Capsid Protein-Derived Nanoparticles and Polymers as Versatile Platforms for Antigen Presentation and Vaccine Development*. *Pharmaceutics*, 2019. **11**(9): p. 472.
80. Tan, M. and X. Jiang, *Norovirus P particle: a subviral nanoparticle for vaccine development against norovirus, rotavirus and influenza virus*. *Nanomedicine (London, England)*, 2012. **7**(6): p. 889-897.
81. Jiang, P., et al., *Hepatitis B virus core antigen as a carrier for Chlamydia trachomatis MOMP multi-epitope peptide enhances protection against genital chlamydial infection*. *Oncotarget*; Vol 6, No 41, 2015.
82. Webster, E.A.-O., et al., *Immunogenicity and Protective Capacity of a Virus-like Particle Vaccine against Chlamydia trachomatis Type 3 Secretion System Tip Protein, CT584*. *LID - 10.3390/vaccines10010111 [doi] LID - 111*. (2076-393X (Print)).
83. Sun, W., et al., *The self-assembled nanoparticle-based trimeric RBD mRNA vaccine elicits robust and durable protective immunity against SARS-CoV-2 in mice*. *Signal Transduction and Targeted Therapy*, 2021. **6**(1): p. 340.
84. Li, H.A.-O., et al., *Self-Assembling Nanoparticle Vaccines Displaying the Receptor Binding Domain of SARS-CoV-2 Elicit Robust Protective Immune Responses in Rhesus Monkeys*. (1520-4812 (Electronic)).
85. Zhang, B., et al., *A platform incorporating trimeric antigens into self-assembling nanoparticles reveals SARS-CoV-2-spike nanoparticles to elicit substantially higher neutralizing responses than spike alone*. *Sci Rep*, 2020. **10**(1): p. 18149.
86. Pollard, A.J. and E.M. Bijker, *A guide to vaccinology: from basic principles to new developments*. *Nature Reviews Immunology*, 2021. **21**(2): p. 83-100.
87. Jennings, G.T. and M.F. Bachmann, *The coming of age of virus-like particle vaccines*. 2008. **389**(5): p. 521-536.
88. Kotsuchibashi, Y., Y. Nakagawa, and M. Ebara, *2.1 - Nanoparticles*, in *Biomaterials Nanoarchitectonics*, M. Ebara, Editor. 2016, William Andrew Publishing. p. 7-23.
89. Lu, L., et al., *Chemical Conjugation Strategies for the Development of Protein-Based Subunit Nanovaccines*. *Vaccines (Basel)*, 2021. **9**(6).
90. Rajabi, M., M. Srinivasan, and S.A. Mousa, *Chapter 1 - Nanobiomaterials in drug delivery*, in *Nanobiomaterials in Drug Delivery*, A.M. Grumezescu, Editor. 2016, William Andrew Publishing. p. 1-37.
91. Wu, Z., et al., *Development of viral nanoparticles for efficient intracellular delivery*. 2012. **4**(11): p. 3567-3576.
92. Rostovtsev, V.V., et al., *A stepwise huisgen cycloaddition process: copper (I)-catalyzed regioselective "ligation" of azides and terminal alkynes*. 2002. **114**(14): p. 2708-2711.
93. Tsuchikama, K. and Z. An, *Antibody-drug conjugates: recent advances in conjugation and linker chemistries*. *Protein & Cell*, 2018. **9**(1): p. 33-46.
94. Oshimura, E. and K. Sakamoto, *Chapter 19 - Amino Acids, Peptides, and Proteins*, in *Cosmetic Science and Technology*, K. Sakamoto, et al., Editors. 2017, Elsevier: Amsterdam. p. 285-303.
95. Hossain, M.K., et al., *Liposomal Fc Domain Conjugated to a Cancer Vaccine Enhances Both Humoral and Cellular Immunity*. *ACS Omega*, 2019. **4**(3): p. 5204-5208.

96. Bloom, S., et al., *Decarboxylative alkylation for site-selective bioconjugation of native proteins via oxidation potentials*. *Nat Chem*, 2018. **10**(2): p. 205-211.
97. Sanchez-Villamil Javier, I., et al., *Development of a Gold Nanoparticle Vaccine against Enterohemorrhagic Escherichia coli O157:H7*. *mBio*. **10**(4): p. e01869-19.
98. Berti, F. and R. Adamo, *Antimicrobial glycoconjugate vaccines: an overview of classic and modern approaches for protein modification*. *Chem Soc Rev*, 2018. **47**(24): p. 9015-9025.
99. Akache, B., et al., *Anti-IgE Qb-VLP Conjugate Vaccine Self-Adjuvants through Activation of TLR7*. *Vaccines*, 2016. **4**(1): p. 3.
100. Maurer, P., et al., *A therapeutic vaccine for nicotine dependence: preclinical efficacy, and Phase I safety and immunogenicity*. 2005. **35**(7): p. 2031-2040.
101. Ambühl, P.M., et al., *A vaccine for hypertension based on virus-like particles: preclinical efficacy and phase I safety and immunogenicity*. 2007. **25**(1): p. 63-72.
102. WinbladB, A.J.L., *Safety, tolerability, and antibody response of active Abeta immunotherapy with CAD106 in patients with Alzheimer's disease: randomised, double-blind, placebo-controlled, first-in-human study*. 2012. **11**(7): p. 597-604.
103. Farlow, M.R., et al., *Long-term treatment with active Aβ immunotherapy with CAD106 in mild Alzheimer's disease*. 2015. **7**(1): p. 1-13.
104. Koho, T., et al., *His-tagged norovirus-like particles: A versatile platform for cellular delivery and surface display*. (1873-3441 (Electronic)).
105. Fairhead, M., et al., *Plug-and-play pairing via defined divalent streptavidins*. (1089-8638 (Electronic)).
106. Thrane, S., et al., *A Novel Virus-Like Particle Based Vaccine Platform Displaying the Placental Malaria Antigen VAR2CSA*. *PLOS ONE*, 2015. **10**(11): p. e0143071.
107. Mazzucchelli, S., et al., *Orientation-controlled conjugation of haloalkane dehalogenase fused homing peptides to multifunctional nanoparticles for the specific recognition of cancer cells*. (1521-3773 (Electronic)).
108. Colombo, M., et al., *Protein oriented ligation on nanoparticles exploiting O6-alkylguanine-DNA transferase (SNAP) genetically encoded fusion*. (1613-6829 (Electronic)).
109. Tang, S., et al., *A Modular Vaccine Development Platform Based on Sortase-Mediated Site-Specific Tagging of Antigens onto Virus-Like Particles*. (2045-2322 (Electronic)).
110. Muik, A., et al., *Covalent coupling of high-affinity ligands to the surface of viral vector particles by protein trans-splicing mediates cell type-specific gene transfer*. (1878-5905 (Electronic)).
111. Reddington, S.C. and M. Howarth, *Secrets of a covalent interaction for biomaterials and biotechnology: SpyTag and SpyCatcher*. (1879-0402 (Electronic)).
112. Brune, K.D. and M. Howarth, *New Routes and Opportunities for Modular Construction of Particulate Vaccines: Stick, Click, and Glue*. *Frontiers in immunology*, 2018. **9**: p. 1432-1432.
113. Pitoiset, F., B. Vazquez T Fau - Bellier, and B. Bellier, *Enveloped virus-like particle platforms: vaccines of the future?* (1744-8395 (Electronic)).
114. Graham, B.A.-O. and N.J. Sullivan, *Emerging viral diseases from a vaccinology perspective: preparing for the next pandemic*. (1529-2916 (Electronic)).
115. Brune, K.D., et al., *Dual Plug-and-Display Synthetic Assembly Using Orthogonal Reactive Proteins for Twin Antigen Immunization*. *Bioconjugate Chemistry*, 2017. **28**(5): p. 1544-1551.
116. Ma, X., et al., *Nanoparticle Vaccines Based on the Receptor Binding Domain (RBD) and Heptad Repeat (HR) of SARS-CoV-2 Elicit Robust Protective Immune Responses*. (1097-4180 (Electronic)).
117. Singh, S.K., et al., *Improving the malaria transmission-blocking activity of a Plasmodium falciparum 48/45 based vaccine antigen by SpyTag/SpyCatcher mediated virus-like display*. *Vaccine*, 2017. **35**(30): p. 3726-3732.
118. Wichgers Schreur, P.J., et al., *Vaccine Efficacy of Self-Assembled Multimeric Protein Scaffold Particles Displaying the Glycoprotein Gn Head Domain of Rift Valley Fever Virus*. *Vaccines*, 2021. **9**(3).
119. Perotti, M. and L. Perez, *Virus-Like Particles and Nanoparticles for Vaccine Development against HCMV*. *Viruses*, 2019. **12**(1): p. 35.

120. Sadeyen, J.-R.é., et al., *Insertion of a foreign sequence on capsid surface loops of human papillomavirus type 16 virus-like particles reduces their capacity to induce neutralizing antibodies and delineates a conformational neutralizing epitope*. *Virology*, 2003. **309**(1): p. 32-40.
121. Zykova, A.A., et al., *Highly Immunogenic Nanoparticles Based on a Fusion Protein Comprising the M2e of Influenza A Virus and a Lipopeptide*. *Viruses*, 2020. **12**(10).
122. Chen, X., J.L. Zaro, and W.-C. Shen, *Fusion protein linkers: property, design and functionality*. *Advanced drug delivery reviews*, 2013. **65**(10): p. 1357-1369.
123. Le, D.T. and K.M. Muller, *In Vitro Assembly of Virus-Like Particles and Their Applications*. *Life (Basel)*, 2021. **11**(4).
124. Tariq, H., et al., *Virus-Like Particles: Revolutionary Platforms for Developing Vaccines Against Emerging Infectious Diseases*. *Frontiers in Microbiology*, 2022. **12**.
125. Zhang, W., et al., *Rationally Designed Protein Building Blocks for Programmable Hierarchical Architectures*. *Frontiers in chemistry*, 2020. **8**: p. 587975-587975.
126. King, N.P., et al., *Computational design of self-assembling protein nanomaterials with atomic level accuracy*. *Science (New York, N.Y.)*, 2012. **336**(6085): p. 1171-1174.
127. Nassal, M. and H. Schaller, *Hepatitis B virus replication*. *Trends in Microbiology*, 1993. **1**(6): p. 221-228.
128. Cohen, B.J. and J.E. Richmond, *Electron microscopy of hepatitis B core antigen synthesized in E. coli*. *Nature*, 1982. **296**(5858): p. 677-678.
129. Crowther, R.A., et al., *Three-dimensional structure of hepatitis B virus core particles determined by electron cryomicroscopy*. (0092-8674 (Print)).
130. Zlotnick, A., et al., *Dimorphism of Hepatitis B Virus Capsids Is Strongly Influenced by the C-Terminus of the Capsid Protein*. *Biochemistry*, 1996. **35**(23): p. 7412-7421.
131. Crowther, R.A., et al., *Three-dimensional structure of hepatitis B virus core particles determined by electron cryomicroscopy*. *Cell*, 1994. **77**(6): p. 943-950.
132. Moradi Vahdat, M., et al., *Hepatitis B core-based virus-like particles: A platform for vaccine development in plants*. *Biotechnology reports (Amsterdam, Netherlands)*, 2021. **29**: p. e00605-e00605.
133. Brown, A., et al., *Foreign epitopes in immunodominant regions of hepatitis B core particles are highly immunogenic and conformationally restricted*. 1991. **9**(8): p. 595-601.
134. Gregson, A.L., et al., *Phase I Trial of an Alhydrogel Adjuvanted Hepatitis B Core Virus-Like Particle Containing Epitopes of Plasmodium falciparum Circumsporozoite Protein*. *PLOS ONE*, 2008. **3**(2): p. e1556.
135. Zahmanova, G., et al., *Efficient Production of Chimeric Hepatitis B Virus-Like Particles Bearing an Epitope of Hepatitis E Virus Capsid by Transient Expression in Nicotiana benthamiana*. *Life (Basel)*, 2021. **11**(1).
136. Walker, A., C. Skamel, and M. Nassal, *SplitCore: an exceptionally versatile viral nanoparticle for native whole protein display regardless of 3D structure*. *Sci Rep*, 2011. **1**: p. 5.
137. Peyret, H., et al., *Tandem Fusion of Hepatitis B Core Antigen Allows Assembly of Virus-Like Particles in Bacteria and Plants with Enhanced Capacity to Accommodate Foreign Proteins*. *PLOS ONE*, 2015. **10**(4): p. e0120751.
138. Yang, M., et al., *Virus-like particles that display Zika virus envelope protein domain III induce potent neutralizing immune responses in mice*. *Scientific Reports*, 2017. **7**(1): p. 7679.
139. Whitacre, D.C., B.O. Lee, and D.R. Milich, *Use of hepadnavirus core proteins as vaccine platforms*. *Expert review of vaccines*, 2009. **8**(11): p. 1565-1573.
140. Golmohammadi, R., et al., *The crystal structure of bacteriophage Q β at 3.5 Å resolution*. *Structure*, 1996. **4**(5): p. 543-554.
141. Takamatsu H Fau - Iso, K. and K. Iso, *Chemical evidence for the capsomeric structure of phage q beta*. (0028-0836 (Print)).
142. Caspar, D.L. and A. Klug, *Physical principles in the construction of regular viruses*. *Cold Spring Harb Symp Quant Biol*, 1962. **27**: p. 1-24.

143. Rumnieks, J. and K. Tars, *Crystal Structure of the Bacteriophage Q β Coat Protein in Complex with the RNA Operator of the Replicase Gene*. *Journal of Molecular Biology*, 2014. **426**(5): p. 1039-1049.
144. Ponchon, L., et al., *Co-expression of RNA-protein complexes in Escherichia coli and applications to RNA biology*. (1362-4962 (Electronic)).
145. Rhee, J.-K., et al., *Colorful Virus-like Particles: Fluorescent Protein Packaging by the Q β Capsid*. *Biomacromolecules*, 2011. **12**(11): p. 3977-3981.
146. Fiedler, J.D., et al., *RNA-directed packaging of enzymes within virus-like particles*. *Angewandte Chemie (International ed. in English)*, 2010. **49**(50): p. 9648-9651.
147. Witherell, G.W. and O.C. Uhlenbeck, *Specific RNA binding by Q beta coat protein*. (0006-2960 (Print)).
148. Ashcroft, A.E., et al., *Engineering thermal stability in RNA phage capsids via disulphide bonds*. (1533-4880 (Print)).
149. Fiedler, J.D., et al., *Engineered mutations change the structure and stability of a virus-like particle*. *Biomacromolecules*, 2012. **13**(8): p. 2339-2348.
150. Freivalds, J., et al., *Assembly of bacteriophage Qbeta virus-like particles in yeast Saccharomyces cerevisiae and Pichia pastoris*. *J Biotechnol*, 2006. **123**(3): p. 297-303.
151. Kozlovska, T.M., et al., *Recombinant RNA phage Q beta capsid particles synthesized and self-assembled in Escherichia coli*. (0378-1119 (Print)).
152. Bundy, B.C., J.R. Franciszkowicz Mj Fau - Swartz, and J.R. Swartz, *Escherichia coli-based cell-free synthesis of virus-like particles*. (1097-0290 (Electronic)).
153. Patel, K.G. and J.R. Swartz, *Surface Functionalization of Virus-Like Particles by Direct Conjugation Using Azide-Alkyne Click Chemistry*. *Bioconjugate Chemistry*, 2011. **22**(3): p. 376-387.
154. Yin, Z., et al., *Antitumor Humoral and T Cell Responses by Mucin-1 Conjugates of Bacteriophage Q β in Wild-type Mice*. *ACS Chemical Biology*, 2018. **13**(6): p. 1668-1676.
155. Guo, Y., et al., *Chimeric Virus-like Particles of Universal Antigen Epitopes of Coronavirus and Phage Q β Coat Protein Trigger the Production of Neutralizing Antibodies*. (1873-4294 (Electronic)).
156. Kündig, T.M., et al., *Der p 1 peptide on virus-like particles is safe and highly immunogenic in healthy adults*. 2006. **117**(6): p. 1470-1476.
157. Senti, G., et al., *Use of A-type CpG oligodeoxynucleotides as an adjuvant in allergen-specific immunotherapy in humans: a phase I/IIa clinical trial*. 2009. **39**(4): p. 562-570.
158. Goldinger, S.M., et al., *Nano-particle vaccination combined with TLR-7 and-9 ligands triggers memory and effector CD 8+ T-cell responses in melanoma patients*. 2012. **42**(11): p. 3049-3061.
159. Palladini, A., et al., *Virus-like particle display of HER2 induces potent anti-cancer responses*. (2162-4011 (Print)).
160. Shishovs, M., et al., *Structure of AP205 Coat Protein Reveals Circular Permutation in ssRNA Bacteriophages*. *J Mol Biol*, 2016. **428**(21): p. 4267-4279.
161. Peabody, D.S., et al., *RNA Phage VLP-Based Vaccine Platforms*. *Pharmaceuticals (Basel, Switzerland)*, 2021. **14**(8): p. 764.
162. Tissot, A.C., et al., *Versatile virus-like particle carrier for epitope based vaccines*. (1932-6203 (Electronic)).
163. Liu, X., et al., *AP205 VLPs Based on Dimerized Capsid Proteins Accommodate RBM Domain of SARS-CoV-2 and Serve as an Attractive Vaccine Candidate*. *LID - 10.3390/vaccines9040403 [doi] LID - 403*. (2076-393X (Print)).
164. Fougereux, C., et al., *Capsid-like particles decorated with the SARS-CoV-2 receptor-binding domain elicit strong virus neutralization activity*. *Nat Commun*, 2021. **12**(1): p. 324.
165. Govasli, M.L., Y. Diaz, and P. Puntervoll, *Virus-like particle-display of the enterotoxigenic Escherichia coli heat-stable toxoid STh-A14T elicits neutralizing antibodies in mice*. (1873-2518 (Electronic)).
166. Thrane, S., et al., *Bacterial superglue enables easy development of efficient virus-like particle based vaccines*. *Journal of nanobiotechnology*, 2016. **14**: p. 30-30.
167. Fredsgaard, L., et al., *Head-to-Head Comparison of Modular Vaccines Developed Using Different Capsid Virus-Like Particle Backbones and Antigen Conjugation Systems*. *Vaccines*, 2021. **9**(6).
168. Bruun, T.U.J., et al., *Engineering a Rugged Nanoscaffold To Enhance Plug-and-Display Vaccination*. *ACS Nano*, 2018. **12**(9): p. 8855-8866.

169. Harrison, P.M. and P. Arosio, *The ferritins: molecular properties, iron storage function and cellular regulation*. Biochimica et Biophysica Acta (BBA) - Bioenergetics, 1996. **1275**(3): p. 161-203.
170. Cho, K.J., et al., *The crystal structure of ferritin from Helicobacter pylori reveals unusual conformational changes for iron uptake*. J Mol Biol, 2009. **390**(1): p. 83-98.
171. Aumiller, W.M., M. Uchida, and T. Douglas, *Protein cage assembly across multiple length scales*. Chemical Society reviews, 2018. **47**(10): p. 3433-3469.
172. Zhang, Y. and B.P. Orner, *Self-assembly in the ferritin nano-cage protein superfamily*. (1422-0067 (Electronic)).
173. Lin, X., et al., *Chimeric ferritin nanocages for multiple function loading and multimodal imaging*. (1530-6992 (Electronic)).
174. Tripathi, N.K. and A. Shrivastava, *Recent Developments in Bioprocessing of Recombinant Proteins: Expression Hosts and Process Development*. Front Bioeng Biotechnol, 2019. **7**: p. 420.
175. Sun, W., et al., *Salt-Dependent Aggregation and Assembly of E coli-Expressed Ferritin*. Dose-response : a publication of International Hormesis Society, 2016. **14**(1): p. 1559325816632102-1559325816632102.
176. Liang, M., et al., *H-ferritin-nanocaged doxorubicin nanoparticles specifically target and kill tumors with a single-dose injection*. (1091-6490 (Electronic)).
177. Zhen, Z., et al., *Ferritin nanocages to encapsulate and deliver photosensitizers for efficient photodynamic therapy against cancer*. (1936-086X (Electronic)).
178. Khoshnejad, M., et al., *Ferritin-based drug delivery systems: Hybrid nanocarriers for vascular immunotargeting*. Journal of controlled release : official journal of the Controlled Release Society, 2018. **282**: p. 13-24.
179. Kanekiyo, M., et al., *Self-assembling influenza nanoparticle vaccines elicit broadly neutralizing H1N1 antibodies*. Nature, 2013. **499**(7456): p. 102-106.
180. Wang, L., et al., *Structure-based design of ferritin nanoparticle immunogens displaying antigenic loops of Neisseria gonorrhoeae*. FEBS Open Bio, 2017. **7**(8): p. 1196-1207.
181. Valdés-Stauber, N. and S. Scherer, *Isolation and characterization of Linocin M18, a bacteriocin produced by Brevibacterium linens*. (0099-2240 (Print)).
182. Giessen, T.W. and P.A. Silver, *Widespread distribution of encapsulin nanocompartments reveals functional diversity*. Nature Microbiology, 2017. **2**(6).
183. Rahmanpour, R. and T.D. Bugg, *Assembly in vitro of Rhodococcus jostii RHA1 encapsulin and peroxidase DypB to form a nanocompartment*. (1742-4658 (Electronic)).
184. Contreras, H., et al., *Characterization of a Mycobacterium tuberculosis nanocompartment and its potential cargo proteins*. (1083-351X (Electronic)).
185. Rurup, W.F., et al., *Self-sorting of foreign proteins in a bacterial nanocompartment*. (1520-5126 (Electronic)).
186. Tamura, A., et al., *Packaging guest proteins into the encapsulin nanocompartment from Rhodococcus erythropolis N771*. (1097-0290 (Electronic)).
187. Cassidy-Amstutz, C., et al., *Identification of a Minimal Peptide Tag for in Vivo and in Vitro Loading of Encapsulin*. (1520-4995 (Electronic)).
188. Moon, H., et al., *Developing genetically engineered encapsulin protein cage nanoparticles as a targeted delivery nanoplatfrom*. (1526-4602 (Electronic)).
189. Toita, R., et al., *Development of human hepatocellular carcinoma cell-targeted protein cages*. (1520-4812 (Electronic)).
190. Moon, H., et al., *Genetically engineering encapsulin protein cage nanoparticle as a SCC-7 cell targeting optical nanoprobe*. (1226-4601 (Print)).
191. Kanekiyo, M., et al., *Rational Design of an Epstein-Barr Virus Vaccine Targeting the Receptor-Binding Site*. Cell, 2015. **162**(5): p. 1090-1100.
192. Lagoutte, P., et al., *Simultaneous surface display and cargo loading of encapsulin nanocompartments and their use for rational vaccine design*. Vaccine, 2018. **36**(25): p. 3622-3628.
193. Rajagopal, K. and J.P. Schneider, *Self-assembling peptides and proteins for nanotechnological applications*. (0959-440X (Print)).

194. Drexler, K.E., *Molecular engineering: An approach to the development of general capabilities for molecular manipulation*. Proceedings of the National Academy of Sciences of the United States of America, 1981. **78**(9): p. 5275-5278.
195. King, N.P. and Y.-T. Lai, *Practical approaches to designing novel protein assemblies*. Current Opinion in Structural Biology, 2013. **23**(4): p. 632-638.
196. King, N.P., et al., *Accurate design of co-assembling multi-component protein nanomaterials*. Nature, 2014. **510**(7503): p. 103-108.
197. Sciore, A., et al., *Flexible, symmetry-directed approach to assembling protein cages*. 2016. **113**(31): p. 8681-8686.
198. Bale, J.B., et al., *Accurate design of megadalton-scale two-component icosahedral protein complexes*. (1095-9203 (Electronic)).
199. Hsia, Y., et al., *Design of a hyperstable 60-subunit protein dodecahedron. [corrected]*. Nature, 2016. **535**(7610): p. 136-9.
200. Griffiths, J.S., et al., *Cloning, isolation and characterization of the Thermotoga maritima KDPG aldolase*. (0968-0896 (Print)).
201. DiMaio, F., et al., *Modeling symmetric macromolecular structures in Rosetta3*. PLoS One, 2011. **6**(6): p. e20450.
202. Leaver-Fay, A., et al., *ROSETTA3: an object-oriented software suite for the simulation and design of macromolecules*. (1557-7988 (Electronic)).
203. Marcandalli, J., et al., *Induction of Potent Neutralizing Antibody Responses by a Designed Protein Nanoparticle Vaccine for Respiratory Syncytial Virus*. Cell, 2019. **176**(6): p. 1420-1431 e17.
204. Tan, T.K., et al., *A COVID-19 vaccine candidate using SpyCatcher multimerization of the SARS-CoV-2 spike protein receptor-binding domain induces potent neutralising antibody responses*. Nature Communications, 2021. **12**(1): p. 542.
205. Vu, M.N., et al., *Current and future nanoparticle vaccines for COVID-19*. eBioMedicine, 2021. **74**: p. 103699.
206. Cohen Alexander, A., et al., *Mosaic nanoparticles elicit cross-reactive immune responses to zoonotic coronaviruses in mice*. Science, 2021. **371**(6530): p. 735-741.
207. Cohen, A.A., et al., *Construction, characterization, and immunization of nanoparticles that display a diverse array of influenza HA trimers*. PLOS ONE, 2021. **16**(3): p. e0247963.
208. Roupheal, N.G. and D.S. Stephens, *Neisseria meningitidis: biology, microbiology, and epidemiology*. Methods in molecular biology (Clifton, N.J.), 2012. **799**: p. 1-20.
209. Stephens, D.S., *Biology and pathogenesis of the evolutionarily successful, obligate human bacterium Neisseria meningitidis*. Vaccine, 2009. **27**: p. B71-B77.
210. Madico, G., et al., *The meningococcal vaccine candidate GNA1870 binds the complement regulatory protein factor H and enhances serum resistance*. 2006. **177**(1): p. 501-510.
211. Schneider, M.C., et al., *Neisseria meningitidis recruits factor H using protein mimicry of host carbohydrates*. 2009. **458**(7240): p. 890-893.
212. Seib, K.L., et al., *Factor H-binding protein is important for meningococcal survival in human whole blood and serum and in the presence of the antimicrobial peptide LL-37*. Infect Immun, 2009. **77**(1): p. 292-9.
213. Beernink, P.T., et al., *A Meningococcal Outer Membrane Vesicle Vaccine with Overexpressed Mutant FHbp Elicits Higher Protective Antibody Responses in Infant Rhesus Macaques than a Licensed Serogroup B Vaccine*. mBio, 2019. **10**(3).
214. Vernikos, G. and D. Medini, *Bexsero® chronicle*. Pathogens and global health, 2014. **108**(7): p. 305-316.
215. Azzari, C. and P. Bonanni, *A new meningococcal B vaccine for adolescents and adults: characteristics and methods of use*. Journal of preventive medicine and hygiene, 2018. **59**(4): p. E257-E260.
216. Cendron, L., et al., *Structure of the uncomplexed Neisseria meningitidis factor H-binding protein fHbp (rLP2086)*. Acta crystallographica. Section F, Structural biology and crystallization communications, 2011. **67**(Pt 5): p. 531-535.

217. Pizza, M., J. Donnelly, and R. Rappuoli, *Factor H-binding protein, a unique meningococcal vaccine antigen*. *Vaccine*, 2008. **26**: p. 146-148.
218. Cantini, F., et al., *Solution structure of the factor H-binding protein, a survival factor and protective antigen of Neisseria meningitidis*. (0021-9258 (Print)).
219. Veggi, D., et al., *The Factor H Binding Protein of Neisseria meningitidis Interacts with Xenosiderophores in Vitro*. *Biochemistry*, 2012. **51**(46): p. 9384-9393.
220. Bianchi, F., et al., *Cocrystal structure of meningococcal factor H binding protein variant 3 reveals a new crossprotective epitope recognized by human mAb 1E6*. *FASEB journal : official publication of the Federation of American Societies for Experimental Biology*, 2019. **33**(11): p. 12099-12111.
221. Malito, E., et al., *Defining a protective epitope on factor H binding protein, a key meningococcal virulence factor and vaccine antigen*. *Proceedings of the National Academy of Sciences of the United States of America*, 2013. **110**(9): p. 3304-3309.
222. Seale, A.C., et al., *Estimates of the Burden of Group B Streptococcal Disease Worldwide for Pregnant Women, Stillbirths, and Children*. *Clinical infectious diseases : an official publication of the Infectious Diseases Society of America*, 2017. **65**(suppl_2): p. S200-S219.
223. Shabayek, S. and B. Spellerberg, *Group B Streptococcal Colonization, Molecular Characteristics, and Epidemiology*. 2018. **9**.
224. Johri, A.K., et al., *Group B Streptococcus: global incidence and vaccine development*. *Nature reviews. Microbiology*, 2006. **4**(12): p. 932-942.
225. Landwehr-Kenzel, S. and P. Henneke, *Interaction of Streptococcus agalactiae and Cellular Innate Immunity in Colonization and Disease*. 2014. **5**.
226. Lazzarin, M., et al., *Contribution of pilus type 2b to invasive disease caused by a Streptococcus agalactiae ST-17 strain*. *BMC microbiology*, 2017. **17**(1): p. 148-148.
227. Rosini, R., et al., *Identification of novel genomic islands coding for antigenic pilus-like structures in Streptococcus agalactiae*. (0950-382X (Print)).
228. Margarit, I., et al., *Preventing bacterial infections with pilus-based vaccines: the group B streptococcus paradigm*. (0022-1899 (Print)).
229. Nuccitelli, A., et al., *Structure-based approach to rationally design a chimeric protein for an effective vaccine against Group B Streptococcus infections*. *Proc Natl Acad Sci U S A*, 2011. **108**(25): p. 10278-83.
230. Cozzi, R., et al., *Structure and assembly of group B streptococcus pilus 2b backbone protein*. *PLoS One*, 2015. **10**(5): p. e0125875.
231. Carboni, F., et al., *Structure of a protective epitope of group B *Streptococcus* type III capsular polysaccharide*. 2017. **114**(19): p. 5017-5022.
232. Uchiyama, S., et al., *Dual actions of group B *Streptococcus* capsular sialic acid provide resistance to platelet-mediated antimicrobial killing*. *Proceedings of the National Academy of Sciences*, 2019. **116**(15): p. 7465.
233. Lemire, P., et al., *Role of capsular polysaccharide in Group B Streptococcus interactions with dendritic cells*. *Microbes and Infection*, 2012. **14**(12): p. 1064-1076.
234. Pezzicoli, A., et al., *Exogenous Sialic Acid Transport Contributes to Group B Streptococcus Infection of Mucosal Surfaces*. *The Journal of Infectious Diseases*, 2012. **206**(6): p. 924-931.
235. Slotved, H.C., et al., *Serotype IX, a Proposed New Streptococcus agalactiae Serotype*. (0095-1137 (Print)).
236. Lancefield, R.C. and E.H. Freimer, *Type-specific polysaccharide antigens of group B streptococci*. *Journal of Hygiene*, 1966. **64**(2): p. 191-203.
237. Baker, C.J., et al., *Immunization of Pregnant Women with a Polysaccharide Vaccine of Group B Streptococcus*. *New England Journal of Medicine*, 1988. **319**(18): p. 1180-1185.
238. Palazzi, D.L., et al., *Use of Type V Group B Streptococcal Conjugate Vaccine in Adults 65–85 Years Old*. *The Journal of Infectious Diseases*, 2004. **190**(3): p. 558-564.
239. Cadoz, M., *Potential and limitations of polysaccharide vaccines in infancy*. *Vaccine*, 1998. **16**(14): p. 1391-1395.

240. Absalon, J., et al., *Safety and immunogenicity of a novel hexavalent group B streptococcus conjugate vaccine in healthy, non-pregnant adults: a phase 1/2, randomised, placebo-controlled, observer-blinded, dose-escalation trial*. *The Lancet Infectious Diseases*, 2021. **21**(2): p. 263-274.
241. Nuccitelli, A., C.D. Rinaudo, and D. Maione, *Group B Streptococcus vaccine: state of the art*. *Therapeutic advances in vaccines*, 2015. **3**(3): p. 76-90.
242. Organization, W.H., *Global incidence and prevalence of selected curable sexually transmitted infections-2008*. 2012: World Health Organization.
243. Workowski, K.A., et al., *Sexually transmitted diseases treatment guidelines, 2015*. 2015. **64**(RR-03): p. 1.
244. Goldenberg, R.L., et al., *Sexually transmitted diseases and adverse outcomes of pregnancy*. 1997. **24**(1): p. 23-41.
245. Galvin, S.R. and M.S. Cohen, *The role of sexually transmitted diseases in HIV transmission*. (1740-1526 (Print)).
246. Ison, C.A., J.W. Dillon Ja Fau - Tapsall, and J.W. Tapsall, *The epidemiology of global antibiotic resistance among Neisseria gonorrhoeae and Haemophilus ducreyi*. (0140-6736 (Print)).
247. Gottlieb, S.L., et al., *Gonococcal vaccines: Public health value and preferred product characteristics; report of a WHO global stakeholder consultation, January 2019*. *Vaccine*, 2020. **38**(28): p. 4362-4373.
248. Gottlieb, S.L., et al., *Advancing vaccine development for gonorrhoea and the Global STI Vaccine Roadmap*. (1449-8987 (Electronic)).
249. Gala, R.P., et al., *Novel Whole-Cell Inactivated Neisseria Gonorrhoeae Microparticles as Vaccine Formulation in Microneedle-Based Transdermal Immunization*. LID - 10.3390/vaccines6030060 [doi] LID - 60. (2076-393X (Print)).
250. Semchenko, E.A. and K.L. Seib, *Outer membrane vesicle vaccines for Neisseria gonorrhoeae*. *Nature Reviews Urology*, 2022. **19**(1): p. 5-6.
251. Gulati, S., et al., *Targeting Lipooligosaccharide (LOS) for a Gonococcal Vaccine*. 2019. **10**.
252. Unemo, M., et al., *Gonorrhoea*. *Nature Reviews Disease Primers*, 2019. **5**(1): p. 79.
253. Baarda, B.I. and A.E. Sikora, *Proteomics of Neisseria gonorrhoeae: the treasure hunt for countermeasures against an old disease*. 2015. **6**.
254. Jerse, A.E., M.C. Bash, and M.W. Russell, *Vaccines against gonorrhea: Current status and future challenges*. *Vaccine*, 2014. **32**(14): p. 1579-1587.
255. Bhat, K.S., et al., *The opacity proteins of Neisseria gonorrhoeae strain MS11 are encoded by a family of 11 complete genes*. *Molecular Microbiology*, 1991. **5**(8): p. 1889-1901.
256. Cole Jessica, G., B. Fulcher Nanette, and E. Jerse Ann, *Opacity Proteins Increase Neisseria gonorrhoeae Fitness in the Female Genital Tract Due to a Factor under Ovarian Control*. *Infection and Immunity*, 2010. **78**(4): p. 1629-1641.
257. Virji, M., et al., *Carcinoembryonic antigens (CD66) on epithelial cells and neutrophils are receptors for Opa proteins of pathogenic neisseriae*. 1996. **22**(5): p. 941-950.
258. Gray-Owen, S.D., et al., *CD66 carcinoembryonic antigens mediate interactions between Opa-expressing Neisseria gonorrhoeae and human polymorphonuclear phagocytes*. 1997. **16**(12): p. 3435-3445.
259. Bos, M.P., D. Hogan, and R.J. Belland, *Selection of Opa+ Neisseria gonorrhoeae by limited availability of normal human serum*. *Infection and Immunity*, 1997. **65**(2): p. 645-650.
260. Malorny, B., et al., *Sequence diversity, predicted two-dimensional protein structure, and epitope mapping of neisserial Opa proteins*. 1998. **180**(5): p. 1323-1330.
261. Cole, J.G. and A.E. Jerse, *Functional characterization of antibodies against Neisseria gonorrhoeae opacity protein loops*. *PLoS One*, 2009. **4**(12): p. e8108.
262. Van Der Ley, P., et al., *Topology of outer membrane porins in pathogenic Neisseria spp*. 1991. **59**(9): p. 2963-2971.
263. Knapp, J.S., et al., *Serological classification of Neisseria gonorrhoeae with use of monoclonal antibodies to gonococcal outer membrane protein I*. 1984. **150**(1): p. 44-48.
264. Kühlewein, C., et al., *Low-phosphate-dependent invasion resembles a general way for Neisseria gonorrhoeae to enter host cells*. 2006. **74**(7): p. 4266-4273.

265. Ram, S., et al., *Binding of complement factor H to loop 5 of porin protein 1A: a molecular mechanism of serum resistance of nonsialylated Neisseria gonorrhoeae*. 1998. **188**(4): p. 671-680.
266. Massari, P., Y. Ho, and L.M.J.P.o.t.N.A.o.S. Wetzler, *Neisseria meningitidis porin PorB interacts with mitochondria and protects cells from apoptosis*. 2000. **97**(16): p. 9070-9075.
267. Zhu, W., et al., *Properly folded and functional PorB from Neisseria gonorrhoeae inhibits dendritic cell stimulation of CD4+ T cell proliferation*. 2018. **293**(28): p. 11218-11229.
268. Yuen, R., et al., *Neisserial PorB immune enhancing activity and use as a vaccine adjuvant*. 2019.
269. Doll, T.A., et al., *Nanoscale assemblies and their biomedical applications*. J R Soc Interface, 2013. **10**(80): p. 20120740.
270. Lee, E.B., et al., *Attachment of flagellin enhances the immunostimulatory activity of a hemagglutinin-ferritin nano-cage*. Nanomedicine, 2019. **17**: p. 223-235.
271. Masignani, V., et al., *Vaccination against Neisseria meningitidis using three variants of the lipoprotein GNA1870*. The Journal of experimental medicine, 2003. **197**(6): p. 789-799.
272. Giuliani, M., et al., *Human protective response induced by meningococcus B vaccine is mediated by the synergy of multiple bactericidal epitopes*. Scientific Reports, 2018. **8**(1): p. 3700.
273. Beernink Peter, T., et al., *Functional Analysis of the Human Antibody Response to Meningococcal Factor H Binding Protein*. mBio. **6**(3): p. e00842-15.
274. Veggi, D., et al., *4CMenB vaccine induces elite cross-protective human antibodies that compete with human factor H for binding to meningococcal fHbp*. PLoS Pathog, 2020. **16**(10): p. e1008882.
275. López-Sagasetta, J., et al., *Crystal structure reveals vaccine elicited bactericidal human antibody targeting a conserved epitope on meningococcal fHbp*. Nature Communications, 2018. **9**(1): p. 528.
276. Moumene, A., et al., *Proteomic profiling of the outer membrane fraction of the obligate intracellular bacterial pathogen Ehrlichia ruminantium*. PLoS One, 2015. **10**(2): p. e0116758.
277. Wu, H.J., A.H. Wang, and M.P. Jennings, *Discovery of virulence factors of pathogenic bacteria*. Curr Opin Chem Biol, 2008. **12**(1): p. 93-101.
278. Rollauer, S.E., et al., *Outer membrane protein biogenesis in Gram-negative bacteria*. Philos Trans R Soc Lond B Biol Sci, 2015. **370**(1679).
279. Puchades, C., et al., *Epitope mapping of diverse influenza Hemagglutinin drug candidates using HDX-MS*. Scientific Reports, 2019. **9**(1): p. 4735.
280. Palumbo, E., et al., *Antigen Identification Starting from the Genome: A "Reverse Vaccinology" Approach Applied to MenB*, in *Neisseria meningitidis: Advanced Methods and Protocols*, M. Christodoulides, Editor. 2012, Humana Press: Totowa, NJ. p. 361-403.
281. Hollingshead, S., et al., *Structure-based design of chimeric antigens for multivalent protein vaccines*. Nat Commun, 2018. **9**(1): p. 1051.
282. Tifrea, D.F., et al., *Protection against a chlamydial respiratory challenge by a chimeric vaccine formulated with the Chlamydia muridarum major outer membrane protein variable domains using the Neisseria lactamica porin B as a scaffold*. npj Vaccines, 2020. **5**(1): p. 37.
283. Cozzi, R., et al., *Structure and assembly of group B streptococcus pilus 2b backbone protein*. PloS one, 2015. **10**(5): p. e0125875-e0125875.
284. Lauer, K.B., R. Borrow, and T.J. Blanchard, *Multivalent and Multipathogen Viral Vector Vaccines*. Clinical and vaccine immunology : CVI, 2017. **24**(1): p. e00298-16.
285. Baicus, A., *History of polio vaccination*. World journal of virology, 2012. **1**(4): p. 108-114.
286. Serruto, D., et al., *The new multicomponent vaccine against meningococcal serogroup B, 4CMenB: immunological, functional and structural characterization of the antigens*. Vaccine, 2012. **30** Suppl 2(0 2): p. B87-B97.
287. Schlingmann, B., et al., *Polyvalent vaccines: High-maintenance heroes*. PLoS pathogens, 2018. **14**(4): p. e1006904-e1006904.
288. Smith, J., J.W. Lipsitch M Fau - Almond, and J.W. Almond, *Vaccine production, distribution, access and uptake*. (1474-547X (Electronic)).
289. Li, H., et al., *Applications of genome editing technology in the targeted therapy of human diseases: mechanisms, advances and prospects*. Signal Transduction and Targeted Therapy, 2020. **5**(1): p. 1.

290. Nilo, A., et al., *Anti-Group B Streptococcus Glycan-Conjugate Vaccines Using Pilus Protein GBS80 As Carrier and Antigen: Comparing Lysine and Tyrosine-directed Conjugation*. ACS Chemical Biology, 2015. **10**(7): p. 1737-1746.
291. Song, Y., et al., *High-resolution comparative modeling with RosettaCM*. Structure (London, England : 1993), 2013. **21**(10): p. 1735-1742.
292. Thompson, J. and D. Baker, *Incorporation of evolutionary information into Rosetta comparative modeling*. Proteins, 2011. **79**(8): p. 2380-8.
293. Bradley, P., K.M. Misura, and D. Baker, *Toward high-resolution de novo structure prediction for small proteins*. Science, 2005. **309**(5742): p. 1868-71.
294. Schrodinger, LLC, *The PyMOL Molecular Graphics System, Version 1.8*. 2015.
295. Pettersen, E.F., et al., *UCSF ChimeraX: Structure visualization for researchers, educators, and developers*. Protein science : a publication of the Protein Society, 2021. **30**(1): p. 70-82.
296. Klock, H.E. and S.A. Lesley, *The Polymerase Incomplete Primer Extension (PIPE) method applied to high-throughput cloning and site-directed mutagenesis*. (1064-3745 (Print)).
297. Bertani, G., *STUDIES ON LYSOGENESIS I*. Journal of Bacteriology, 1951. **62**(3): p. 293-300.
298. Froger, A. and J.E. Hall, *Transformation of plasmid DNA into E. coli using the heat shock method*. Journal of visualized experiments : JoVE, 2007(6): p. 253-253.
299. Battye, T.G., et al., *iMOSFLM: a new graphical interface for diffraction-image processing with MOSFLM*. (1399-0047 (Electronic)).
300. McCoy A.J. - Grosse-Kunstleve, R.W., et al., *Phaser crystallographic software*. (0021-8898 (Print)).
301. Krissinel, E. and K. Henrick, *Inference of macromolecular assemblies from crystalline state*. (0022-2836 (Print)).
302. Salfeld, J., et al., *Antigenic determinants and functional domains in core antigen and e antigen from hepatitis B virus*. Journal of virology, 1989. **63**(2): p. 798-808.
303. van Rosmalen, M., M. Krom, and M. Merckx, *Tuning the Flexibility of Glycine-Serine Linkers To Allow Rational Design of Multidomain Proteins*. Biochemistry, 2017. **56**(50): p. 6565-6574.
304. DiMaio, F., et al., *Modeling symmetric macromolecular structures in Rosetta3*. (1932-6203 (Electronic)).
305. Rappuoli, R. and D. Serruto, *Self-Assembling Nanoparticles Usher in a New Era of Vaccine Design*. Cell, 2019. **176**(6): p. 1245-1247.
306. Joyce, M.G., et al., *Efficacy of a Broadly Neutralizing SARS-CoV-2 Ferritin Nanoparticle Vaccine in Nonhuman Primates*. bioRxiv, 2021.
307. Aston-Deville, S., et al., *An assessment of the use of Hepatitis B Virus core protein virus-like particles to display heterologous antigens from Neisseria meningitidis*. Vaccine, 2020. **38**(16): p. 3201-3209.
308. Tao, P., et al., *A Bacteriophage T4 Nanoparticle-Based Dual Vaccine against Anthrax and Plague*. mBio, 2018. **9**(5): p. e01926-18.
309. Kamp, H.D., et al., *Design of a broadly reactive Lyme disease vaccine*. npj Vaccines, 2020. **5**(1): p. 33.
310. Correia, B.E., et al., *Proof of principle for epitope-focused vaccine design*. (1476-4687 (Electronic)).
311. Nussinov, R., et al., *AlphaFold, Artificial Intelligence (AI), and Allostery*. The Journal of Physical Chemistry B, 2022.
312. Gao, K., R. Oerlemans, and M.R. Groves, *Theory and applications of differential scanning fluorimetry in early-stage drug discovery*. Biophysical Reviews, 2020. **12**(1): p. 85-104.
313. Gotschlich, E.C., et al., *Porin protein of Neisseria gonorrhoeae: cloning and gene structure*. Proceedings of the National Academy of Sciences of the United States of America, 1987. **84**(22): p. 8135-8139.
314. Zeth, K., et al., *Structure and function of the PorB porin from disseminating Neisseria gonorrhoeae*. Biochemical Journal, 2013. **449**(3): p. 631-642.
315. Fox, D.A., et al., *Structure of the Neisserial outer membrane protein Opa(6)(0): loop flexibility essential to receptor recognition and bacterial engulfment*. J Am Chem Soc, 2014. **136**(28): p. 9938-46.
316. Jumper, J.A.-O., et al., *Applying and improving AlphaFold at CASP14*. (1097-0134 (Electronic)).
317. Spraggon, G., et al., *Supramolecular Organization of the Repetitive Backbone Unit of the Streptococcus pneumoniae Pilus*. PLOS ONE, 2010. **5**(6): p. e10919.

318. Campisi, E., et al., *Group B Streptococcus chimeric capsular polysaccharides as novel multivalent vaccine candidates*. Glycoconjugate Journal, 2021. **38**(4): p. 447-457.
319. Möglinger, U., et al., *Cross Reactive Material 197 glycoconjugate vaccines contain privileged conjugation sites*. Scientific Reports, 2016. **6**(1): p. 20488.
320. Garçon, N., A.M. Vaughn Dw Fau - Didierlaurent, and A.M. Didierlaurent, *Development and evaluation of AS03, an Adjuvant System containing α -tocopherol and squalene in an oil-in-water emulsion*. (1744-8395 (Electronic)).
321. Cid, R. and J. Bolívar, *Platforms for Production of Protein-Based Vaccines: From Classical to Next-Generation Strategies*. Biomolecules, 2021. **11**(8): p. 1072.
322. Sáez-Llorens, X., et al., *Four-year antibody persistence and response to a booster dose of a pentavalent MenABCWY vaccine administered to healthy adolescents and young adults*. Human vaccines & immunotherapeutics, 2018. **14**(5): p. 1161-1174.
323. Caradonna, T.A.-O. and A.A.-O. Schmidt, *Protein engineering strategies for rational immunogen design*. (2059-0105 (Electronic)).
324. Maphis, N.M., et al., *Q β Virus-like particle-based vaccine induces robust immunity and protects against tauopathy*. (2059-0105 (Electronic)).
325. Rodrigues, M.Q., P.M. Alves, and A. Roldao, *Functionalizing Ferritin Nanoparticles for Vaccine Development*. Pharmaceutics, 2021. **13**(10).
326. Brune, K.D., et al., *Plug-and-Display: decoration of Virus-Like Particles via isopeptide bonds for modular immunization*. Sci Rep, 2016. **6**: p. 19234.

